Peak-to-Average Power Ratio Reduction of DOCSIS 3.1 Downstream Signals

A Thesis Submitted
to the College of Graduate and Postdoctoral Studies
in Partial Fulfillment of the Requirements
for the Degree of Master of Science
in the Department of Electrical and Computer Engineering
University of Saskatchewan

by

Quang Nguyen

Saskatoon, Saskatchewan, Canada

Permission to Use

In presenting this thesis in partial fulfillment of the requirements for a Postgraduate degree from the University of Saskatchewan, it is agreed that the Libraries of this University may make it freely available for inspection. Permission for copying of this thesis in any manner, in whole or in part, for scholarly purposes may be granted by the professors who supervised this thesis work or, in their absence, by the Head of the Department of Electrical and Computer Engineering or the Dean of the College of Graduate and Postdoctoral Studies at the University of Saskatchewan. Any copying, publication, or use of this thesis, or parts thereof, for financial gain without the written permission of the author is strictly prohibited. Proper recognition shall be given to the author and to the University of Saskatchewan in any scholarly use which may be made of any material in this thesis.

Request for permission to copy or to make any other use of material in this thesis in whole or in part should be addressed to:

Head of the Department of Electrical and Computer Engineering
57 Campus Drive
University of Saskatchewan
Saskatoon, Saskatchewan S7N 5A9
Canada

OR

Dean
College of Graduate and Postdoctoral Studies
University of Saskatchewan
116 Thorvaldson Building, 110 Science Place
Saskatoon, Saskatchewan S7N 5C9
Canada

Abstract

Tone reservation (TR) is an attractive and widely used method for peak-to-average power ratio (PAPR) reduction of orthogonal frequency division multiplexing (OFDM) signals, where both transmitter and receiver agree upon a number of subcarriers or tones to be reserved to generate a peak canceling signal that can reduce the peak power of the transmitted signals. The tones are selected to be mutually exclusive with the tones used for data transmission, which allows the receiver to extract the data symbols without distortions.

This thesis presents two novel PAPR reduction algorithms for OFDM signals based on the TR principle, which do not distort the transmitted signals. The first proposed algorithm is performed in the time domain, whereas the second algorithm is a new clipping-and-filtering method. Both algorithms consist of two stages. The first stage, which is done off-line, creates a set of canceling signals based on the settings of the OFDM system. In particular, these signals are constructed to cancel signals at different levels of maximum instantaneous power that are above a predefined threshold. The second stage, which is online and iterative, reduces the signal peaks by using the canceling signals constructed in the first stage. The precalculated canceling signals can be updated when different tone sets are selected for data transmission, accommodating many practical applications. Simulation results show that the proposed algorithms achieve slightly better PAPR reduction performance than the conventional algorithms. Moreover, such performance is achieved with much lower computational complexity in terms of numbers of multiplications and additions per iteration. Among the two proposed algorithms, the time-domain algorithm gives the best peak reduction performance but the clipping-and-filtering algorithm requires considerably less number of multiplications per iteration and can be efficiently implemented using the fast Fourier transform (FFT)/inverse fast Fourier transform (IFFT) structure.

Acknowledgments

I would like to express my deepest appreciation and gratitude to my supervisor, Professor Ha Nguyen, for his great support during my studies and research. He has been a great source of knowledge and has inspired me with many ideas which are very important for my research. The useful discussion and advice from him during our weekly meetings made my studies and research flow easily and smoothly. This thesis definitely cannot be finished without his meticulous reviews.

My special thanks go to Professor Eric Salt who taught me wonderful courses. His passionate attitudes towards his students and digital signal processing techniques are highly influential for me to pursue my dream of becoming a professional in the digital signal processing area.

I would like to send my special thanks to Dr. Brian Berscheid for his committed tutoring during my research period. His open-minded thoughts and discussions help to shape my skills of understanding research problems in a practical way.

I feel a deep sense of gratitude for my wife Trinh Nguyen. It is impossible to finish this thesis without her encouragement and help. She devotes her time taking care of me and our two lovely children so that I can focus on studying. I dedicate this thesis to her and our children.

I would also like to thank my parents for the endless love and support they provide through my entire life. They continuously inspire me to work harder in every stage of my life.

I wish to express my appreciation to all of those who gave me help when I studied at the University of Saskatchewan.

Finally, I gratefully acknowledge Vecima Networks Inc., Natural Sciences and Engineering Research Council of Canada (NSERC) and the University of Saskatchewan for their financial supports of my studies.

Table of Contents

List of Abbreviations

ACE	Active Constellation Extension
AM	Amplitude Modulation
BPSK	Binary Phase Shift Keying
CATV	Community Antenna TeleVision
CCDF	Complimentary Cumulative Distribution Function
CFTR	Clipping-and-Filtering Tone Reservation
CM	Cable Modem
CMTS	Cable Modem Termination System
CP	Cyclic Prefix
DFT	Discrete Fourier Transform
DOCSIS	Data Over Cable System Interface Specification
FDX	Full Duplex
FFT	Fast Fourier Transform
FPGA	Field Programmable Gate Array
GTR	Gradient-based Tone Reservation
HPA	High Power Amplifier
I	Inphase
IBO	Input back off
IDFT	Inverse Discrete Fourier Transform

IFFT	Inverse Fast Fourier Transform
ISI	Inter-Symbol Interference
OFDM	Orthogonal Frequency Division Multiplexing
OFDMA	Orthogonal Frequency Division Multiple Access
PAPR	Peak to Average Power Ratio
PM	Phase Modulation
PTS	Partial Transmit Sequence
Q	Quadrature
QAM	Quadrature Amplitude Modulation
QPSK	Quadrature Phase Shift Keying
RC	Raised Cosine
RX	Receiver
SC-QAM	Single-Carrier Quadrature Amplitude Modulation
SLM	Selective Mapping
SNR	Signal to Noise Ratio
SRRC	Square Root Raised Cosine
SSPA	Solid State Power Amplifer
TR	Tone Reservation
TWTA	Travelling Wave Tube Amplifier
TX	Transmitter

List of Figures

List of Tables

1. Introduction

The CATV systems that we have today originated as a well-placed "Community Antenna" connected to a few televisions that could not get reception of a commercial broadcasting station with a roof-mounted antenna. In fact, CATV is a legacy acronym for Community Antenna TeleVision network.

Over time, there were changes that increased the number of TV channels delivered over the network. The changes continued, but took a turn in the late 1990's when service providers started to develop a new type of set-top box that could be uniquely addressed and remotely monitored. This transformed the broadcast cable network into a network that handled two-way communication. Advancements in digital communication technology provided the means to put several channels over the bandwidth used for a single TV signal. Further improvement allowed data to be transmitted over the system designed for TV signals. Data transmission give rise to interactive TV guides, news, weather, and later on, Internet services.

The revenue that came from the rapid expansion of the CATV network was shared between service providers and equipment manufacturers. However, service providers found themselves held hostage by the equipment manufacturers as their equipment was proprietary and had to be sourced by them. The manufacturers overpriced their equipment to capture revenue that should have gone to the service providers. The CATV service providers remedied this by banding together and forming a not-for-profit organization, called CableLabs [3].

CableLabs redefined the CATV systems as a set of well-defined subsystems of sufficiently small sizes that each could be manufactured by small companies. They provided a functional description of these components in a document referred to as "Data-over-cable service interface specification", or DOCSIS. This document, while technically not an official standard,

has been adopted by virtually every CATV service provider, so is a de-facto standard [4, 5].

1.1 DOCSIS

A simplified infrastructure of a typical CATV network is shown in Figure 1.1. There are two main components in a DOCSIS network: *cable modems* (CMs) located at the user's premises, and a *cable modem termination system* (CMTS) resided at the cable company's head-end. The CMTS is responsible to communicate with multiple CMs installed at subscribers' households. The two-way communication between CMTS and CMs is realized by downstream and upstream traffics. The downstream direction refers to the distribution of data streams from the CMTS to cable modems. Upstream communication is used by CMs to upload their data contents to the company's head-end. In order to accommodate multiple users, the CMTS allocates channel resources to different CMs and schedules times to send and receive data packets. At the head-end, the CMTS connects with an Internet Service Provider via its Internet interface. Thereby, the Internet data can be streamed through the coaxial cable networks and reach the subscribers' CMs.

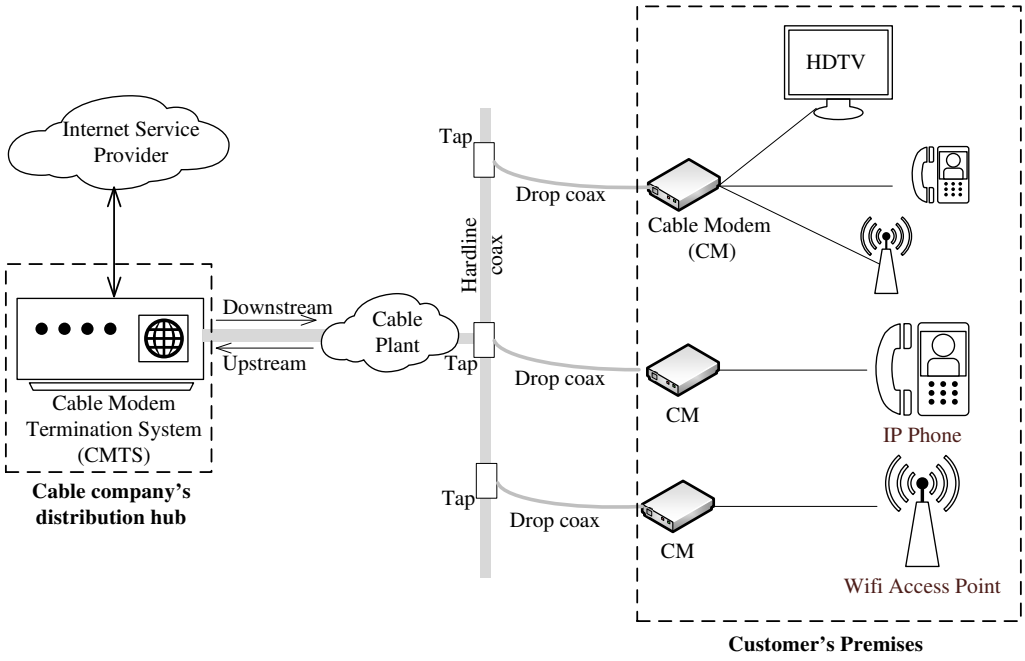

Figure 1.1 General structure of a DOCSIS network.

The first DOCSIS standards, referred to as DOCSIS 1.0, was released in 1997. The sub-

Table 1.1 Different DOCSIS versions.

DOCSIS version	Release date	Modulation	Downstream throughput	Upstream throughput
1.0	03/1997	Single-carrier QAM	42.88 Mbps	10.24 Mbps
2.0	12/2001		42.88 Mbps	30.72 Mbps
3.0	08/2006		1372.16 Mbps	245.76 Mbps
3.1	10/2013	Multi-carrier OFDM	10 Gbps	1 Gbps
3.1 FDX	05/2018	Multi-carrier OFDM with FDX	10 Gbps	4 Gbps

sequent versions were 1.1, 2.0, 3.0, 3.1 and 3.1 FDX. The latest version was released in May 2018, which is version 3.1 expanded with the *full duplex* (FDX) feature. Table 1.1 shows different versions of DOCSIS standards with different capacities for upstream and downstream traffics. The original DOCSIS 1.0 standard supported only a single channel with 42.88 *mega bits per second* (Mbps) in downstream and 10.24 Mbps in upstream. DOCSIS 2.0 extended the upstream bandwidth by 3 times 4 years later in responding to a higher demand in upstream traffic. DOCSIS 3.0 was introduced in 2006 as a substantial update for CATV network to make it comparable to other competitive services using *digital subscriber line* (DSL) and fiber optics technology. This version of DOCSIS was able to support simultaneously multiple *single-carrier quadrature amplitude modulation* (SC-QAM) channels and combine them together to provide 1372.16 Mbps downstream and 245.76 Mbps upstream traffics. After 7 years, in 2013, DOCSIS 3.1 was released with an adoption of multi-carrier modulation schemes, which were *orthogonal frequency division modulation* (OFDM) in the downstream direction, and *orthogonal division multiple access* (OFDMA) in the reverse direction. In addition, DOCSIS 3.1 substantially increases the performance of the coaxial networks via downstream and upstream spectrum expansion incorporation of modern *forward error coding* (FEC) with *low density parity check* (LDPC) codes, high modulation orders of *quadrature amplitude modulation* (QAM) with OFDM and multiple downstream modulation profiles [4].

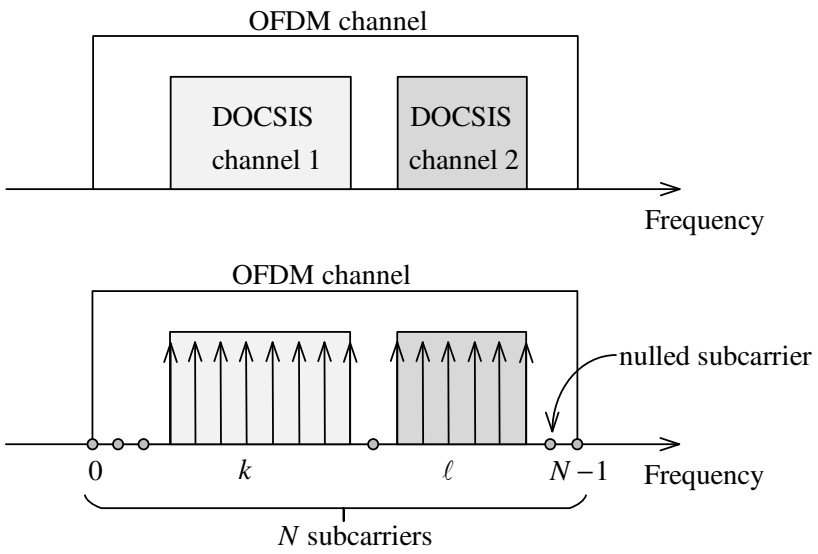

Figure 1.2 OFDM channel with nulled subcarriers to accommodate legacy channels.

The multi-carrier modulation utilizes a number of orthogonal subcarriers which can be efficiently implemented using the *fast Fourier transform* (FFT). The change from single-carrier QAM modulation to multi-carrier modulation provides a number of benefits. The multi-carrier scheme produces a longer symbol time duration, which has better immunity to impulse noise present in the channel. By the nature of using multiple subcarriers, the system can flexibly null individual subcarriers to accommodate legacy channels as well as avoiding ingress noise (see illustration in Figure 1.2). With OFDM, impulse noise and narrowband interference can also be effectively mitigated by using time and frequency interleaving [4]. Moreover, the multi-carrier modulation allows the use of high-order QAM constellations as high as $16,384$-QAM on downstream and $4,096$-QAM on upstream. More details on SC-QAM and OFDM systems will be presented later in Chapter 2.

The recently released version 3.1 of DOCSIS includes *full-duplex* (FDX) capability, which allows the upstream and downstream transmissions to concurrently use the same spectrum. Thereby, the FDX-enabled DOCSIS technology has the potential of doubling the spectral efficiency. However, in order to be backward compatible with the previous versions of DOCSIS, the FDX band is specified in portions of the available spectrum. Figure 1.3 illustrates

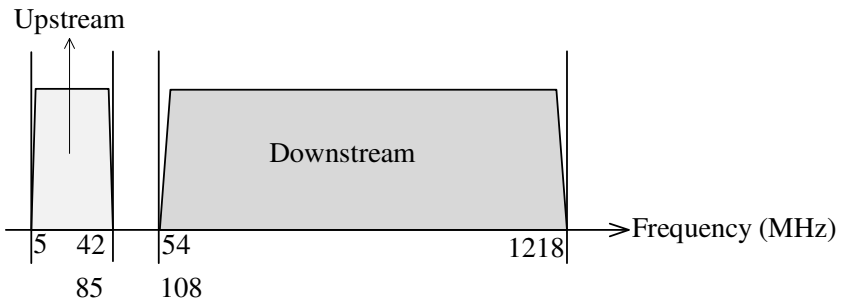

(a) DOCSIS 3.1 spectrum

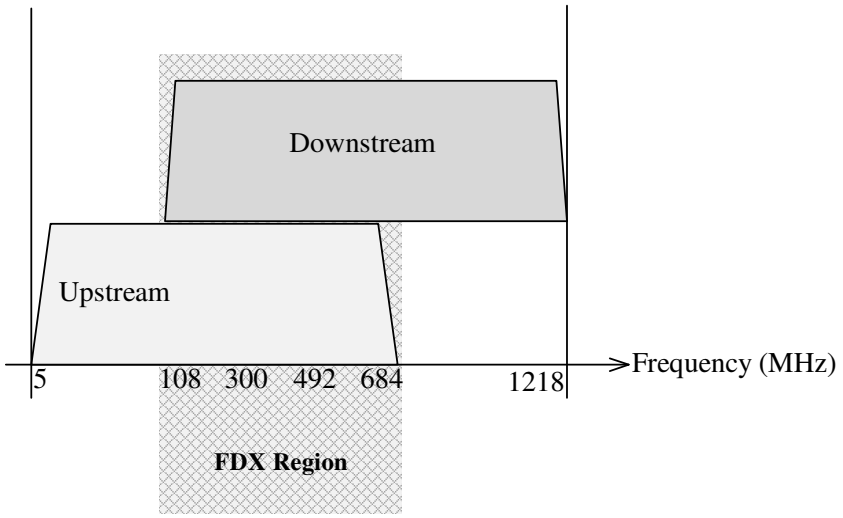

(b) DOCSIS 3.1 with FDX spectrum

Figure 1.3 The augmentation in spectrum from (a) DOCSIS 3.1 to (b) DOCSIS 3.1 with FDX.

the augmentation in the standard. Previous DOCSIS standards use a split-spectrum architecture between downstream and upstream traffic, in which there is a cross-over region between the upstream spectrum and downstream spectrum and the bandwidth available for downstream made up most of the total frequency spectrum. Full-duplex DOCSIS expands the upstream spectrum by a factor of 8 when compared to the 2013 standard and allows it to overlap with the downstream spectral region. The configurable allocated spectrum bandwidths for an FDX node can be 96 MHz, 192 MHz, 288 MHz, 384 MHz and 576 MHz, which can occupy the frequency range from 108 MHz up to 684 MHz. The expected *media access control* (MAC) data rates for the FDX node is $4-5$ *giga bits per second* (Gbps) in upstream and $9-10$ Gbps in downstream operation [4]. The significant expansion of the

upstream spectrum would allow customers to share more interactive high-resolution videos and media content, and help the CATV network to gain advantages over its competitive networks which use the *fiber to home* (FTTH) technology.

1.2 DOCSIS 3.1 with FDX

The addition of full-duplex operation adds management complexity and introduces challenges in designing transceivers over a coaxial cable to meet the demand for higher speeds of downstream and upstream traffics as well as to maintain backward compatibility with transceivers of previous DOCSIS versions.

One of the biggest challenges in designing a full-duplex transceiver is to suppress the downstream signal leakage from the receiving upstream signal due to the spectral overlap. In the FDX DOCSIS 3.1 network, the CM still operates in *frequency division duplex* mode in which on any FDX channel, the CM is either transmitting in the upstream or receiving in the downstream [4]. Thus, the full-duplex transceiver is the one residing at the CMTS.

To illustrate, the structure of a half-duplex DOCSIS transceiver node which is placed at the CMTS head-end is shown in Figure 1.4. Transforming this node into a full-duplex one would require a number of modifications which are discussed next.

In the downstream path, the transceiver takes broadcasting data packets from the upper layers of the CMTS, converts into radio frequency signals, and couples them into the coaxial cable. The upstream path is the same as the downstream path but in a reversed order, in which the transceiver gets radio frequency signals from the coaxial cable, processes and extracts data traffic and transports them to the upper layers for further processing tasks.

The downstream path begins with a *downstream medium access control* (DS MAC) block which converts data packets into appropriate symbol sequences. The *downstream physical layer* (DS PHY) block digitally modulates those symbols onto some carrier frequencies, and then converts them into analog signals using a *digital-to-analog converter* (DAC). A *low pass filter* (LPF) is applied after the DAC, which is a reconstruction filter that suppresses frequency components caused by digital sampling. A crucial component, namely a *high power*

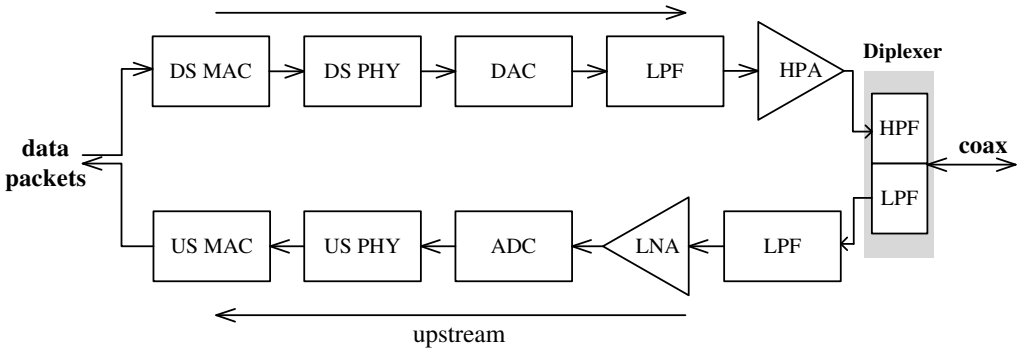

Figure 1.4 General structure of a half-duplex DOCSIS node.

amplifier (HPA) is then used to amplify the power of the RF signal to some level, which conforms with the specifications in DOCSIS 3.1. The final component in the downstream path is a *diplexer*, which performs the final spectral shaping of the signal before it goes through the coax to subscribers' modems. It is the diplexer which enables the half-duplex operations of the transceiver.

The diplexer is basically a combination of two RF filters, a low-pass filter (LPF) and a high-pass filter (HPF). The LPF and HPF have responses such that they allow only one type of streaming signal, either downstream signal or upstream signal, transporting through while effectively removing the other. Figure 1.5 illustrates the frequency responses of these filters. The filters would have a high attenuation in the stop-band region so as to suppress most of the high-power downstream and prevent it from leaking into the upstream signal. This means that only one type of signal can be transmitted over a specified spectrum at a time.

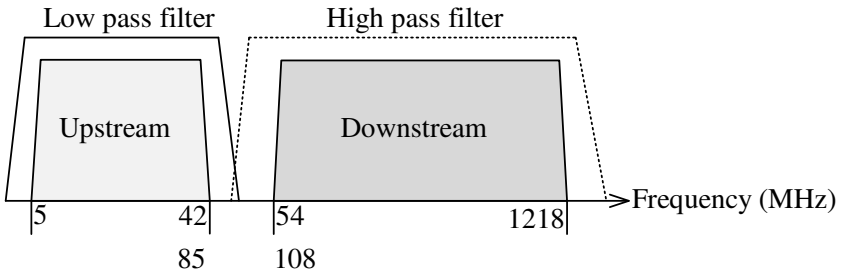

Figure 1.5 Filter responses of a diplexer used in a half-duplex DOCSIS transceiver.

Regarding the upstream path, the low-pass filtered upstream signal first goes to the *low noise amplifier* (LNA) to boost its signal level, and is converted into digital samples by an *analog-to-digital converter* (ADC). The next blocks are *upstream physical layer* (US PHY) and *upstream medium access control* (US MAC), which process the digital samples further to bring the upstream traffic to higher processing levels in the CMTS. Intuitively, a half-duplex node can be viewed as a pair of a downstream transmitter and an upstream receiver that operate on a split spectrum and are combined by the diplexer.

To allow simultaneous operation of the upstream receiver and the downstream transmitter on the same frequencies, the diplexer must be replaced by a *hybrid coupler* (HC). This device has three ports , namely TX, RX and T/R, in which, two of them (TX and RX) are single direction ports used to transmit or receive radio frequency signals, respectively. A remaining port (T/R) is bidirectional and utilized to couple with the coaxial cable. The principle of a HC is shown in Figure 1.6.

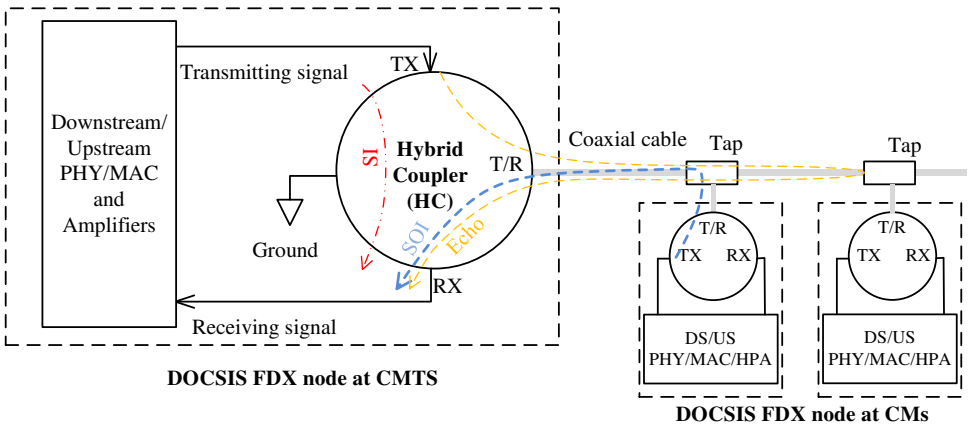

Figure 1.6 A FDX node with a hybrid coupler where RX, TX, T/R represents the receiving port, transmitting port and bidirectional port, respectively.

The downstream signal which comes into the HC's TX port would appear on the bidirectional port with a small degradation in power. Because of the imperfection of an isolation between the TX port and the RX port, some portion of the transmit signal leaks into the receiving port. This leakage is referred to as a *self interference* (SI).

On the other hand, the upstream signal from subcribers' CMs traverses through the coaxial cable, comes into the bidirectional port and appears at the receiving port, which is the so-called *signal of interest* (SOI). Due to the HC's imperfection, the TX port also experiences some fraction of the receiving upstream signal. However, since the upstream signal has been transmitted from the subscriber's CM with a lower power than the power of the CMTS passed through a number of taps along the coaxial cable, the receive signal which appears at the head-end's T/R port would be considerably smaller in power when compared to the downstream signal coming in the head-end's TX port.

Besides, due to the mismatch between the input impedance of the HC and the channel's characteristic impedance, there are multiple copies of the downstream transmit signal that has reached taps along the coaxial channel and reflected back to the source, which are often referred to as *echoes* [4].

Overall, the received signal coming out from the HC's RX port consists of three components: SOI, SI and echoes, which is illustrated in Figure 1.6. Comparing the power levels of these three components, the SI signal is the strongest component. The second largest component is made up of echoes. The challenging part of the FDX operation is to be able to suppress as much as possible the SI and the echoes from the signal of interest, i.e., the upstream signal. SI suppression and echo cancellation therefore become the most important tasks in enabling the FDX technology, which is also a very active research area in wireless communications [6].

1.3 Motivation

Adding full-duplex capability into a half-duplex DOCSIS 3.1 system will increase the amount of power needed in the nodes. The main reason for this has to do with the 4-wire to 2-wire interface that connects the nodes to the coaxial cables. As explained before, the full-duplex capable system uses a hybrid in place of the diplexer and unfortunately the insertion loss of the hybrid, which is approximately 3.5 dB, is about 3 dB more than that of the

diplexer[1]. To compensate for the increased insertion loss, the output of the HPA must be about 3 dB higher.

The power supplied to the transceiver nodes in a DOCSIS system is limited by the existing HFC infrastructure. Since incorporating FDX into the node requires extra power, either the infrastructure could be upgraded to supply more power or the signal power delivered to the cable plant could be reduced. Changing the infrastructure is impractical and reducing the signal power would come at a cost since more nodes would be needed. Unfortunately, reducing the signal power is not an option as it would not maintain backward compatibility with the half-duplex version. This is to say that the only practical alternative is to somehow reduce the power consumption in the node. This could possibly be done by making the HPA more efficient.

The minimum voltage level that can be used to supply the HPA is determined by the maximum value of the output signal. Therefore, reducing the maximum value of the output signal will allow the voltage supply to be reduced and thereby increase the efficiency of the HPA.

The objective of this thesis is to explore the possibility of reducing the maximum value of signals transmitted in the downstream of DOCSIS 3.1 systems by at least 3 dB. In other words, the objective of this thesis is to reduce the peak-to-average power ratio (i.e., the maximum-to-average ratio) of DOCSIS 3.1 downstream signals by at least 3 dB.

1.4 Scope of the Thesis

The transmit signals in multi-carrier OFDM systems exhibit higher peak values in the time domain when compared to the transmit signals in single-carrier systems since many subcarrier components are combined (added) simultaneously. Therefore, OFDM signals are known to have a high *peak to average power ratio* (PAPR) [2]. High peaks encountered in the time domain signal cause detrimental effects to the performance of the power amplifier

[1]Macom's hybrid coupler MAPD-009918-C209C0 [7] and Macom's diplexer MAEL-007988-CD0550 [8] have insertion losses of 3.5 dB and 0.5 dB, respectively.

in the OFDM system. This is due to the limited linear working region of the PA where any peaks present in the signal can drive it into saturation. Forcing the amplifier to work in its saturation condition causes nonlinear distortions and spectral spreading. In order to amplify the signal with less distortions, the PA is required to have some *input back off* (IBO) which shifts the operating point towards the linear region where the PA creates the output signal with less power. Ideally, the IBO is chosen to be equal to the PAPR of the OFDM signal. However, this negatively affects the power efficiency of the whole system. Moreover, the magnitude of the signal peaks can grow proportionally to the number of subcarriers, making the dynamic range of the OFDM signal theoretically much higher than the practical limitation of the PA. Various techniques, therefore, have been proposed to reduce the PAPR of OFDM signals [2].

The objective of this thesis is to investigate possible approaches to carry out PAPR reduction for the downstream OFDM signals in a DOCSIS 3.1 system. The downstream signal is generated from the CMTS resided at the cable company's head-end and is broadcasted via coaxial cables to subscribers' CMs. The signal at the output of the downstream power amplifier consists of a number of different OFDM channels, of which the subcarriers' locations have been clearly defined in DOCSIS 3.1. The standard specifies each downstream OFDM channel must use a FFT size of 4096 (4K mode) or 8192 (8K mode). In other words, if operating in the 4K mode, each OFDM channel consists of 4096 subcarriers with a spacing between adjacent subcarriers being 50 kHz. In the 8K mode, 8192 subcarriers can be used and the spacing between adjacent subcarriers is 25 kHz.

Although different PAPR reduction algorithms are available, they cannot be easily applied to DOCSIS systems due to a number of reasons. First, the PAPR reduction can only be applied to the CMTS side and not at the CM side. This is to say that the selected methods need to satisfy the property called *downward compatibility* where the changes in the transmitter's side need not to be propagated to the receivers of the network. The demodulation operation at the OFDM receivers must be kept unchanged, which disqualifies those techniques involving changing the order of data sequences or adding more information to the receiver's side. Second, the chosen PAPR reduction algorithms must have small

computational cost. It is required that the proposed techniques should be suitable to *field programmable gate arrays* (FPGAs). The reconfigurability of FPGA devices provides an economical solution in system design since they can be easily updated to meet changes in standards. However, they do have a limited number of logic resources, such as a number of multipliers used or the amount of *random memory access* (RAM) can be utilized. As a consequence, sophisticated algorithms requiring off-line processing techniques with a large amount of memory or optimization assistance from other third-parties will be impractical especially for real-time applications. This is to say that the processing time for each instance of the signal should be limited to some constant time duration. Most of the available PAPR reduction algorithms work in an iterative manner [2]. However, with upper bounded processing time, techniques which reduce the signal's PAPR for some undetermined number of iterations will not be permitted. Third, DOCSIS 3.1 has clearly defined spectral masks for each OFDM channel that must be conformed to in order to make the system compatible with both legacy channels and new channels released in the recent standards. This puts another constraint on the PAPR reduction techniques to be applied. The constraint is that the PAPR reduction techniques are not allowed to severely distort the transmit signal or create spectral spreading.

It is pointed out that the techniques investigated and proposed in this thesis serve as proof-of-concept rather than fully hardware implemented techniques. MATLAB is therefore used as a simulation platform to evaluate the feasibility and compare the performance of different techniques with the proposed ones.

1.5 Organization of the Thesis

This thesis has five chapters. The first chapter introduces the CATV networks and its evolutionary development from an analog transmission network into a multi-user data transmission network. The chapter then discusses DOCSIS as a de-facto standard that governs the operability of CATV network using coaxial cables and its different versions introduced over the years. The latter part of the chapter explains the challenges in data communication over coaxial cables which motivates the objective of this research.

Chapter 2 starts with some background on SC-QAM and OFDM systems. It reviews the implementation of an OFDM system using DFT/IDFT blocks and modeling the downstream OFDM signal path in the discrete time domain. Also introduced in Chapter 2 are the definition of PAPR of an OFDM signal and a *complimentary cumulative distributive function* (CCDF) curve as a tool to quantify the PAPR reduction performance. The last section of the chapter discusses the property of an HPA and its theoretical models to illustrate the effect of its limited linear range in amplifying OFDM signals.

A taxonomy of different PAPR reduction techniques is briefly overviewed in Chapter 3, in which the two main classes of PAPR reduction techniques, namely signal distortion techniques and signal distortion-less techniques, are categorized. The subsequent sections in Chapter 3 describe principles of some well-known candidates of PAPR reduction techniques for OFDM signals that have been proposed in literature.

Chapter 4 proposes two novel PAPR reduction techniques based on the principle of *tone reservation* (TR). The chapter first discusses in detail conventional TR-based PAPR reduction techniques. The last two sections of the chapter present two novel algorithms for peak reduction of OFDM signals, a time-domain algorithm and clipping-and-filtering algorithm. The performance and computational cost of the proposed techniques and the conventional techniques are compared by simulating in different scenarios. The implementation complexity in terms of numbers of multipliers and additions required per each application of the proposed algorithms and the conventional algorithms are also given.

Finally, Chapter 5 summarizes the main contributions, discusses some further research issues and concludes the thesis.

2. OFDM Signals

As discussed in Chapter 1, OFDM has been adopted in DOCSIS 3.1 to greatly improve the overall systems' throughput. The objective of this thesis is to find techniques for reducing the dynamic range of OFDM signals presented at the output of the downstream amplifiers. Therefore, this chapter will discuss a general OFDM-based communication system. Because OFDM is an extension of SC-QAM (single carrier QAM), the first section reviews the basics of QAM theory.

2.1 Single-Carrier Quadrature Amplitude Modulation (SC-QAM)

Figure 2.1 shows the major components in a transmitter and a receiver of a SC-QAM system. For simplicity, some components such as timing, frequency and phase recovery are not shown.

First, data bits are grouped into blocks where each block has λ bits and is mapped to a QAM symbol by the QAM mapping module. The number of QAM symbols is therefore $M = 2^{\lambda}$, which is also known as the *modulation order*. Each QAM symbol is represented by a complex value consisting of an in-phase (I) component and a quadrature (Q) component, denoted by $v_{\mathrm{I}}[n]$ and $v_{\mathrm{Q}}[n]$, respectively. The collection of $M-$QAM symbols $s_0, s_1, \ldots, s_{M-1}$, can be visualized on a $2-$dimensional complex plane, resulting in a diagram normally referred to as a constellation diagram. Figure 2.2 shows constellation diagrams of a binary phase shift keying (BPSK), quadrature phase shift keying (i.e., $4-$QAM), $8-$QAM and $16-$QAM, corresponding to $M = 2, M = 4, M = 8$ and $M = 16$, respectively.

The discrete sequences of I, Q symbols (i.e., $v_{\mathrm{I}}[n]$ and $v_{\mathrm{Q}}[n]$) are converted into trains of

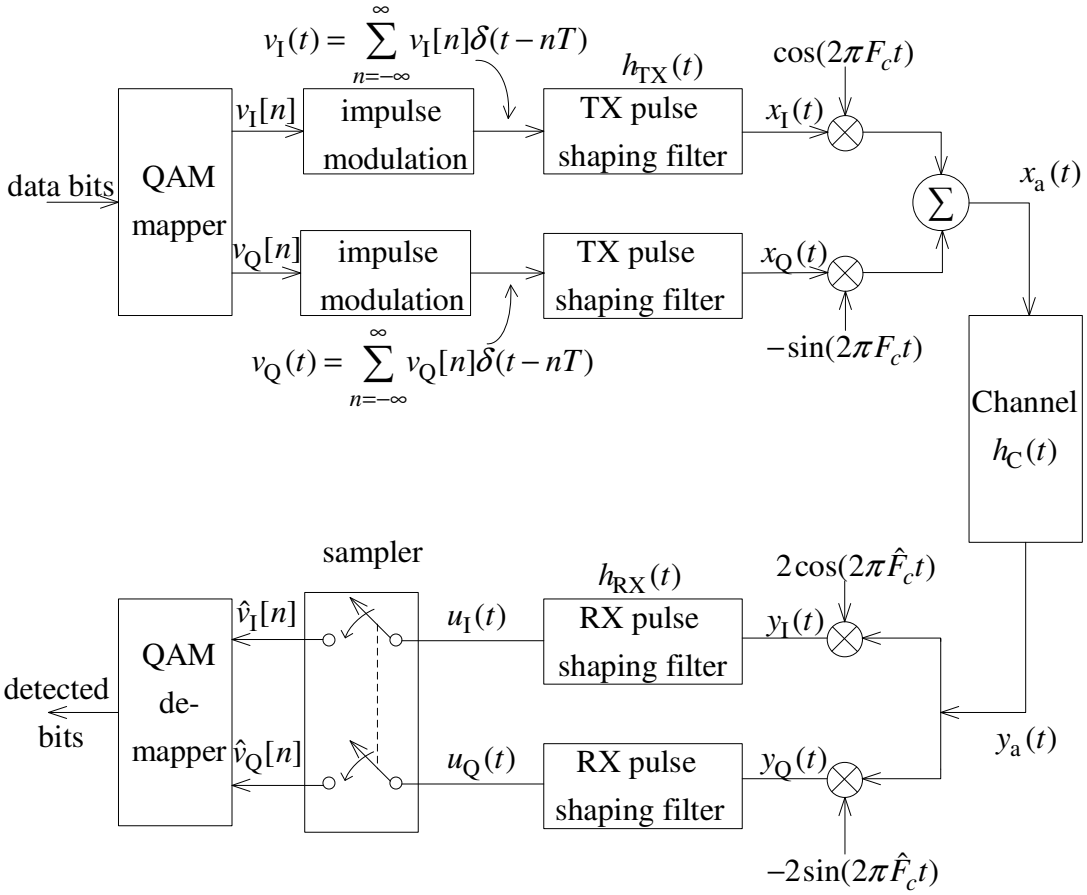

Figure 2.1 A simplified SC-QAM system.

impulses by the impulse modulators. That is:

$$\begin{aligned} v_{\mathrm{I}}(t) &= \sum_{n=-\infty}^{\infty} v_{\mathrm{I}}[n]\delta(t-nT) \\ v_{\mathrm{Q}}(t) &= \sum_{n=-\infty}^{\infty} v_{\mathrm{Q}}[n]\delta(t-nT) \end{aligned} \tag{2.1}$$

where T is the time duration of each symbol.

Next, the impulse trains are passed through a *pulse shaping filter*, $h_{\mathrm{TX}}(t)$, which is a low-pass filter that limits the bandwidth of the transmit signal to meet the spectrum mask required by transmission standards. Thus, the resulting signals are called *baseband signals*

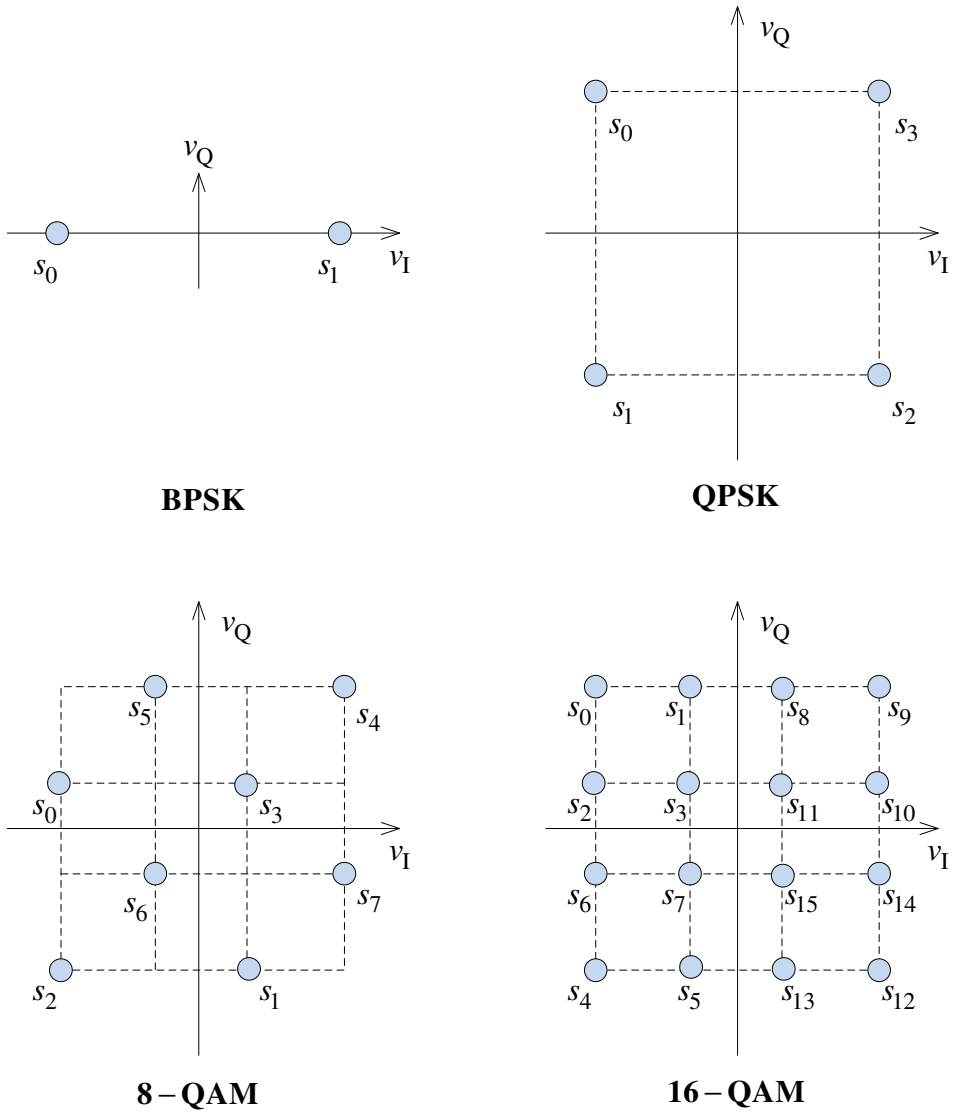

Figure 2.2 QAM symbol constellations with $M = 2$ for *binary phase shift keying* (BPSK), $M = 4$ for *quadrature phase shift keying* (QPSK), $M = 8$ for 8-QAM and $M = 16$ for 16-QAM.

and given by:

$$\begin{aligned} x_{\mathrm{I}}(t) &= v_{\mathrm{I}}(t) * h_{\mathrm{TX}}(t) = \sum_{n=-\infty}^{\infty} v_{\mathrm{I}}[n] h_{\mathrm{TX}}(t - nT) \\ x_{\mathrm{Q}}(t) &= v_{\mathrm{Q}}(t) * h_{\mathrm{TX}}(t) = \sum_{n=-\infty}^{\infty} v_{\mathrm{Q}}[n] h_{\mathrm{TX}}(t - nT) \end{aligned} \tag{2.2}$$

The baseband signals are then up converted to radio frequency F_c with a pair of sinusoidal

carriers whose phases differ by $\pi/2$ radians (i.e., quadrature carriers). The modulated signals are added together to form a passband signal $x_a(t)$, which is:

$$x_a(t) = x_{\mathrm{I}}(t)\cos(2\pi F_c t) - x_{\mathrm{Q}}(t)\sin(2\pi F_c t) \tag{2.3}$$

The RF signal $x_a(t)$ is then sent over a channel, whose impulse response is $h_{\mathrm{C}}(t)$. The received signal is:

$$y_a(t) = x_a(t) * h_{\mathrm{C}}(t) + w(t) \tag{2.4}$$

where $w(t)$ represents *additive white Gaussian noise* (AWGN).

In the simplest case, the channel is assumed to be $h_{\mathrm{C}}(t) \equiv \delta(t)$, resulting in $y_a(t) = x_a(t) + w(t)$, which is known as an AWGN channel.

At the receiver, the received RF signal is first down-converted to baseband signals using quadrate down-conversion with frequency $\hat{F}_c$. Again, it is assumed that a perfect synchronization can be established at the receiver, making $\hat{F}_c = F_c$. Ignoring AWGN $w(t)$, the down-conversion process produces:

$$\begin{aligned} y_{\mathrm{I}}(t) &= x_a(t) 2\cos(2\pi F_c(t)) \\ &= \left(x_{\mathrm{I}}(t)\cos(2\pi F_c t) - x_{\mathrm{Q}}(t)\sin(2\pi F_c t)\right) 2\cos(2\pi F_c(t)) \\ &= x_{\mathrm{I}}(t)\left(1 + \cos(4\pi F_c t)\right) - x_{\mathrm{Q}}(t)\sin(4\pi F_c t) \\ &= x_{\mathrm{I}}(t) + \underbrace{\left(\cos(4\pi F_c t)x_{\mathrm{I}}(t) - \sin(4\pi F_c t)x_{\mathrm{Q}}(t)\right)}_{\text{filtered by } h_{\mathrm{RX}}(t)} \end{aligned} \tag{2.5}$$

and

$$\begin{aligned} y_{\mathrm{Q}}(t) &= -x_a(t) 2\sin(2\pi F_c(t)) \\ &= -\left(x_{\mathrm{I}}(t)\cos(2\pi F_c t) - x_{\mathrm{Q}}(t)\sin(2\pi F_c t)\right) 2\sin(2\pi F_c(t)) \\ &= -x_{\mathrm{I}}(t)\sin(4\pi F_c t) + x_{\mathrm{Q}}(t)\left(1 - \cos(4\pi F_c t)\right) \\ &= x_{\mathrm{Q}}(t) - \underbrace{\left(\cos(4\pi F_c t)x_{\mathrm{I}}(t) + \sin(4\pi F_c t)x_{\mathrm{Q}}(t)\right)}_{\text{filtered by } h_{\mathrm{RX}}(t)} \end{aligned} \tag{2.6}$$

In equations (2.5) and (2.6), there are low frequency components and high frequency components. A low-pass filter $h_{\mathrm{RX}}(t)$ is applied to remove the high frequency components.

In practice, this filter is often chosen to be a *matched filter*, which is identical to the pulse shaping filter used at the transmitter, but in a reverse order, that is, $h_{\mathrm{RX}}(t) = h_{\mathrm{TX}}(-t)$. This filter also serves to mitigate distortions occurring in the communication channel and to maximize the *signal-to-noise ratio* (SNR) at the correct sample points [9].

Outputs of the receiving filters are baseband quadrature signals:

$$\begin{aligned} u_{\mathrm{I}}(t) = x_{\mathrm{I}}(t) * h_{\mathrm{RX}}(t) &= \sum_{n=-\infty}^{\infty} v_{\mathrm{I}}[n] h_{\mathrm{TX}}(t - nT) * h_{\mathrm{RX}}(t) \\ &= \sum_{n=-\infty}^{\infty} v_{\mathrm{I}}[n] \left(h_{\mathrm{TX}}(t - nT) * h_{\mathrm{RX}}(t) \right) \\ &= \sum_{n=-\infty}^{\infty} v_{\mathrm{I}}[n] h_{\mathrm{TR}}(t - nT) \end{aligned}$$

where $h_{\mathrm{TR}}(t) = h_{\mathrm{TX}}(t) * h_{\mathrm{RX}}(t)$ is the impulse response of a linear system obtained by cascading $h_{\mathrm{TX}}(t)$ and $h_{\mathrm{RX}}(t)$, and:

$$u_{\mathrm{Q}}(t) = \sum_{n=-\infty}^{\infty} v_{\mathrm{Q}}[n] h_{\mathrm{TR}}(t - nT)$$

When no timing delay and noise are introduced in the signal path from the transmitter to the receiver, the sampler captures data samples after every symbol duration T. At the sampling time $t = mT$ the samplers' outputs are:

$$\begin{aligned} \hat{v}_{\mathrm{I}}[m] = u_{\mathrm{I}}(t)|_{t=mT} &= \sum_{n=-\infty}^{\infty} v_{\mathrm{I}}[n] h_{\mathrm{TR}}(mT - nT) \\ &= v_{\mathrm{I}}[m] h_{\mathrm{TR}}(0) + \underbrace{\sum_{n=-\infty, n\neq m}^{\infty} v_{\mathrm{I}}[n] h_{\mathrm{TR}}((m-n)T)}_{\text{ISI term}} \end{aligned} \tag{2.7}$$

and

$$\hat{v}_{\mathrm{Q}}[m] = u_{\mathrm{Q}}(t)|_{t=mT} = v_{\mathrm{Q}}[m] h_{\mathrm{TR}}(0) + \underbrace{\sum_{n=-\infty, n\neq m}^{\infty} v_{\mathrm{Q}}[n] h_{\mathrm{TR}}((m-n)T)}_{\text{ISI term}} \tag{2.8}$$

The second terms in Equations (2.7) and (2.8) represent *inter-symbol interference* (ISI) since the value of the current transmitting symbol is interfered by the value of symbols

transmitted in other time slots. Ideally, if the overall impulse response satisfies the condition of:

$$h_{\mathrm{TR}}(t) = \begin{cases} 1, & \text{if } t = 0 \\ \\ 0, & \text{if } t = kT \end{cases} \tag{2.9}$$

then the system will experience no ISI. The condition stated in (2.9) is therefore called a zero-ISI criterion [9]. In order to meet this criterion, the pulse shaping filter and its matched filter can be chosen as *square-root raised-cosine* (SRRC) filters. An SRRC filter has a frequency response equal to square root of the raised cosine spectrum. In other words, this means:

$$H_{\mathrm{TX}}(F) = H_{\mathrm{RX}}(F) = \sqrt{H_{\mathrm{RC}}(F)} \tag{2.10}$$

where $H_{\mathrm{TX}}(F), H_{\mathrm{RX}}(F)$ are the frequency responses of $h_{\mathrm{TX}}(t), h_{\mathrm{RX}}(t)$, respectively, and $H_{\mathrm{RC}}(F)$ is the frequency response of a raised cosine filter (or a Nyquist filter) defined as [9]:

$$H_{\mathrm{RC}}(F) = \begin{cases} 1, & \text{if } |F| \leq \frac{1-\beta}{2T} \\ \frac{1}{2}\left[1 + \cos\left(\frac{\pi T}{\beta}\left(|F| - \frac{1-\beta}{2T}\right)\right)\right], & \text{if } \frac{1-\beta}{2T} < |F| \leq \frac{1+\beta}{2T} \\ 0, & \text{otherwise} \end{cases} \tag{2.11}$$

In (2.11), β is a roll-off factor and T is the symbol period. As in (2.10) cascading two SRRC filters forms an RC filter, whose impulse response is zero at every sampling instance $t = mT$. The frequency responses and time responses of RC filters with different roll-off factors are shown in Figure 2.3 to illustrate how they meet the zero-ISI criterion.

Figure 2.4 shows an example of symbol recovery for an in-phase (I) channel using the BPSK modulation where $v_{\mathrm{I}}[n] = +1, -1$. Since no channel impairment is introduced, the sampler's output exhibits a perfect recovery of the transmit symbols.

In practice, the channel is not ideal and its imperfections cause the received signal to be distorted. The major impairments of the channel are noise, timing and frequency offsets, as well as multi-path effects. A discussion of the details of these impairments is outside the scope of this thesis, but can be found in [9] or other references on digital communication theory.

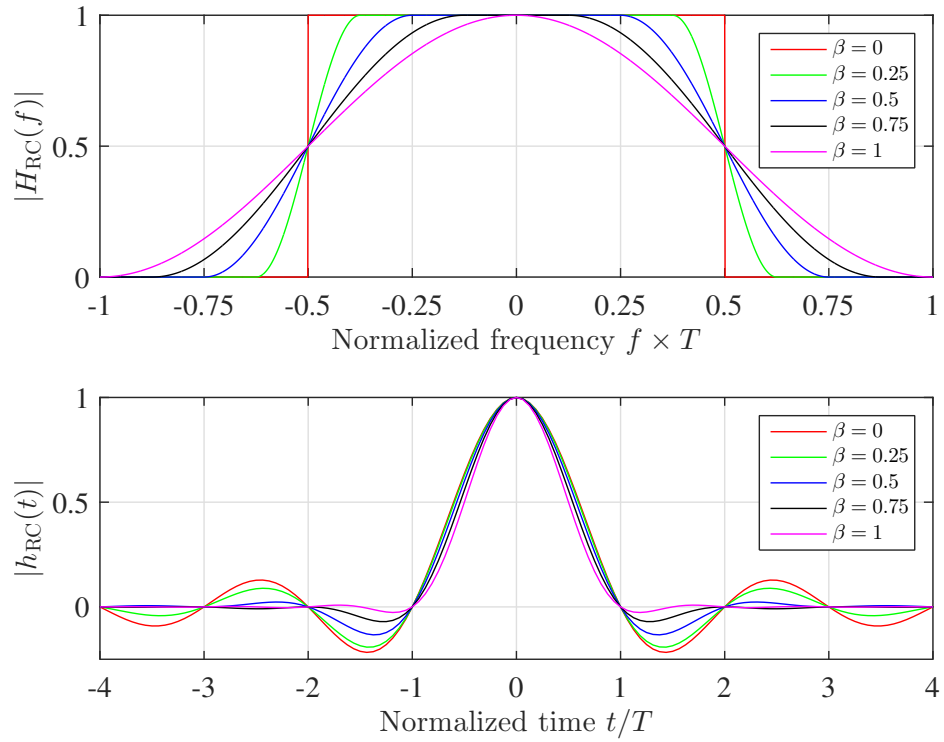

Figure 2.3 Frequency responses of RC filters with different roll-off factors and their time-domain responses that show the zero-ISI condition at sampling instances $t = mT$ for $m = \ldots, -1, 0, 1, \ldots$.

To illustrate, Figure 2.5 shows scatter plots of QAM constellations at the receiver's side being affected by different levels of noise power. Each transmit symbol is represented by a dot in the scatter plot, where the blue and red points denote the transmit and receive signal points, respectively. The dash lines in the plot show decision boundaries for each constellation point, which specify the regions used by the QAM de-mapper to recover the transmit symbols. It can be seen that while the transmit signal points are exactly located at the positions of the 16−QAM constellation, the receive points are made deviated from those constellations points because of the noise. In general, there are 16 clusters of points centered around the transmit points. When the noise power is high (or the *signal to noise ratio* (SNR) is low), there are more points that cross the decision boundaries when compared to the case with the lower noise power (or with the higher SNR). Thus, the resulting *bit-error-rate* (BER) of the system under higher noise power is higher than the BER of the system corrupted with less noise power.

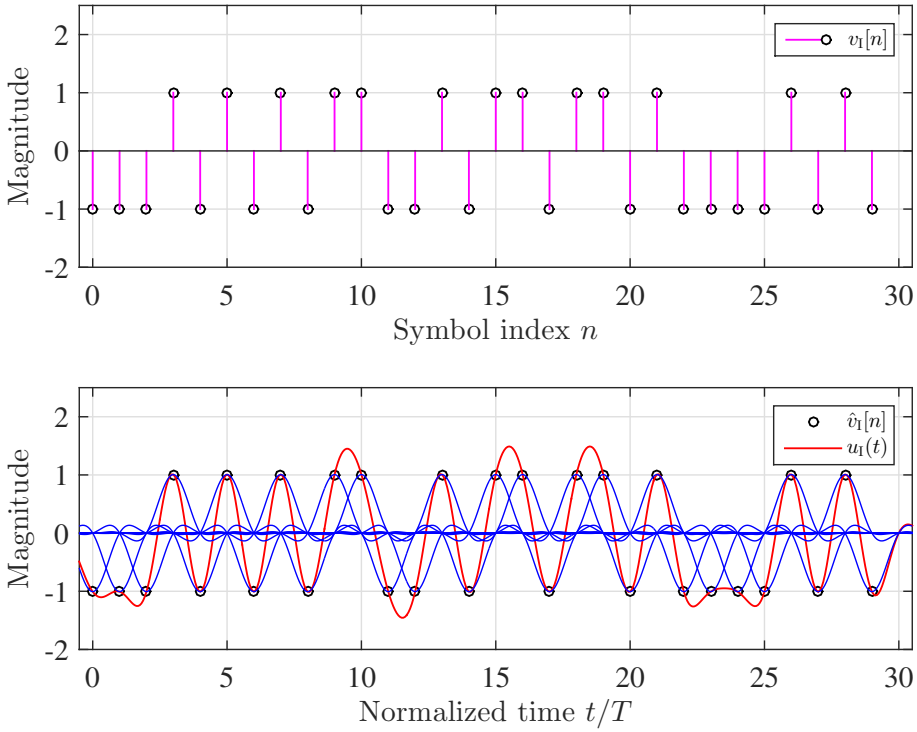

Figure 2.4 Output of the receiver's matched SRRC filter (I channel) with roll-off factor $\beta = 0.5$ using the BPSK modulation.

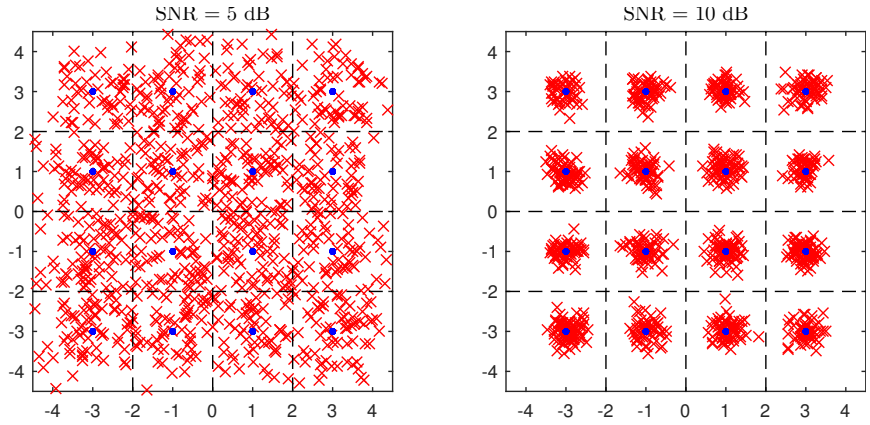

Figure 2.5 Scatter plot of 16−QAM signals under different signal-to-noise ratios, where blue and red points represent the transmit and receive signal points, respectively.

2.2 Orthogonal Frequency-Division Multiplexing (OFDM) Modulation

OFDM provides a better use of the allocated frequency bandwidth by utilizing multiple subcarriers. An OFDM system can be viewed as a combination of N SC-QAM subchannels, each centered around its own carrier frequency. The power spectrum of OFDM signals is illustrated in Figure 2.6 and a general structure of an OFDM transmitter and an OFDM receiver is shown in Figure 2.7.

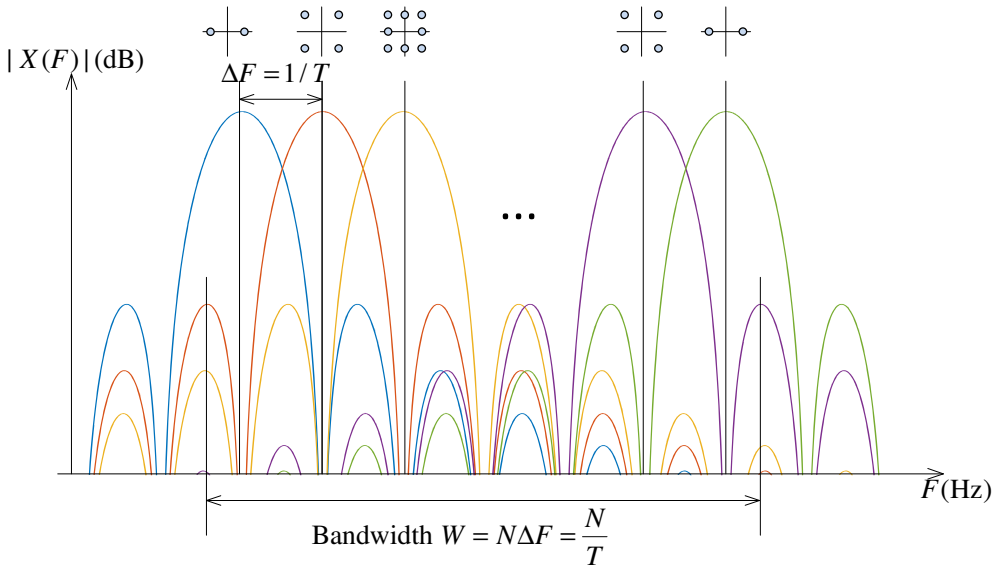

Figure 2.6 Spectrum of theoretical OFDM signals.

Let T be the duration of each OFDM symbol and $X_m[k] = I_m[k] + jQ_m[k]$ denote the QAM symbol transmitted over the kth subcarrier during the mth OFDM symbol. Then the time waveform of the mth OFDM symbol can be expressed as:

$$\begin{aligned} x_m(t) &= \sum_{k=0}^{N-1} \Re\{X_m[k]p(t)e^{j2\pi F_k t}\} \\ &= p(t)\sum_{k=0}^{N-1} [I_m[k]\cos(2\pi F_k t) - Q_m[k]\sin(2\pi F_k t)] \end{aligned} \tag{2.12}$$

where m is the symbol index, $p(t)$ is a pulse shaping filter defined within $0 \le t \le T$, and $F_0, F_1, \ldots, F_{N-1}$ are the subcarrier frequencies. To ensure the orthogonality between the subcarriers over the duration of T, the subcarriers are selected to be equally spaced with a

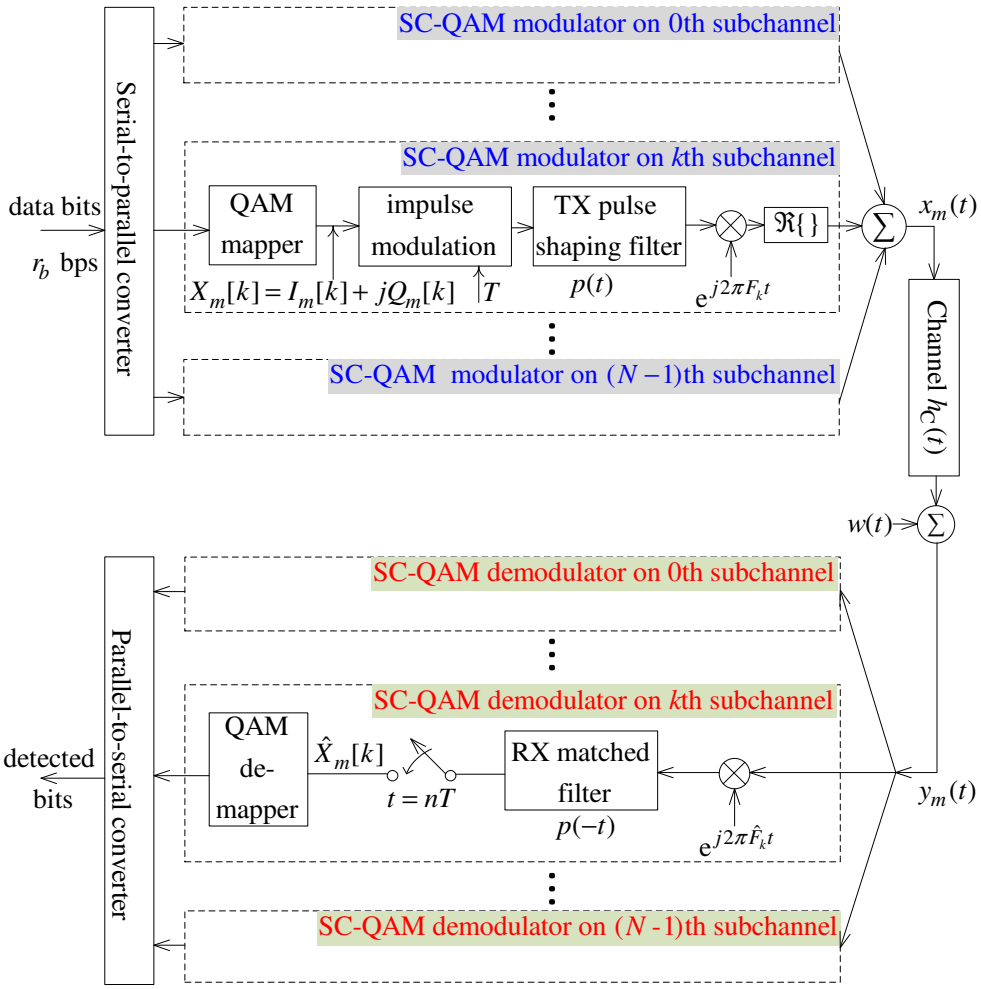

Figure 2.7 An OFDM system viewed as multiple SC-QAM modulators/demodulators [1].

spacing of $\Delta F = \frac{1}{T}$, that is $F_k = F_0 + k/T, \quad 0 \leq k \leq N-1$. If the bandwidth of each subchannel is approximated as $1/T$, the bandwidth of an OFDM signal in (2.12) is:

$$W = (N-1)\Delta F + \frac{1}{T} = (N-1)\frac{1}{T} + \frac{1}{T} = \frac{N}{T}. \tag{2.13}$$

When a pulse shaping filter is a rectangular window of unit height over the duration $[0, T]$, the spectrum of OFDM signals is a combination of the QAM signals spectra having a sinc-function shape shifted at different subcarriers as shown in Figure 2.6. Note that adjacent QAM signals overlap in frequency but are still orthogonal under the condition that their carrier frequency spacing satisfies $\Delta F = \frac{1}{T}$. The sum of these signals produces a signal

with a much wider bandwidth, approximately from $F_0 - \frac{1}{2T}$ to $F_{N-1} + \frac{1}{2T}$.

The OFDM signal is sent over a *wide band channel* $h_C(t)$ having a frequency response of $H_C(F)$. The frequency response of a wide band channel is typically *frequency-selective* as it varies over different frequency bands. The frequency selectivity of the channel is characterized by a *coherence bandwidth* of the channel, denoted by B_c [1]. In other words, B_c is the frequency bandwidth over which the channel exhibits approximately constant frequency response. The reciprocal of B_c is the *delay spread* of the channel, given by $T_m = 1/B_c$. This means, if a short pulse of duration T_p is sent over a channel with a delay spread T_m, then the received signal will have its duration roughly of $T_p + T_m$. As a consequence, if T_m is large compared to T_p, a symbol sent in a previous time duration interferes with the current symbol, which results in ISI. The bandwidth of each QAM subchannel in OFDM is $W_N = 1/T$. If this bandwidth is made smaller than the coherence bandwidth, i.e., $W_N < B_c$ or $T_m < T$, then each subchannel experiences approximately flat frequency response over its bandwidth, resulting in $T > T_m$. When this happens, the effect of ISI can be completely avoided by introducing a guard interval which is often in the form of a *cyclic prefix* (CP) [1]. The CP extension shall be discussed in the following section.

With the simplest *additive white Gaussian noise* (AWGN) channel model, the transmit signals are disturbed by noise, which is modelled as a random process $w(t)$ in Figure 2.7. The signal is then down converted to baseband, passed through a matched filter, the sampler and QAM de-mapper.

The next section elaborates on a DFT/IDFT based implementation of an OFDM system, which can effectively produce multicarrier signals using just one oscillator at the transmitter and one at the receiver. The section that comes after analyzes the signal path in the OFDM transmitter, which is the main focus of the thesis.

OFDM Implementation Using DFT/IDFT

A more effective implementation of OFDM transmitter and receiver is given in Figure 2.8. The input information bit stream is organized into N blocks using a *serial-to-parallel converter* (S/P). Each block is then input to a QAM modulator of order M_k, which pro-

duces a set of complex QAM symbols $X_m[0], X_m[1], \ldots, X_m[N-1]$. These symbols form a complex vector $\boldsymbol{X}_m = [X_m[0], X_m[1], \ldots, X_m[N-1]]^T$, which represents discrete frequency components of the mth OFDM symbol. As such, $\boldsymbol{X}_m$ is also referred to as the mth frequency symbol.

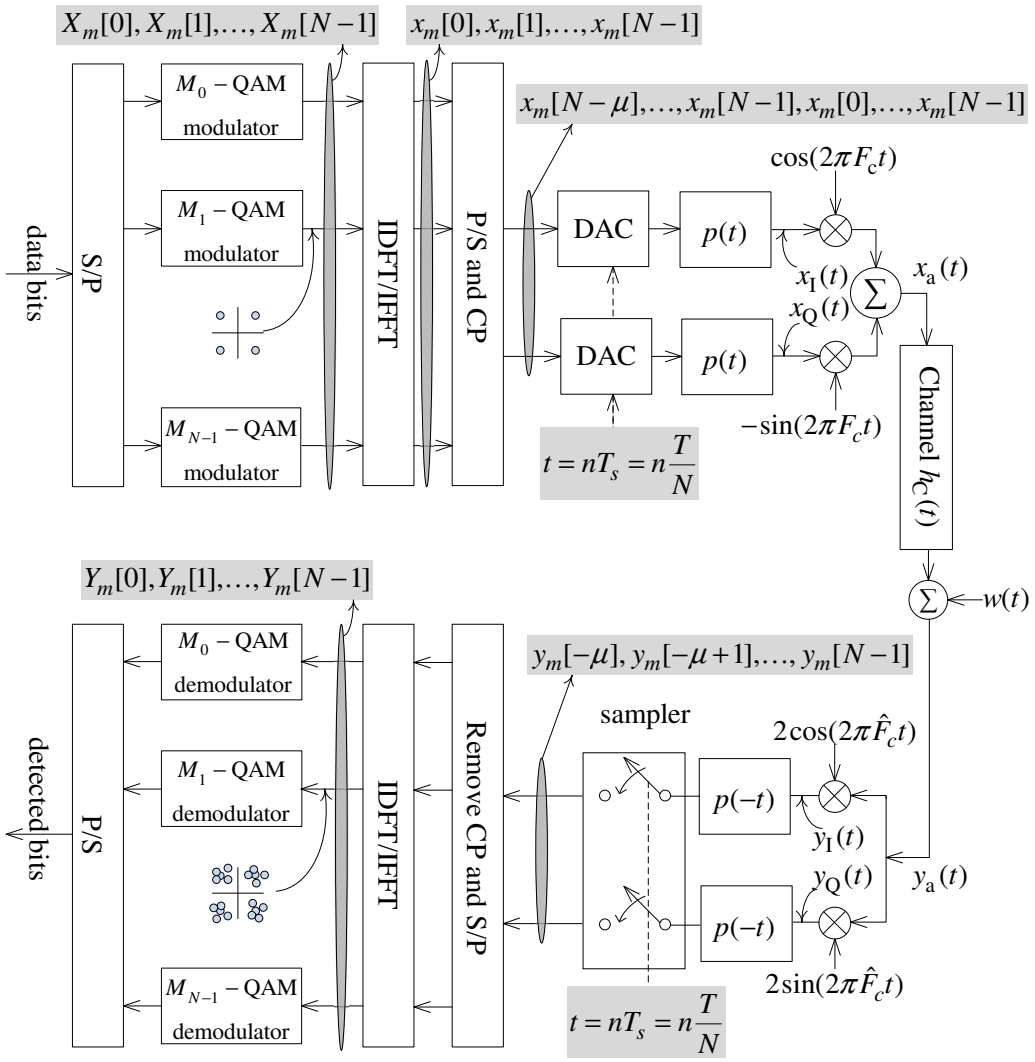

Figure 2.8 OFDM implementation using DFT/IDFT [1].

The conversion from the frequency-domain symbol into N time-domain samples is performed by an IDFT block (or IFFT if N is a power of 2). The IDFT/IFFT yields an OFDM time-domain symbol represented as a complex-valued vector $\boldsymbol{x}_m = [x_m[0], \ldots, x_m[N-1]]^T$,

where:

$$x_m[n] = \frac{1}{\sqrt{N}} \sum_{k=0}^{N-1} X_m[k] \mathrm{e}^{j2\pi kn/N}, \quad n = 0, 1, \ldots, N-1 \tag{2.14}$$

Next, a *cylic prefix* (CP) extension is performed on the symbol by duplicating the last μ samples and appending those samples to the beginning of $\boldsymbol{x}_m$. This yields a prolonged vector of time samples:

$$\boldsymbol{x}_m^{(\mathrm{CP})} = \Big[\underbrace{x_m[N-\mu], \ldots, x_m[N-1]}_{\text{CP extension}}, x_m[0], \ldots, x_m[N-1] \Big]^T \tag{2.15}$$

This extension is illustrated in Figure 2.9.

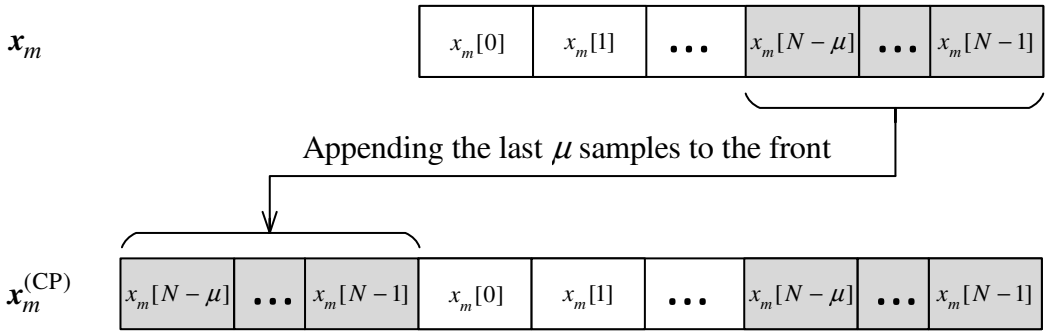

Figure 2.9 CP extension prolongs the mth OFDM symbol $\boldsymbol{x}_m$ into $\boldsymbol{x}_m^{(\mathrm{CP})}$.

Note that the duration between two adjacent time samples is $T_s = T/N$. So the length of CP in its continuous-time domain is $T_{\mathrm{CP}} = \mu T_s = \mu T/N$. The purpose of this extension is to mitigate the delay spread causing ISI when receiving the data signal from a wide-band channel as discussed in the previous section.

After having extended with a CP, the complex sequence $\boldsymbol{x}_m^{(\mathrm{CP})}$ is converted into a pair of analog signals using *digital-to-analog converters* (DACs), and then passed through pulse shaping filters. Since OFDM time samples are transmitted sequentially, the output of the *P/S and CP* block in Figure 2.8 is a discrete-time signal:

$$x^{(\mathrm{CP})}[n] = \sum_{m=-\infty}^{\infty} x_m^{(\mathrm{CP})}[n] * \delta[n - m(N+\mu)] = \sum_{m=-\infty}^{\infty} x_m^{(\mathrm{CP})}[n - m(N+\mu)] \tag{2.16}$$

where for any integer m: $x_m^{(\mathrm{CP})}[n] = 0$ if $n \notin [-\mu, N-1]$.

Two identical filters are applied to the complex signals to produce a pair of *baseband quadrature* OFDM signals.

$$\begin{aligned} x_{\mathrm{I}}(t) &= \left[\sum_{n=-\infty}^{\infty} \Re\{x^{(\mathrm{CP})}[n]\} h_{\mathrm{DAC}}\left(t - nT_s\right) \right] * p(t) \\ x_{\mathrm{Q}}(t) &= \left[\sum_{n=-\infty}^{\infty} \Im\{x^{(\mathrm{CP})}[n]\} h_{\mathrm{DAC}}\left(t - nT_s\right) \right] * p(t) \end{aligned} \tag{2.17}$$

where $h_{\mathrm{DAC}}(t)$ represents the DAC response and its reconstruction filter, and $p(t)$ is the pulse shaping filter. The baseband signals are then upconverted to a carrier frequency F_c as:

$$x_{\mathrm{a}}(t) = x_{\mathrm{I}}(t)\cos(2\pi F_c t) - x_{\mathrm{Q}}(t)\sin(2\pi F_c t) \tag{2.18}$$

The transmit signal is filtered by the channel impulse response $h_{\mathrm{C}}(t)$ and corrupted by additive white Gaussian noise $w(t)$, forming a received analog signal as $y_{\mathrm{a}}(t) = x_{\mathrm{a}}(t) * h_{\mathrm{C}}(t) + w(t)$. The next steps in the receiver are down-conversion, matched filtering, and sampling at T_s to produce a complex sequence

$$\boldsymbol{y}_m^{(\mathrm{CP})} = \left[y_m[-\mu], \ldots, y_m[-1], y_m[0], \ldots, y_m[N-1] \right]^T .$$

The sequence then has its μ prefix samples removed and is converted back to the frequency domain using a DFT or FFT block. The obtained frequency symbols are input to the corresponding QAM demodulator to recover the transmitted data.

This section discussed an efficient OFDM implementation which decomposes the wideband channel $H_{\mathrm{C}}(F)$ into a set of narrowband orthogonal subchannels with different QAM modulation over each subchannel. The following section elaborates on a practical implementation of the OFDM transmitter, which is relevant to the PAPR problem.

Practical Implementation of an OFDM Transmitter

In practical OFDM applications, baseband OFDM signals are typically generated in the discrete-time domain, whereas the upconversion to a carrier frequency F_c can then be done either before or after the DAC. The block diagram of an OFDM transmitter to generate baseband signals is shown in Figure 2.10.

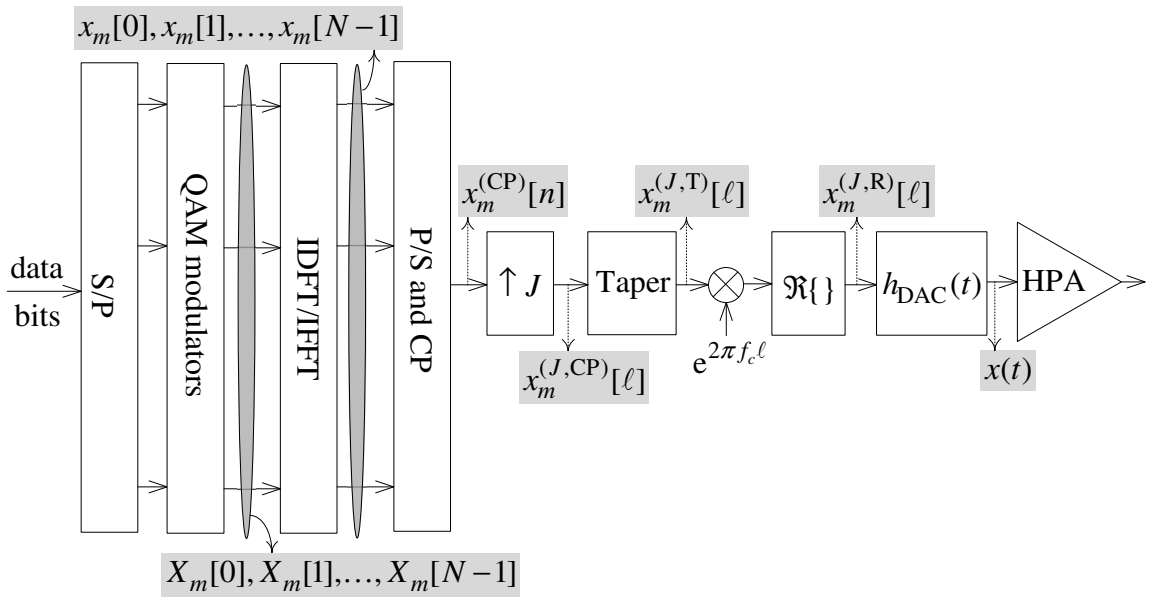

Figure 2.10 Block diagram of an OFDM transmitter.

The time samples of the mth OFDM symbol after the IDFT/IFFT block in (2.14) can be rewritten as:

$$x_m[n] = \frac{1}{\sqrt{N}} \sum_{k=0}^{N-1} X_m[k] \mathrm{e}^{j2\pi kn/N} w_N[n] \tag{2.19}$$

where $w_N[n]$ is a discrete-time rectangular window of unit height over the interval $[0, N-1]$. With the introduction of $w_N[n]$ and thanks to the cyclic property of the exponential sum, the symbol with a CP extension given in (2.15) can be expressed in formula as:

$$x_m^{(\mathrm{CP})}[n] = \frac{1}{\sqrt{N}} \sum_{k=0}^{N-1} X_m[k] \mathrm{e}^{j2\pi kn/N} w_{N+\mu}^{(\mathrm{CP})}[n] \tag{2.20}$$

where $w_{N+\mu}^{(\mathrm{CP})}[n]$ is a unit-height rectangular window defined over $[-\mu, N-1]$. If these time samples are transmitted sequentially, the infinite length sequence of time samples can be described by:

$$x^{(\mathrm{CP})}[n] = \sum_{m=-\infty}^{\infty} x_m^{(\mathrm{CP})}\left[n - m(N+\mu)\right] \tag{2.21}$$

It can be easily seen that $x^{(\mathrm{CP})}[n]$ is not band-limited due to the sinc-shape spectrum introduced by the windowing operation of $w_{N+\mu}^{(\mathrm{CP})}[n]$.

Oversampling by a factor of J is normally required in a practical OFDM transmitter. The notation $x_m^{(J)}[\ell]$ is then used to denote an oversampled sequence of $x_m[n]$ as shown in Figure

2.11. If the original sequence $x_m[n]$ has a length of N, the J-times oversampled sequence $x_m^{(J)}[\ell]$ has a length of JN.

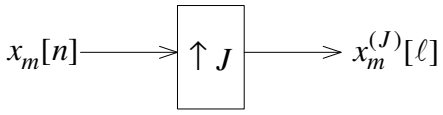

Figure 2.11 Illustration of a J-times up-sampler.

There might be different approaches to obtain an oversampled version of $x[n]$. One approach is to pad $(J-1)N$ zero values in the middle of its frequency symbol $\boldsymbol{X}_m$ to obtain:

$$\begin{aligned}\boldsymbol{X}_m^{(\mathbf{0})} &= \left[X_m^{(\mathbf{0})}[0], \ldots, X_m^{(\mathbf{0})}[JN-1]\right]^T \\ &= \left[X_m[0], \ldots, X_m[\frac{N}{2}-1], \underbrace{0, \ldots, 0}_{(J-1)N}, X_m[\frac{N}{2}], \ldots, X_m[N-1]\right]^T\end{aligned} \tag{2.22}$$

Then performing a length-JN IDFT/IFFT operation on the padded frequency symbol $\boldsymbol{X}_m^{(\mathbf{0})}$ produces $x_m^{(J)}[\ell]$ for $0 \leq \ell \leq JN-1$. An example of an up-sampler with $J=2$ is shown in Figure 2.12.

The oversampled signal $\boldsymbol{x}_m^{(J)} = \left[x_m^{(J)}[0], \ldots, x_m^{(J)}[NJ-1]\right]$ is thus:

$$\begin{aligned}x_m^{(J)}[\ell] &= \frac{1}{\sqrt{JN}} \sum_{k=0}^{JN-1} X_m^{(\mathbf{0})}[k] \mathrm{e}^{j2\pi k\ell/JN} w_{JN}[\ell] \\ &= \frac{w_{JN}[\ell]}{\sqrt{JN}} \left(\sum_{k=0}^{\frac{N}{2}-1} X_m[k] \mathrm{e}^{j2\pi k\ell/JN} + \sum_{k=JN-\frac{N}{2}}^{JN-1} X_m[k-J(N-1)] \mathrm{e}^{j2\pi k\ell/JN} \right) \\ &= \frac{w_{JN}[\ell]}{\sqrt{JN}} \sum_{k=-\frac{N}{2}}^{\frac{N}{2}-1} X_m[k] \mathrm{e}^{j2\pi k\ell/JN}\end{aligned} \tag{2.23}$$

where $w_{JN}[\ell]$ is a window of unit height over $[0, JN-1]$. The signal is then CP extended,

$$x_m^{(J,\mathrm{CP})}[\ell] = \frac{w_{JN+J\mu}^{(\mathrm{CP})}[\ell]}{\sqrt{JN}} \sum_{k=-\frac{N}{2}}^{\frac{N}{2}-1} X_m[k] \mathrm{e}^{j2\pi k\ell/JN} \tag{2.24}$$

with $w_{JN+J\mu}^{(\mathrm{CP})}[\ell]$ a unit-height window over $[-J\mu, JN-1]$. The resulting infinite-length sequence of time samples is then:

$$x^{(J,\mathrm{CP})}[\ell] = \sum_{m=-\infty}^{+\infty} x_m^{(J,\mathrm{CP})}\left[\ell - m(NJ+J\mu)\right]. \tag{2.25}$$

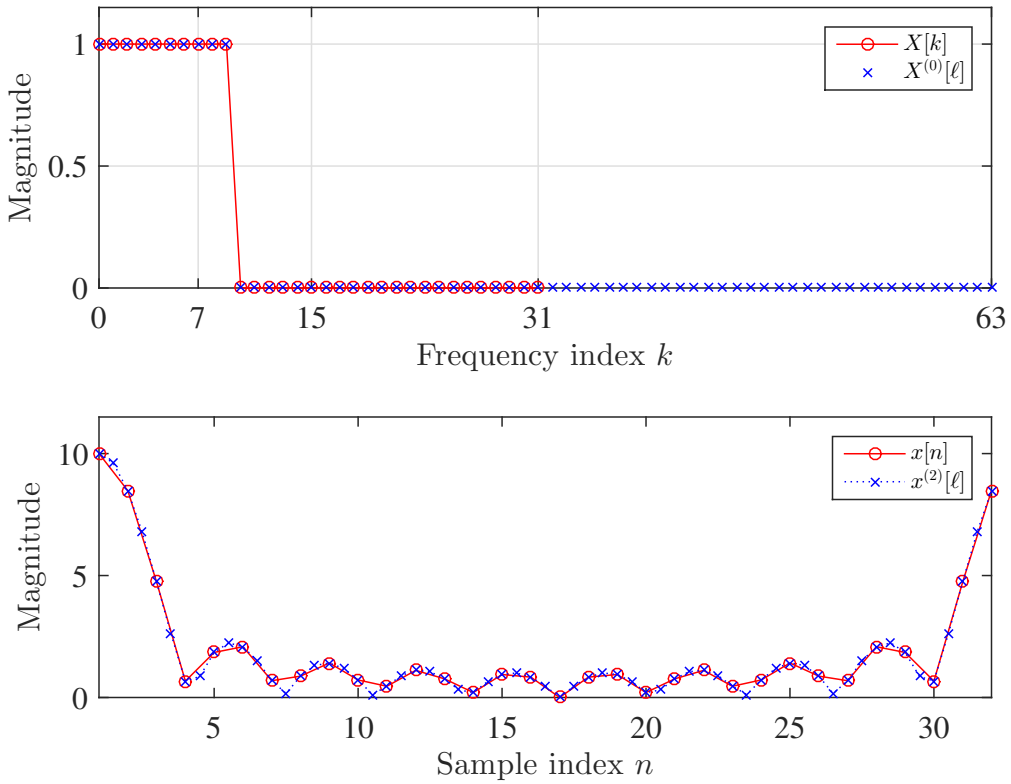

Figure 2.12 A 2-times (i.e., $J = 2$) upsample sequence obtained by zero padding a frequency symbol and perform IDFT: $N = 32$ subcarriers.

Windowing and Tapering OFDM Symbols

It is very common that communication standards, such as DOCSIS 3.1 [4], require that the transmit signals conform to some spectral masks, in which the out-of-band spectral emissions are not allowed to be above some threshold. This is mandatory for OFDM applications to share the broadband spectrum with other modulation schemes or to allow multiple OFDM transmitters/receivers simultaneously operate. This is why pulse-shaping filters are applied to help sharpen the edges of the spectrum of the transmitting signal. However the application of pulse shaping filters can cause the OFDM signal to lose the orthogonality between subcarriers if care is not taken. In DOCSIS 3.1, the shaping is implemented by appending $x_m^{(J,\mathrm{CP})}[\ell]$ with $J\beta$ samples at the beginning and tapering on its start and end with a shaping function $w^{(\mathrm{T})}_{JN+J\beta+J\mu}[\ell]$. The tapered signal is given by:

$$x_m^{(J,\mathrm{T})}[\ell] = \frac{w^{(\mathrm{T})}_{JN+J\beta+J\mu}[\ell]}{\sqrt{JN}} \sum_{k=-\frac{N}{2}}^{\frac{N}{2}-1} X_m[k] \mathrm{e}^{j2\pi k\ell/JN} \tag{2.26}$$

where $w^{(\mathrm{T})}_{JN+J\beta+J\mu}[\ell]$ is the taper window of length $(NJ + J\beta + J\mu)$ defined over $[-J\mu, JN + J\beta]$. A pulse shaping window function is also called a taper window since it tapers off the two endings of length $J\beta/2$ samples of the symbol. The CP extending and tapering operations are illustrated in Figure 2.13.

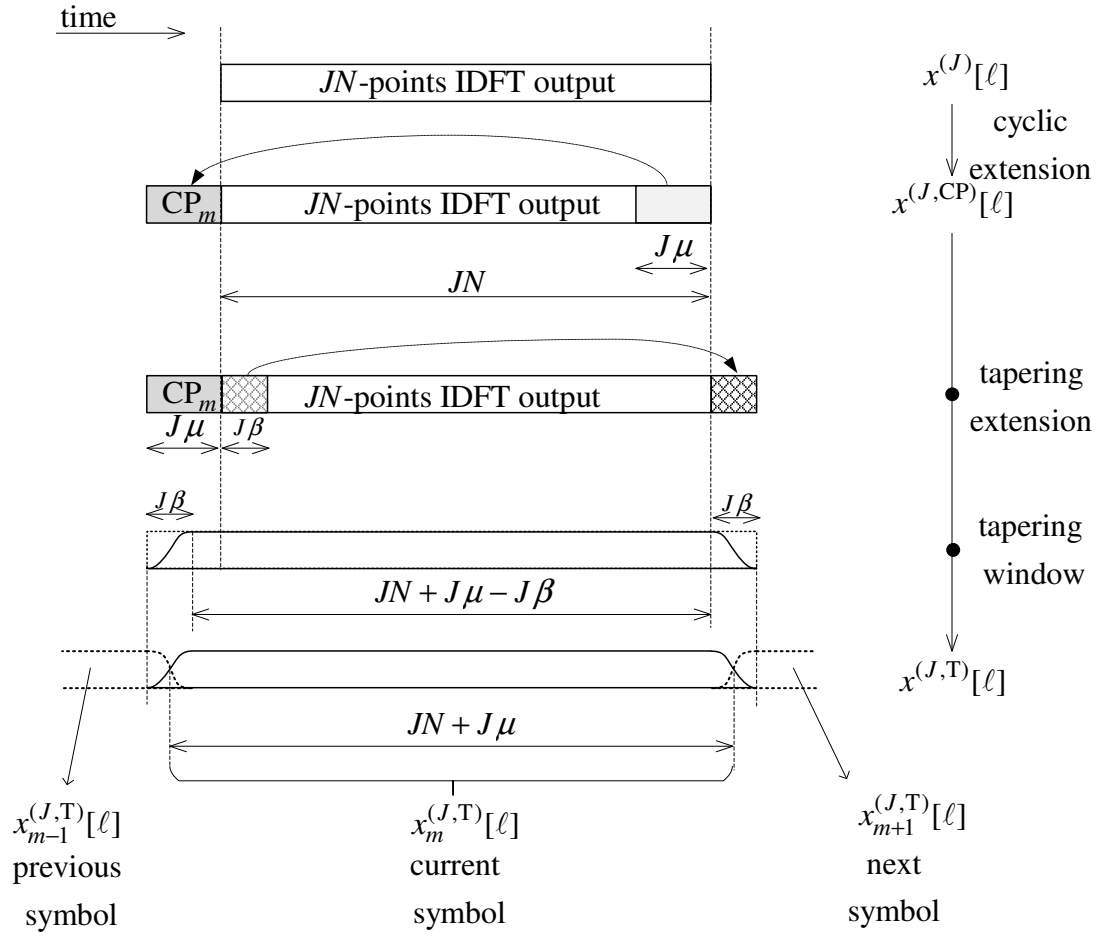

Figure 2.13 *Cylic prefix* extension and *tapering* of the mth OFDM symbol.

The infinite time-domain tapered signal is then:

$$x^{(J,\mathrm{T})}[\ell] = \sum_{m=-\infty}^{+\infty} x_m^{(J,\mathrm{T})}\left[\ell - m(NJ + J\mu + J\beta/2)\right]. \tag{2.27}$$

With the tapered endings, each symbol is overlapped by $J\beta/2$ samples and added with the tapered beginning samples of the next symbol, which is illustrated in Figure 2.14.

The tapering window can be implemented using a raised cosine (RC) window. Let $p[n]$,

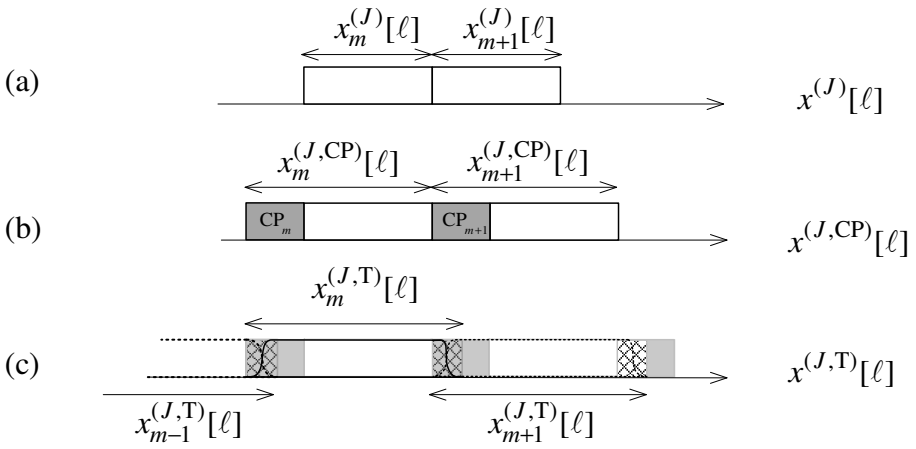

Figure 2.14 Continuous stream of OFDM symbols (a) Without cyclic prefix (b) With cyclic prefix (c) With cyclic prefix and tapering.

$0 \leq n \leq N+\beta+\mu-1$, be the RC window coefficients, specified as [4]:

$$p\left[i+\frac{N+\mu+\beta}{2}\right] = \begin{cases} 1, & i = 0,1,\ldots,\frac{N+\mu-\beta}{2}-1 \\ \frac{1}{2}\left[1-\sin\left(\frac{\pi}{\beta}\left(i-\frac{N+\mu}{2}+\frac{1}{2}\right)\right)\right] & i = \frac{N+\mu-\beta}{2},\ldots,\frac{N+\mu+\beta}{2}-1 \end{cases} \tag{2.28}$$

Then the corresponding tapering window before oversampling is

$$w_{N+\mu+\beta}^{(\mathrm{T})}[n] = p[n+\mu], \quad -\mu \leq n \leq N+\beta-1 \tag{2.29}$$

From (2.29), the oversampled $w_{JN+J\beta+J\mu}^{(\mathrm{T})}[\ell]$, $-J\mu \leq \ell \leq JN+J\beta-1$ can be obtained, which results in CP length of $J\mu$ and a tapering extension of $J\beta$. The *roll-off parameter* of the RC window is defined as:

$$\alpha = \frac{J\beta}{JN+J\mu} = \frac{\beta}{N+\mu} \tag{2.30}$$

As seen in (2.30), α does not depend on the value of J. In addition, different values of α affect the sharpness of the output spectra. This is illustrated in Figure 2.15 where the *power spectral density* (PSD) of the OFDM signals becomes sharper with larger values of the roll-off factor.

The upconversion in (2.18) is realized in the discrete-time domain by multiplying the complex sequence $x^{(J,\mathrm{T})}[\ell]$ with a complex sinusoid $\mathrm{e}^{j2\pi f_c \ell}$ and then taking the real component

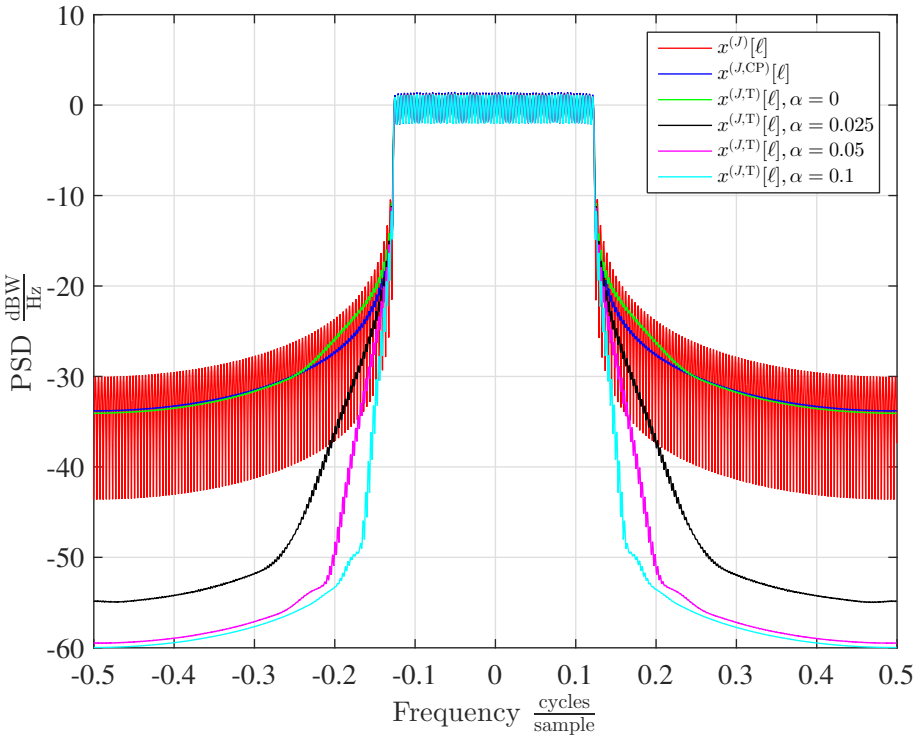

Figure 2.15 Power spectral density of OFDM signals with $N = 64, M = 16, J = 4, \mu = 16$ and a raised cosine window of different roll-off factors: $\alpha = 0, 0.025, 0.05, 0.1$.

of the result. Note that f_c is connected to the carrier frequency F_c in (2.18) by

$$f_c = \frac{F_c}{F_s}$$

where F_s is the sampling frequency. Because of oversampling, the duration between two adjacent time samples is

$$T_s^{(J)} = \frac{T_s}{J} = \frac{T}{NJ},$$

which results in

$$F_s = \frac{1}{T_s^{(J)}} = \frac{NJ}{T}.$$

The passband discrete-time signal is thus:

$$\begin{aligned} x^{(J,\mathrm{R})}[\ell] &= \Re\{x^{(J,\mathrm{T})}[\ell] \mathrm{e}^{j2\pi f_c \ell}\} \\ &= \Re\{x^{(J,\mathrm{T})}[\ell]\} \cos(2\pi f_c \ell) - \Im\{x^{(J,\mathrm{T})}[\ell]\} \sin(2\pi f_c \ell) \\ &= x_{\mathrm{I}}^{(J,\mathrm{T})}[\ell] \cos(2\pi f_c \ell) - x_{\mathrm{Q}}^{(J,\mathrm{T})}[\ell] \sin(2\pi f_c \ell) \end{aligned} \tag{2.31}$$

where $x_{\mathrm{I}}^{(J,\mathrm{T})}[\ell] = \Re\{x^{(J,\mathrm{T})}[\ell]\}$ and $x_{\mathrm{Q}}^{(J,\mathrm{T})}[\ell] = \Im\{x^{(J,\mathrm{T})}[\ell]\}$.

The real discrete-time signal is then fed into a DAC to produce the continuous time signal $x(t)$

$$x(t) = \sum_{\ell=-\infty}^{\infty} x^{(J,\mathrm{R})}[\ell]\, h_{\mathrm{DAC}}\left(t - \ell T_s^{(J)}\right) \tag{2.32}$$

where $h_{\mathrm{DAC}}(t)$ represents the DAC response which incorporates a sample-and-hold filter and a reconstruction filter.

The final stage in Figure 2.10 is denoted by a HPA block, which is a *high power amplifier* that amplifies the OFDM signal before it is sent over the physical channel. The characteristics and effects of HPA will be discussed in more detail in Section 2.4.

2.3 Peak-to-Average Power Ratio (PAPR)

The dynamic range of OFDM signals poses a major concern in the system design. Due to the nature of multicarrier signals, the resulting time waveform can have a very high peak in the instantaneous power with respect to the average power. This high ratio between the peak power and the average power, called the *peak-to-average power ratio* (PAPR), causes significant in-band distortion and out-of-band radiation when the signal passes through a nonlinear device such as a power amplifier.

The PAPR of the analog OFDM signal $x(t)$ is evaluated over a symbol interval T as

$$\mathrm{PAPR}_{\mathrm{C}}(x(t)) = \frac{\max_{0\le t\le T} |x(t)|^2}{E\{|x(t)|^2\}} \tag{2.33}$$

where $\max_{0\le t\le T} |x(t)|^2$ denotes the maximum symbol-wise instantaneous power, and $E\{|x(t)|^2\}$ is the average power of the OFDM signal $x(t)$.

The definition given in (2.33) is difficult to use in a practical system. Instead, the measurement is typically done using discrete time samples. The PAPR defined using discrete time samples of $x(t)$ is given by:

$$\mathrm{PAPR}_{\mathrm{D}}(x[\ell]) = \frac{\max_{0\le \ell\le NJ-1} |x[\ell]|^2}{E\{|x[\ell]|^2\}} \tag{2.34}$$

The discrete time signal $x[\ell]$ in (2.34) can be $x^{(J,\mathrm{CP})}[\ell]$, $x^{(J,\mathrm{T})}[\ell]$ or $x^{(J,\mathrm{R})}[\ell]$ as described in Figure 2.10.

There is a well-known result established in [10], which states that the minimum value of J should be at least 4 so that the observed PAPR of the discrete-time signal approximates that of the analog signal.

In the literature, it is customary to use the complimentary cumulative distribution function (CCDF) of the PAPR as a performance criterion. It is defined as:

$$\text{CCDF}(\psi) = \Pr\{\text{PAPR}_{\text{D}}(x) \geq \psi\} \tag{2.35}$$

In essence $\text{CCDF}(\psi)$ is the probability of an OFDM symbol having its PAPR exceeding ψ. As an example, the CCDFs of PAPR for different oversampling factors are shown in Figure 2.16. The results show that $J = 4$ can provide good enough approximation of the PAPR distribution of the continuous-time signal.

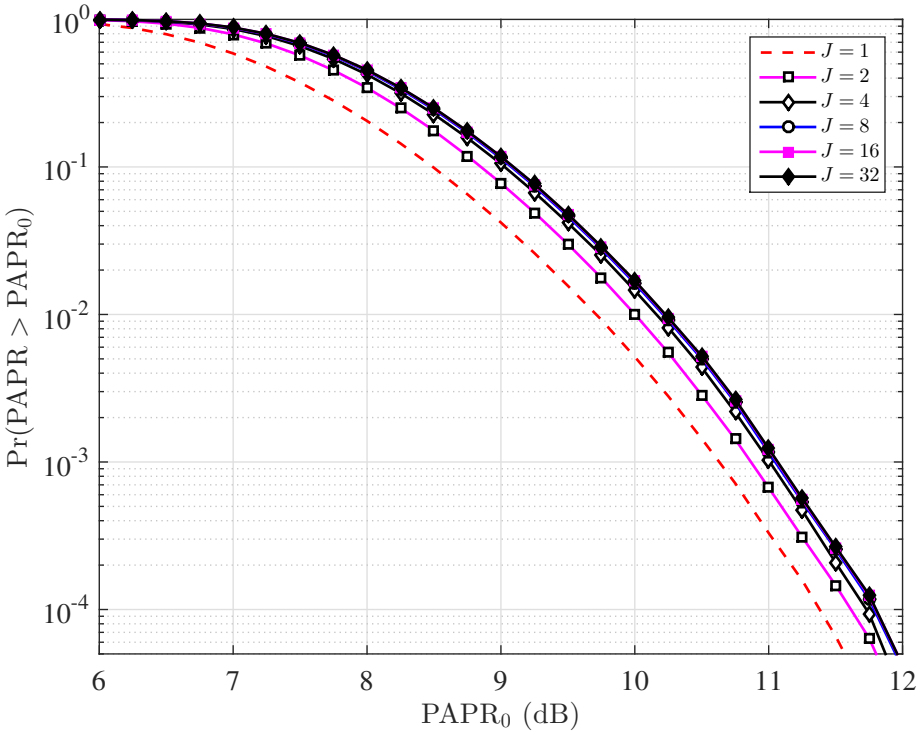

Figure 2.16 CCDF of $\text{PAPR}_{\text{D}}(x^{(J,\text{T})}[\ell])$ for different oversampling factors.

If the number of subcarriers N is large enough ($N \geq 64$ is practically good), then based on the central limit theorem, the real and imaginary parts of $x[n]$ have Gaussian distributions, hence the envelope of $x[n]$ follows a Rayleigh distribution [2]. Also, in theory, PAPR can be proportional to the number of active subcarriers, which happens when all the subcarriers

align in phase. The CCDF curves of OFDM symbols corresponding to different numbers of subcarriers and $J = 4$ are plotted in Figure 2.17.

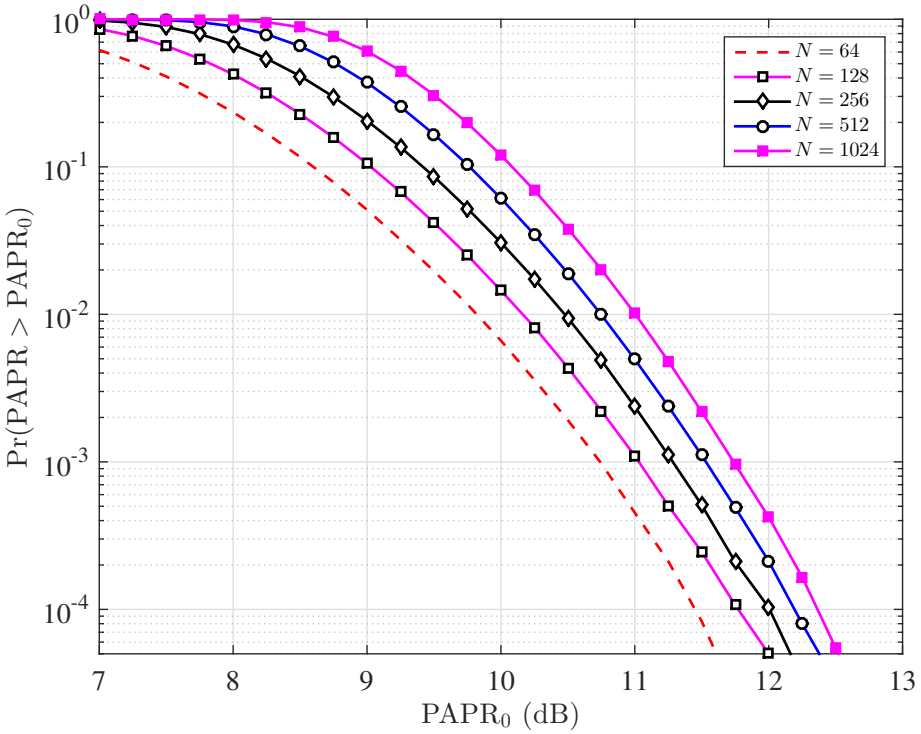

Figure 2.17 CCDF of $\text{PAPR}_\text{D}(x^{(4,\text{T})}[\ell])$ for different numbers of subcarriers.

The PAPR measured with the real signal $x^{(J,\text{R})}[\ell]$ is slightly different from that measured with the complex signal $x^{(J,\text{T})}[\ell]$. Given the modulation in (2.31) and assuming the carrier frequency is much larger than the bandwidth of the OFDM symbol, i.e. $f_c >> W = N/T$, the peak instantaneous magnitude of the real signal is the same as the peak instantaneous envelope of the complex signal:

$$\max_{0\le\ell\le NJ-1} |x^{(J,\text{R})}[\ell]| \approx \max_{0\le\ell\le NJ-1} |x^{(J,\text{T})}[\ell]| \tag{2.36}$$

For square QAM modulation, the I and Q channels are made up from the same set of signals. It follows that:

$$E\{|x_\text{I}^{(J,\text{T})}[\ell]|^2\} = E\{|x_\text{Q}^{(J,\text{T})}[\ell]|^2\} = \frac{1}{2}E\{|x^{(J,\text{R})}[\ell]|^2\} \tag{2.37}$$

Furthermore, because of (2.31), one has:

$$E\{|x^{(J,\text{R})}[\ell]|^2\} = \frac{1}{2}E\{|x_\text{I}^{(J,\text{T})}[\ell]|^2\} + \frac{1}{2}E\{|x_\text{Q}^{(J,\text{T})}[\ell]|^2\} = \frac{1}{2}E\{|x^{(J,\text{T})}[\ell]|^2\}, \tag{2.38}$$

which results in:

$$\begin{aligned}\mathrm{PAPR_D}(x^{(J,\mathrm{R})}[\ell]) &= \frac{\max\limits_{0\le\ell\le NJ-1}|x^{(J,\mathrm{R})}[\ell]|^2}{E\{|x^{(J,\mathrm{R})}[\ell]|^2\}} \\ &= \frac{\max\limits_{0\le\ell\le NJ-1}|x^{(J,\mathrm{T})}[\ell]|^2}{E\{|x^{(J,\mathrm{T})}[\ell]|^2\}/2} = 2\mathrm{PAPR_D}(x^{(J,\mathrm{T})}[\ell])\end{aligned} \tag{2.39}$$

Hence, the PAPR of the real passband signal is 3 dB higher than the PAPR of the baseband signal.

2.4 Models of a Power Amplifier

OFDM signals are more sensitive to the nonlinearities encountered in the transmitting path than constant-envelope signals. Common sources of nonlinearities are: nonlinearity in the FFT/IFFT blocks due to the limited word lengths; quantization noise introduced in the DAC and *analog-to-digital conversion* (ADC); the nonlinearity due to the amplifying characteristic of a HPA. Due to the high PAPR nature of multicarrier signals, the nonlinearities of a HPA have the dominant effect. Therefore, a model of a HPA is needed to fully understand the impact of high PAPR.

HPAs are commonly characterized as memory-less amplifiers with frequency-non-selective response [11]. Provided that the input signal is

$$x(t) = |x(t)|\mathrm{e}^{j\phi(t)} \tag{2.40}$$

where $|x(t)|$ and $\phi(t)$ are the amplitude and phase of the signal, the output of the HPA is represented by [2]:

$$y(t) = G\left(|x(t)|\right)\mathrm{e}^{j\{\phi(t)+\Phi(|x(t)|)\}} \tag{2.41}$$

where $G(\cdot)$ and $\Phi(\cdot)$ are, respectively, the amplitude/amplitude (AM/AM) and the amplitude/phase (AM/PM) distortion functions. In particular, $G(\cdot)$ captures the effect of nonlinearity on the amplitude $|x(t)|$, whereas $\Phi(\cdot)$ accounts for the effect of nonlinearity on the phase $\phi(t)$.

There are three HPA models that are commonly used in literature: the *soft limiter* (SL) model, the *solid state power amplifier* (SSPA) model, and the *traveling wave tube amplifier* (TWTA) model [2]. The following subsections discuss them briefly.

Soft Limiter

The *soft limiter* (SL) is the simplest model of the power amplifiers. It's AM/AM response is a constant and AM/PM response is ideally zero. Therefore, the output of the SL HPA is given by:

$$y(t) = \begin{cases} A\mathrm{e}^{j\phi(t)}, & |x(t)| \geq A, \\ x(t), & \text{otherwise}, \end{cases} \tag{2.42}$$

where A is the limiting threshold of the SL HPA.

Solid State Power Amplifier

The *solid state power amplifier* (SSPA) model is expressed as [12] :

$$G\left(|x(t)|\right) = \frac{g_0|x(t)|}{\left[1 + \left(\frac{|x(t)|}{A}\right)^{2p}\right]^{1/2p}}, \tag{2.43}$$

and

$$\Phi\left(|x(t)|\right) = 0, \tag{2.44}$$

where g_0 is the amplifier gain; A is the threshold or the saturation level of the HPA; p is a parameter that controls the AM/AM sharpness of the saturation region. This model is widely used in wireless communications [2]. It can be seen from (2.44) that the SSPA introduces no distortion in the signal phase. Note also that when $p \to \infty$, the SSPA model becomes the SL model.

Traveling Wave Tube Amplifier

The *traveling wave tube amplifier* (TWTA) model is given by [13] :

$$G\left(|x(t)|\right) = \frac{\alpha_1|x(t)|}{1 + \beta_1|x(t)|^2}, \tag{2.45}$$

and

$$\Phi\left(|x(t)|\right) = \frac{\alpha_2|x(t)|}{1 + \beta_2|x(t)|^2}, \tag{2.46}$$

where $\alpha_1, \beta_1, \alpha_2, \beta_2$ are parameters that control the characteristics of the AM/AM and AM/PM responses. Common choices of these parameters are [2]:

$$\alpha_1 = 2A,\ \beta_1 = \frac{1}{A^2},\ \alpha_2 = \frac{\pi}{12},\ \beta_2 = 0.25. \tag{2.47}$$

As a comparison, the AM/AM distortion functions of the SL model, SSPA model for $p = 1, 2, 4, 10$ and the TWTA model with the suggested parameter values in (2.47) are shown in Figure 2.18. Note that, due to the non-zero phase response, the TWTA model exhibits stronger nonlinearity when compared to the SSPA and SL models.

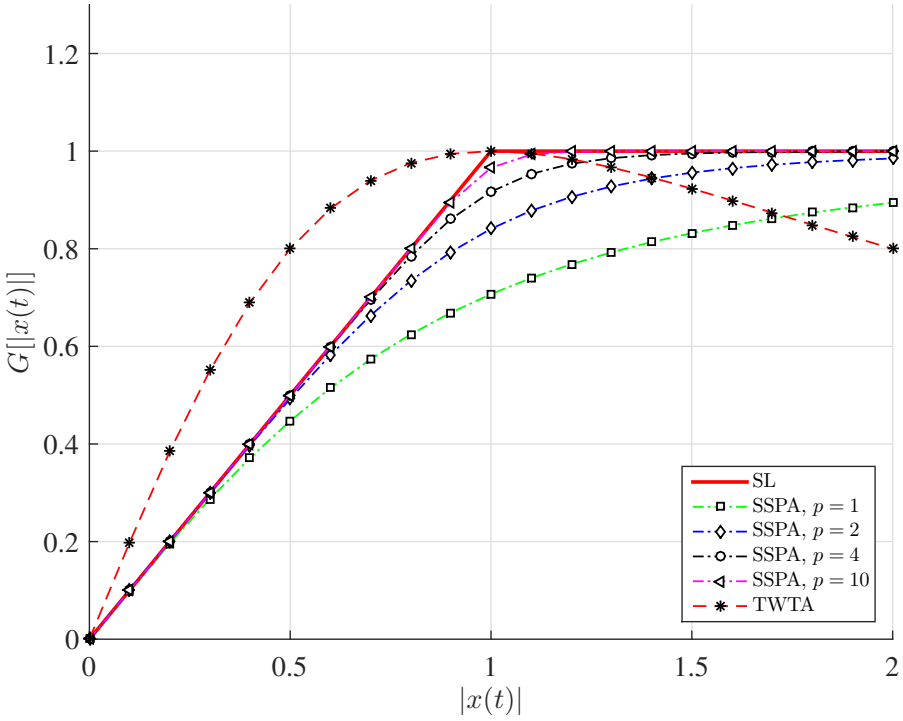

Figure 2.18 Simulations of AM/AM distortion functions of SL model in (2.42), SSPA model with $p = 1, 2, 4, 10$ in (2.43) and TWTA model in (2.45) with suggested values in (2.47).

Input Back-Off

The most efficient working point of a PA is at its saturation level. However, the high peaks encountered in OFDM signals can drive the PA into saturation. Therefore some *input back-off* (IBO) is required to shift the operating point towards the lower input power, which is illustrated in Figure 2.20. The IBO factor is defined as the ratio between the input saturation power level of the HPA and the average power of the input signal:

$$\text{IBO} = 10 \log_{10} \left(\frac{P_{\text{sat}}}{P_{\text{avg}}} \right) = [P_{\text{sat}}]_{\text{dB}} - [P_{\text{avg}}]_{\text{dB}} \tag{2.48}$$

where $P_{\text{sat}}, P_{\text{avg}}$ are the input saturation power and the average power of the input signal,

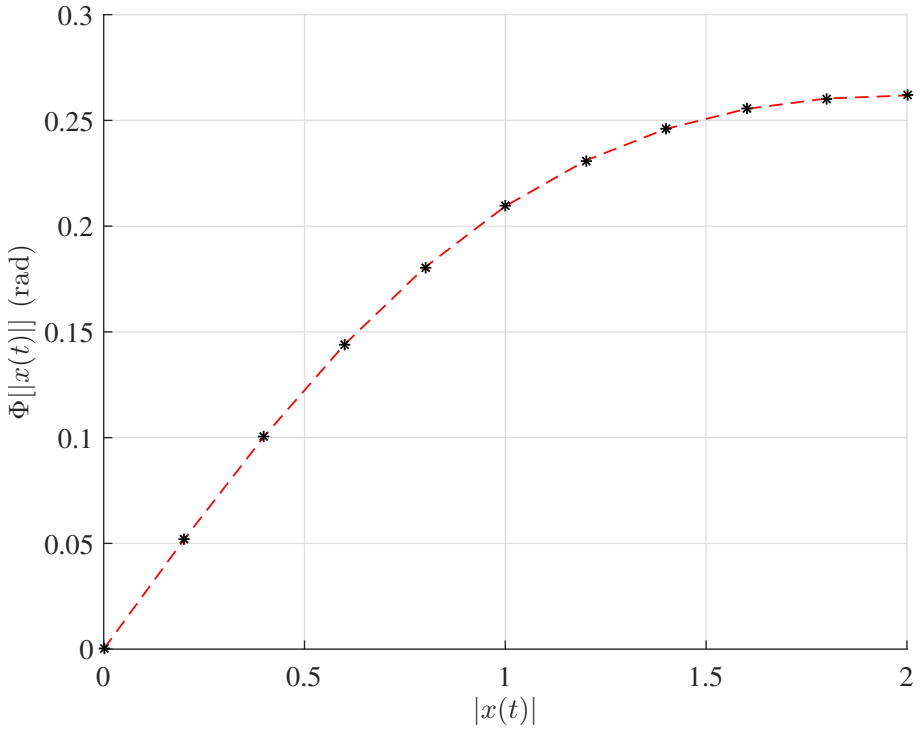

Figure 2.19 Simulation of AM/PM distortion function of TWTA model in (2.46) with suggested values in (2.47).

respectively.

The amplified peaks in OFDM signals are clipped in the saturation region of the HPA, which causes spectral spreading and distortions. To limit this effect, the IBO should be at least equal to the PAPR of the input signal. However, such solution forces the HPA to work at a reduced efficiency. Figure 2.21 shows the spectral spreading effect for different values of IBO.

2.5 Summary

In this chapter, a review of single-carrier QAM systems is first given. Then the concept of OFDM as a combination of multiple SC-QAM subchannels is presented, in which the effect of a wide-band channel causing ISI at the receiver is also discussed. After that, the implementation of an OFDM system utilizing DFT/IDFT is reviewed. As the objective of the thesis is on the problem of PAPR reduction for OFDM signals, a definition of PAPR to

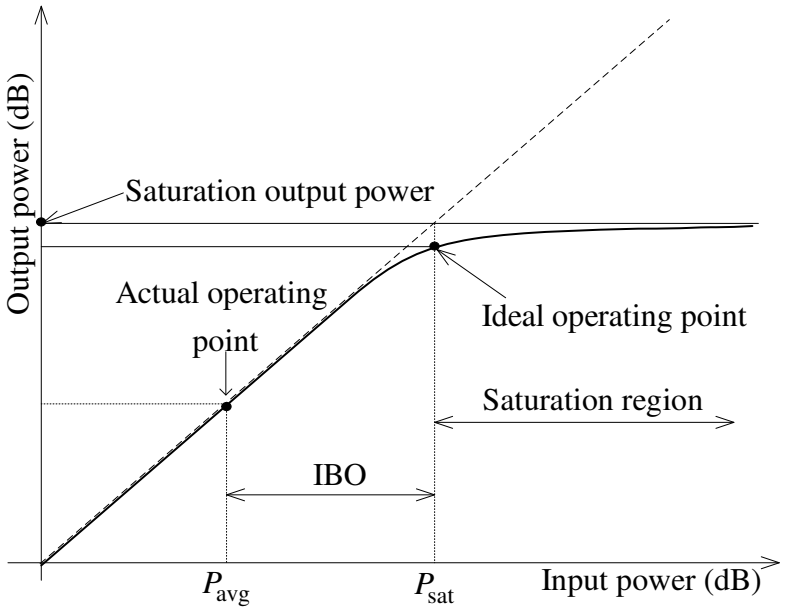

Figure 2.20 Typical input power versus output power characteristics curve for a HPA [2].

quantify the dynamic range of OFDM signals is introduced. The last section discussed the property of an HPA and its theoretical models to illustrate the affect of limited linear range in amplifying OFDM signals. As the PAPR of OFDM signals is theoretically unlimited, PAPR reduction is crucial to obtain signals with a smaller dynamic range so that they can be amplified more effectively and less distorted. The next chapter gives an overview of different techniques in literature to reduce PAPR and discusses some of their principles.

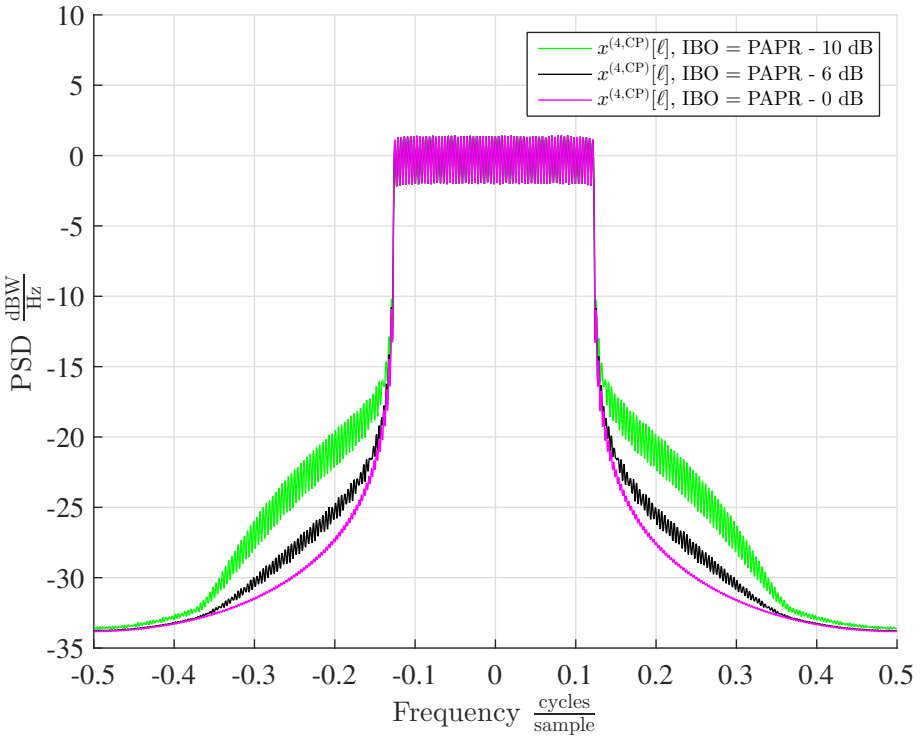

Figure 2.21 Simulation of spectral spreading effect of SSPA model with $p = 2$ for $\mathrm{PAPR} - \mathrm{IBO} = 10, 6$ and 0 dB on the OFDM signal spectrum ($N = 64, N_{\mathrm{CP}} = 16, M = 16$).

3. PAPR Reduction Techniques

There are numerous techniques proposed to reduce the PAPR of OFDM signals in the literature. These techniques can be classified into two categories: (i) distortion techniques, and (ii) distortion-less techniques. A categorized view of PAPR reduction techniques is given in Figure 3.1 and an example of PAPR reduction is shown in Figure 3.2.

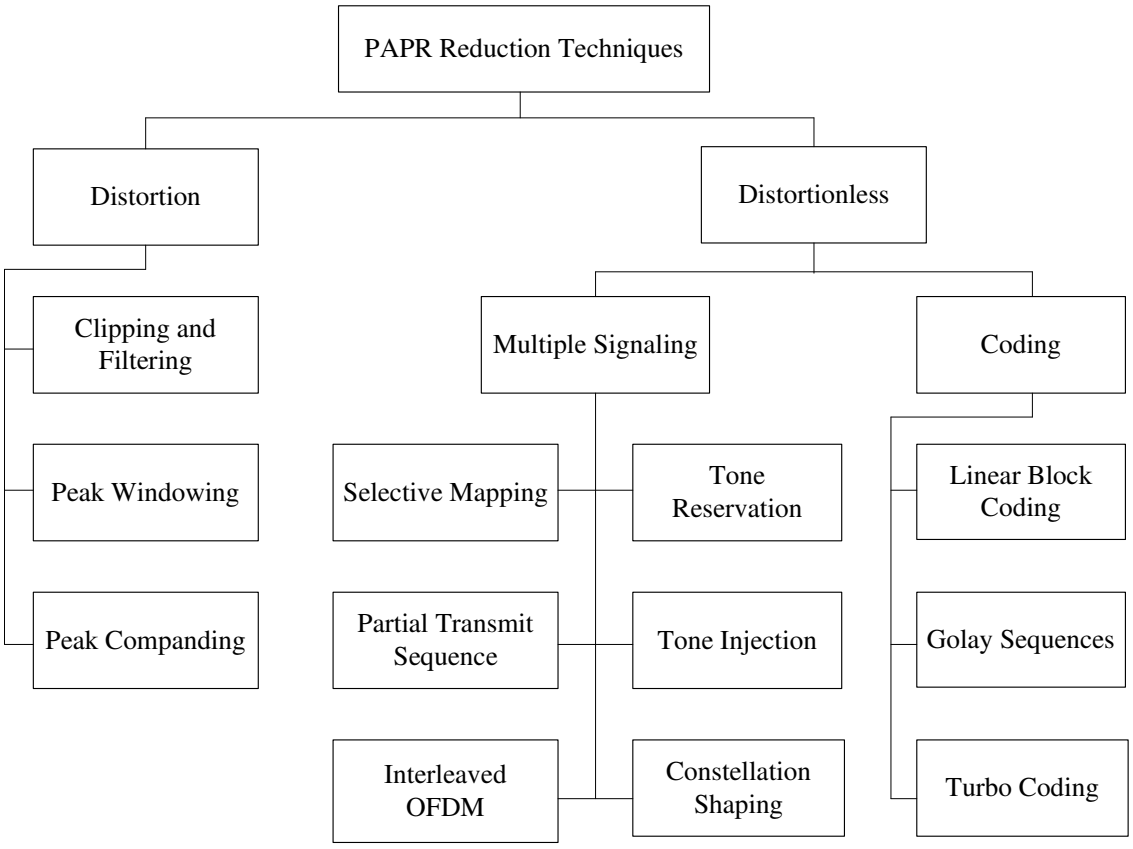

Figure 3.1 Categories of PAPR reduction algorithms [2].

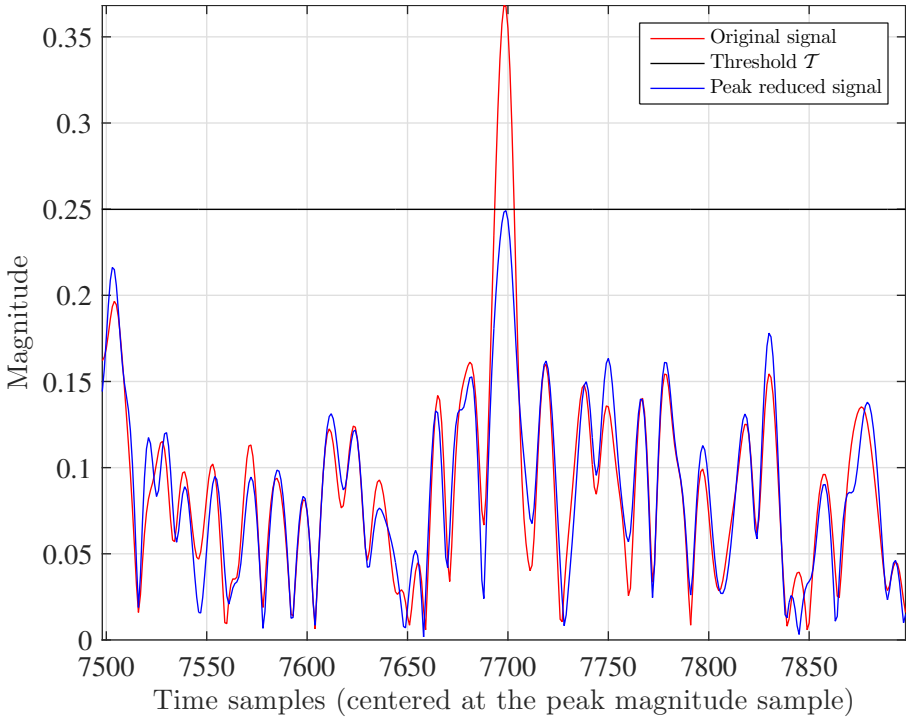

Figure 3.2 Example of PAPR reduction of an OFDM symbol using a TR technique.

The distortion techniques reduce the PAPR by distorting the OFDM signal before it passes through the HPA. Some well-known techniques in this category are clipping-and-filtering [14–16], peak windowing [17–22] and peak companding [23–25]. These techniques provide good PAPR reduction, but introduce both in-band and out-of-band distortions, which increases the *bit-error-rate* (BER). Because the probability of having a high peak in OFDM signals is quite small [2], most of the signal power is contributed by low magnitude samples. At the expense of some tolerable increase in the BER, some level of PAPR reduction can be achieved by distorting the OFDM signals.

The distortion-less techniques are more attractive since they do not increase the BER. They can be further categorized into two sub-categories: multiple signaling techniques and coding techniques. The multiple signaling techniques reduce the PAPR of the transmit signals by generating multiple permutations of the original OFDM signal, then choosing the one with the minimum PAPR. On the other hand, the coding techniques modify the redundancy part of the data block, which is used for error detection and correction purpose,

to obtain the resulting signal having the minimum PAPR. Consequently, all the distortionless techniques requires side-information that must be made known to the receiver in order to demodulate the transmitted data correctly.

The multiple signaling sub-category includes selective mapping [26–28], partial transmit sequence [29–32], interleaved OFDM [33–35], tone reservation [36], tone rejection [37], and constellation shaping techniques [38–40] . The coding techniques make use of linear block coding [41–43], Golay sequences [44–46], and turbo coding [47–49].

The following subsections elaborate further on the clipping-and-filtering, selective mapping, partial transmit sequences, interleaved OFDM and tone reservation techniques.

As discussed in Section 2.3, the oversampled discrete-time signal provides a good approximation of the PAPR of the continuous-time signal. So from this point onwards, all the mathematical derivations will consider only oversampled discrete-time OFDM symbols. In addition, because the major cause of the high dynamic range of OFDM signals is due to the combination of subcarriers, not the extensions of symbol durations such as CP or roll-off intervals, it is reasonable to analyze OFDM symbols that are generated without any cyclic prefix or roll-off interval extensions.

3.1 Clipping-and-Filtering Technique

Reducing PAPR by clipping is the simplest approach, which limits the high peaks of OFDM signals to a pre-specified level prior to passing it to the HPA. There are different ways to clip the signal. The classical method [14] employs a clipping function given by:

$$g_{\mathcal{T}}(\xi) = \begin{cases} \xi, & \text{if } |\xi| \leq \mathcal{T} \\ \mathcal{T}\, \mathrm{e}^{j\angle\xi}, & \text{if } |\xi| > \mathcal{T} \end{cases} \tag{3.1}$$

where ξ is a complex variable; $\mathcal{T}$ is a predefined threshold. This means that any sample having its magnitude exceed $\mathcal{T}$ is clipped in magnitude but its phase is unchanged; otherwise, it is passed to the HPA without change.

Deep clipping is another method which is proposed in [50]. This method modifies the

classical clipping function in order to deeply clip the high magnitude samples. A parameter called a clipping depth factor is then used to control the clipping depth. The deep clipping function is defined by:

$$d_{\mathcal{T}}(\xi) = \begin{cases} \xi, & \text{if } |\xi| \leq \mathcal{T} \\ [\mathcal{T} - \beta(|\xi| - \mathcal{T})]\, \mathrm{e}^{j\angle\xi}, & \text{if } \mathcal{T} < |\xi| < \frac{1+\beta}{\beta}\mathcal{T} \\ 0, & \text{if } |\xi| > \frac{1+\beta}{\beta}\mathcal{T} \end{cases} \tag{3.2}$$

where β is a clipping depth factor.

Another clipping operation, called *smooth clipping* is reported in [51]. In this paper, the smooth clipping function is defined as:

$$m_{\mathcal{T}}(\xi) = \begin{cases} \left(|\xi| - \frac{1}{\kappa}|\xi|^3\right) \mathrm{e}^{j\angle\xi}, & \text{if } |\xi| \leq \frac{3}{2}\mathcal{T} \\ \mathcal{T}\mathrm{e}^{j\angle\xi}, & \text{if } |\xi| > \frac{3}{2}\mathcal{T} \end{cases} \tag{3.3}$$

where $\kappa = \frac{27}{4}\mathcal{T}^2$.

For comparison, the magnitude responses of the three clipping functions discussed above are plotted in Figure 3.3.

The clipping operations cause in-band signal distortion, resulting in BER degradation. Because of the probability of large peaks is small, the in-band distortion is not severe under the condition that the clipping threshold is sufficiently large. Therefore a small increase in in-band distortion can be tolerated when a low-order QAM modulation, for instance a 4-QAM modulation, is used. For high-order QAM modulation, even a small increase in in-band distortion is not acceptable. To illustrate this, the effects of 6 dB clipping with the clipping function in (3.1) for OFDM signals using 16-QAM and 64-QAM are shown in Figure 3.4. It is obvious that the distortion caused by clipping leads to a higher error rate for 64-QAM as compared to 16-QAM.

In addition, clipping also creates out-of-band radiation, which causes out-of-band interference signals to the neighboring frequency bands. This is why the filtering operations are needed. Filtering out-of-band radiation can be done in the time domain by using a low-pass

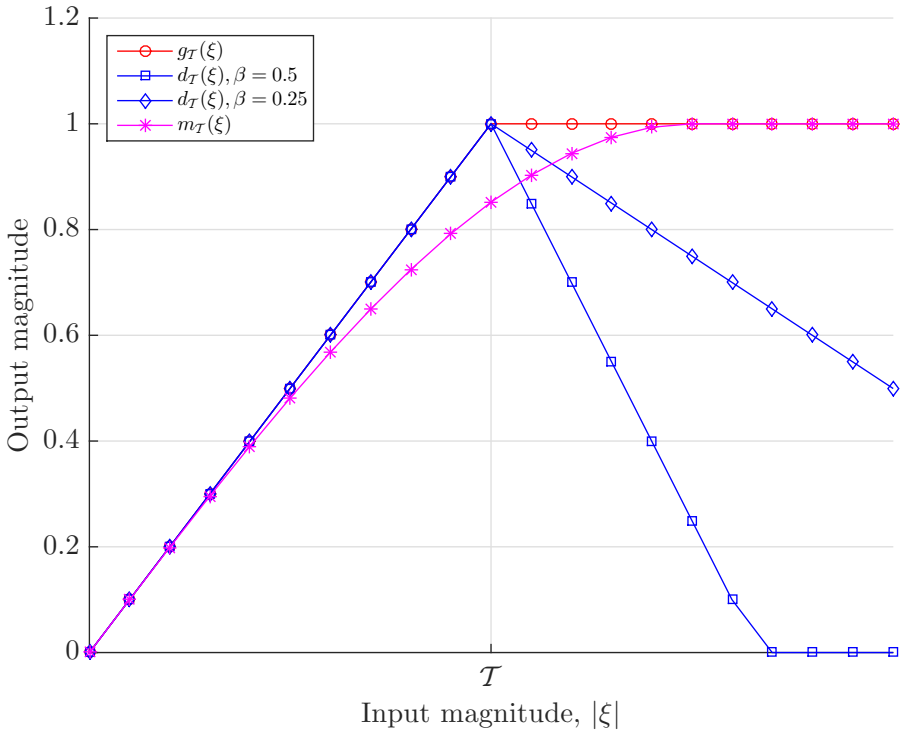

Figure 3.3 Different clipping functions used for PAPR reduction.

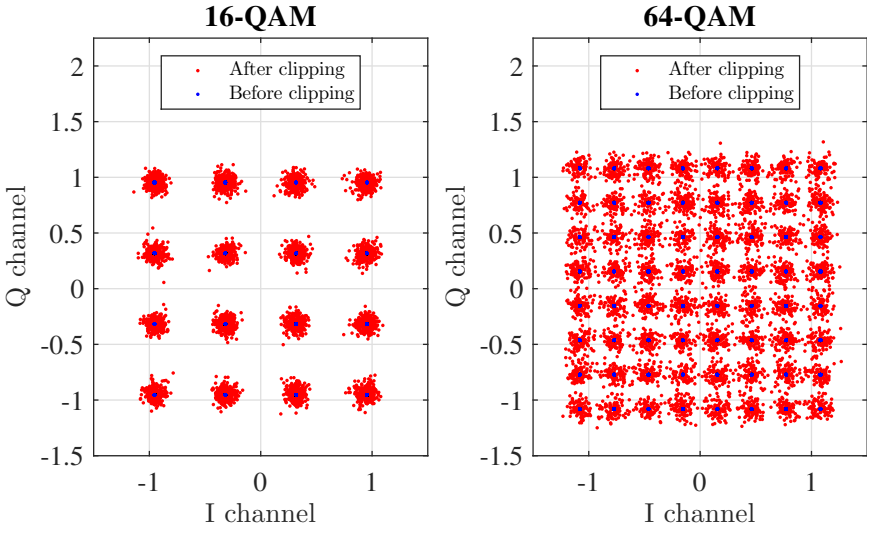

Figure 3.4 Clipping at 6 dB causes more severe distortions for 64-QAM than for 16-QAM.

filter [52] or in the frequency domain utilizing a pair of DFT and IDFT [14]. Filtering in the frequency domain is simpler than in the time domain since the DFT/IDFT operations can be effectively implemented using the FFT algorithms. The clipped signal is transformed

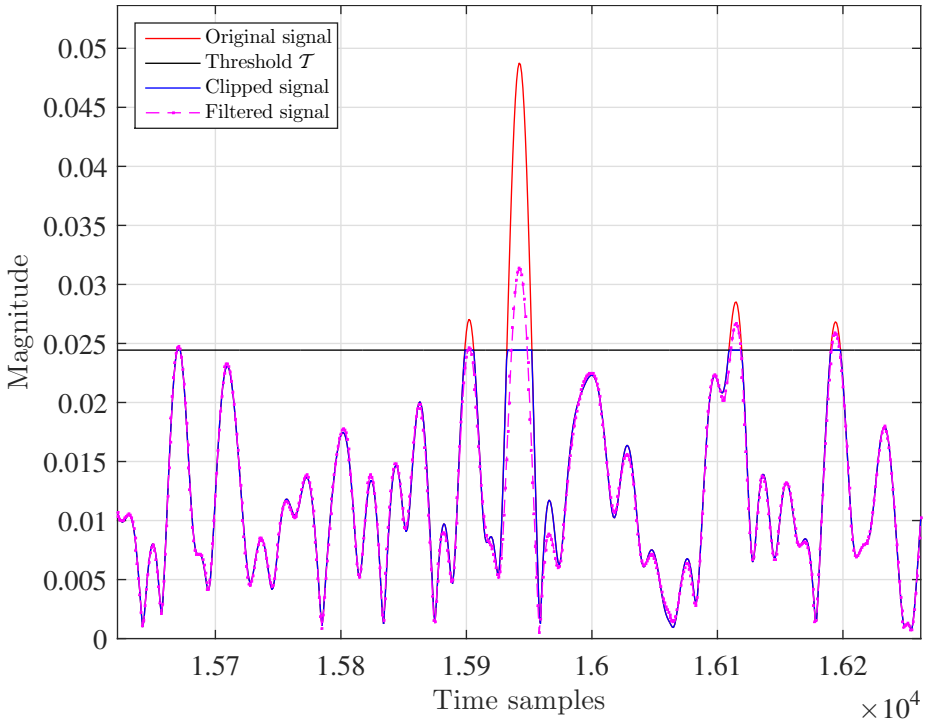

Figure 3.5 Peak regrowth ($N = 1024, J = 16, M = 64$; clipping at 6 dB).

into the frequency domain, where all the out-of-band terms are set to zero. After that, an inverse FFT (IFFT) is used to convert the filtered signal back to the time domain. Nonetheless, a side-effect of filtering is peak regrowth. The peaks appear again after filtering but having lower magnitudes than that of the original peaks. The peak regrowth phenomenon is illustrated in Figure 3.5.

3.2 Selective Mapping Technique

Figure 3.6 shows the general scheme of PAPR reduction using the *selective mapping* (SLM) technique. The general idea is to generate a set of $M-$different OFDM symbols $\{\boldsymbol{x}_{(0)}, \ldots, \boldsymbol{x}_{(M-1)}\}$, that are all generated from the same block of input data sequence $\boldsymbol{X} = [X_0, \ldots, X_{N-1}]$. The transmit signal is selected to be the one having the minimal PAPR.

Mathematically, the transmitted OFDM symbol is expressed as:

$$\tilde{\boldsymbol{x}} = \arg \min_{0 \leq m \leq M-1} \left\{ \text{PAPR}(\boldsymbol{x}_{(0)}), \ldots, \text{PAPR}(\boldsymbol{x}_{(M-1)}) \right\} \tag{3.4}$$

The M OFDM symbol sets can be generated by multiplying $\boldsymbol{X}$ by M different length-N

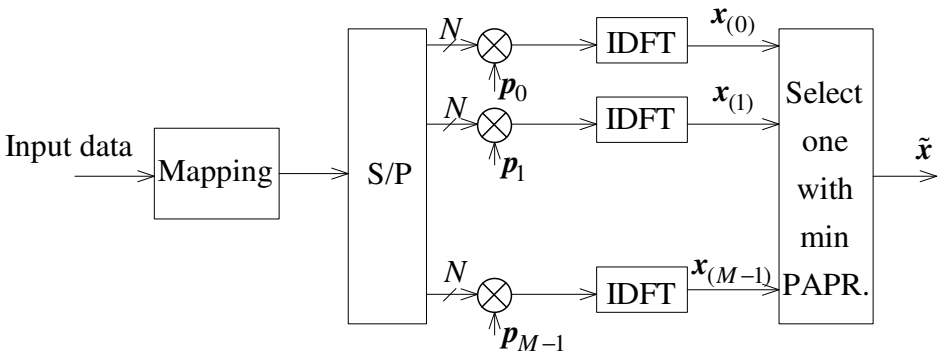

Figure 3.6 PAPR reduction using the SLM technique.

phase sequences, element-by-element, prior to performing IDFT. The phase sequences are denoted by:

$$\boldsymbol{p}_i = \left[\mathrm{e}^{j\phi_{i,0}}, \ldots, \mathrm{e}^{j\phi_{i,N-1}}\right]^T, \quad 0 \leq i \leq M-1 \tag{3.5}$$

where $\phi_{i,k} \in [0, 2\pi)$ for $0 \leq i \leq M-1$; $0 \leq k \leq N-1$. The modified OFDM symbols are then formed by taking the IDFT on the phase-altered data, which is:

$$\boldsymbol{x}_{(i)} = \text{IDFT}\left\{X_0 \mathrm{e}^{j\phi_{i,0}}, \ldots, X_{N-1}\mathrm{e}^{j\phi_{i,N-1}}\right\}, \quad 0 \leq i \leq M-1 \tag{3.6}$$

The multiplication with the phase sequence causes the data symbols to rotate within the QAM constellation. As an example, a phase sequence can consist of 0° or 180° phase rotation, i.e., $\phi_{i,k} \in \{0, \pi\}$. In such a case, the phase shifting can be done without the need of multiplications. Different phase sequences can give different amounts of PAPR reduction and designing good phase sequences is an important task.

In order for the receiver to detect the correct data, information of a selected phase sequence must be transmitted along with the OFDM symbol. This in turn reduces the data transmission rate. Moreover this side information also needs to be protected since a corrupted phase sequence results in an erroneous recovery of a whole OFDM symbol. Thus numerous schemes, called blind-SLM schemes, have been proposed to avoid the need of transmitting side information over the channel [2].

The optimization process of choosing the minimal PAPR signal among M generated signals can become prohibitively complicated when the number of carriers becomes large,

and more importantly, when the number of phase sequences is increased. Note that as higher PAPR reduction is required, a larger number of phase sequences needs to be generated. Besides, the implementation of the SLM technique requires M blocks of IFFT for the frequency-to-time domain conversion. All of these factors translate to high computation cost.

The authors in [28] suggest using multiple all-pass filters to rotate the OFDM symbol sequence instead of performing complex multiplication along with IFFT as in the conventional SLM approach. This technique helps to significantly reduce the work load in the transmitter thanks to IFFT operations. However the performance of PAPR reduction is slightly degraded when compared to the conventional SLM scheme. The authors provide an example of using 8 first-order all-pass filters for an OFDM system with $N = 2048$ subcarriers. The proposed scheme is able to reduce the number of required multiplications by 69.2% and the number of additions by 63.1% at a sacrifice of 0.25 dB PAPR increase when compared to the conventional SLM scheme using 8 IFFT blocks [2].

3.3 Partial Transmit Sequence Technique

In the *partial transmit sequence* (PTS) technique, the input data block $\boldsymbol{X}$ is partitioned into M disjoint subblocks as $\boldsymbol{X} = [\boldsymbol{X}_0, \ldots, \boldsymbol{X}_{M-1}]^T$. The IDFT is then operated on each subblock. The IDFT's outputs are weighted with complex phase factors $b_0, \ldots, b_{M-1}$. The block diagram is shown in Figure 3.7.

The transmit signal is formed by summing all scaled outputs of IDFT blocks, which yields:

$$\tilde{\boldsymbol{x}} = \sum_{i=0}^{M-1} b_i \text{IDFT}\{\boldsymbol{X}_i\} = \sum_{i=0}^{M-1} b_i \boldsymbol{x}_i \tag{3.7}$$

where $\boldsymbol{x}_i$ is the ith partial sequence; $b_i = \mathrm{e}^{j\phi_i}$ with $\phi_i \in [0, 2\pi)$ is the ith scaling factor. The phase vector is chosen so that the PAPR of $\tilde{\boldsymbol{x}}$ can be minimized, which can be expressed as:

$$[b_0, \ldots, b_{M-1}] = \arg \min_{[b_0,\ldots,b_{M-1}] \in \mathbb{C}^M} \left(\max_{0 \le n \le N-1} \left| \sum_{i=0}^{M-1} b_i x_i[n] \right| \right) \tag{3.8}$$

where $\mathbb{C}^M$ is the M-dimensional complex number space.

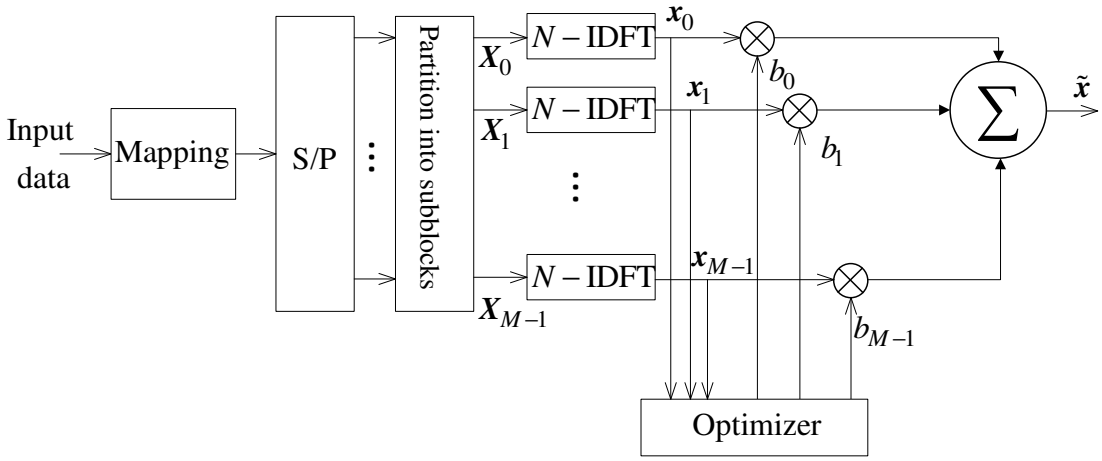

Figure 3.7 PAPR reduction using the PTS technique.

In general, the search space for the optimal length-M phase vector is too large to have an effective search. As such, searching in a subspace with a finite number of elements is usually conducted. Specifically, the phase factors are chosen to be in the set $\{b_i = \mathrm{e}^{j\frac{2\pi i}{Q}},\ 0 \leq i \leq Q-1\}$ where Q is the number of allowed phase values. Since the first factor is 1, the search objective is to find $M-1$ phase factors, which is equivalent to search for an element in the set of Q^{M-1} elements. This means the search complexity still increases exponentially with the number of subblocks.

The performance of PAPR reduction depends on the values of M and Q. Higher PAPR reduction can be obtained for a larger number of subblocks. However, the PTS operations require Q IDFT operations for each data block and $\lfloor \log_2 Q^{M-1} \rfloor$ additional bits of information to be transmitted to the receiver. Therefore, having a larger number of subblocks increase considerably the resources required and the complexity. In addition, the partitioning scheme is an important factor determining how well the PAPR reduction scheme performs. There are three prevalent methods to partition the input block: adjacent partitioning, interleaved partitioning and pseduo-random partitioning [2], in which the pseudo-random partitioning has been found to provide the best performance.

Due to the high complexity of searching for a suitable transmitting sequence, various schemes are proposed to reduce this complexity. One particular example is a suboptimal combinational algorithm, which uses the binary phase factors of $\{1, -1\}$ instead of general

complex phase factors as in [30].

3.4 Interleaved OFDM Technique

Instead of using different phase sequences as in the SLM method, different OFDM symbols can be generated by using an interleaver. Given the same input block of data, different interleavers generate different permutations of data over different subcarriers, which creates different symbols with different PAPR values. To achieve a substantial PAPR reduction, multiple interleavers are exploited to generate a set of sufficiently large permutations from the original data block. The reordered data is then put onto IDFT blocks and the resulting signal having the smallest value of PAPR is chosen. This technique is illustrated in Figure 3.8.

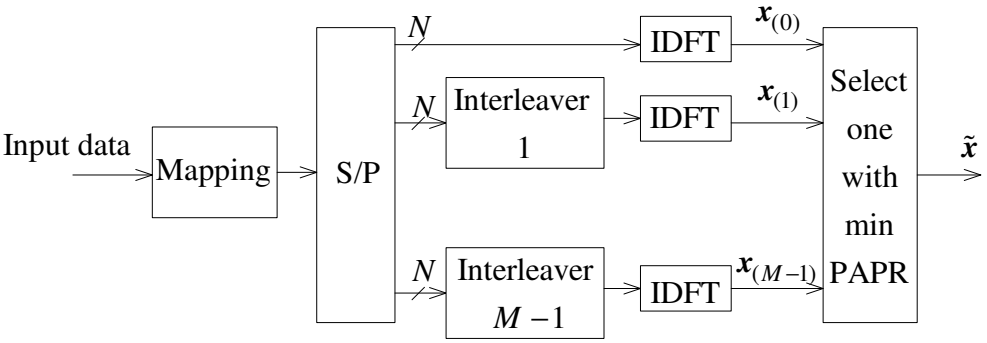

Figure 3.8 PAPR reduction using the interleaved OFDM technique.

The permutations can be conducted on the data bits or the data symbols. Moreover the interleaving operations can also be applied for the case of multiple channel OFDM signal as in orthogonal frequency-division multiple access (OFDMA) system [53], which is also known as the DFT-spreading technique.

The interleaved OFDM symbols are selected amongst M candidate symbols, which requires $M-1$ interleavers and M IDFT blocks. Additionally, $\lfloor \log_2 M \rfloor$ side information bits have to be transmitted to the receiver since the receiver must know which interleaver was used for the transmitted symbols in order to detect the data correctly. These bits are used to store the index of the interleaver used, which must be stored in both the transmitter and receiver.

3.5 Tone Reservation Technique

In the *tone reservation* (TR) method, the transmitter and receiver must agree to reserve a set of G subcarriers for peak reduction, while the remaining $(N-G)$ subcarriers are used for data transmission. An oversampled peak canceling signal $\boldsymbol{c} = [c[0], \ldots, c[NJ-1]]$ is constructed from the reserved tones. The peak-reduced signal $\boldsymbol{y} = [y[0], \ldots, y[NJ-1]]$ is given by:

$$y[n] = x[n] + c[n] = \frac{1}{\sqrt{JN}} \sum_{k=0}^{N-1} (X_k + C_k) e^{j2\pi \frac{nk}{NJ}}, \tag{3.9}$$

where $0 \leq n \leq NJ-1$ and

$$\boldsymbol{C} = \left[C_0, \ldots, C_{N/2-1}, 0, \ldots, 0, C_{N/2}, \ldots, C_{N-1}\right]^T$$

is the frequency symbol used to construct $\boldsymbol{c}$. The principle of this method is illustrated in Figure 3.9.

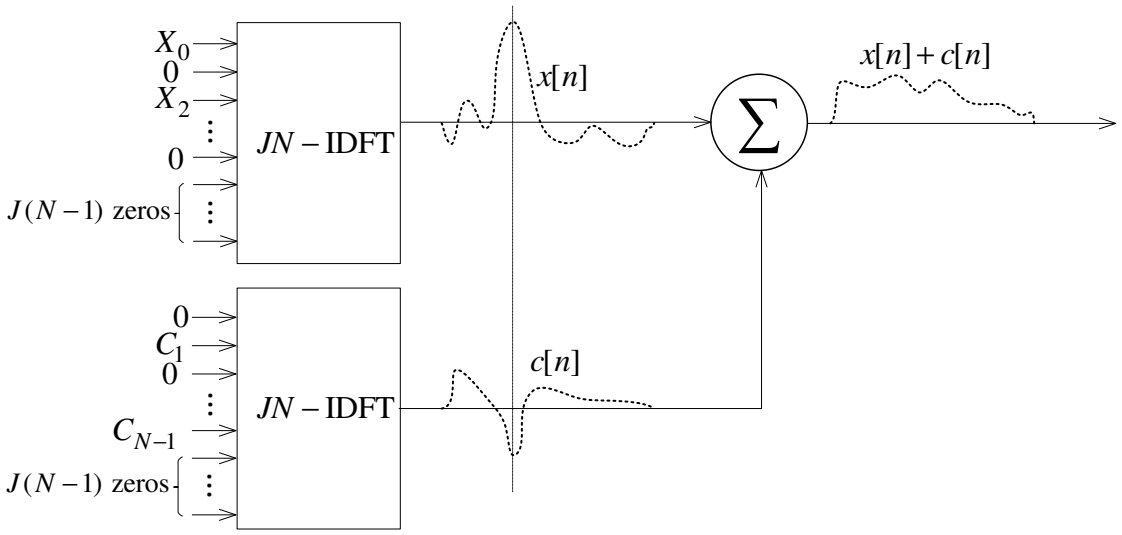

Figure 3.9 PAPR reduction using the TR technique.

The set of subcarriers used is referred to as a peak reservation tone set (PRT), denoted as $\mathcal{R} = \{i_0, i_1, \ldots, i_{G-1}\}$. The frequency vector $\boldsymbol{C}$ is restricted to have non-zero elements only at the reserved tones. That is:

$$X_k + C_k = \begin{cases} X_k, & k \in \mathcal{D} \\ C_k, & k \in \mathcal{R} \end{cases} \tag{3.10}$$

where $\mathcal{D}$ is the set of data tones, and $\mathcal{D} \cap \mathcal{R} = \emptyset$.

The PAPR of the peak-reduced OFDM signal is then computed as [37]

$$\text{PAPR}(y) = \frac{\max_{0 \le n \le NJ-1} |x[n] + c[n]|^2}{E\left\{|x[n]|^2\right\}} \tag{3.11}$$

Since the denominator of (3.11) does not depend on $\boldsymbol{C}$, the optimal peak canceling signal is chosen to minimize the peak power of $y[n]$:

$$\begin{aligned} &\boldsymbol{C} = \arg \min_{\boldsymbol{C} \in \mathbb{C}^N} \left\{\max_{0 \le n \le NJ-1} |x[n] + c[n]|^2\right\} \\ &\text{subject to: } \mathcal{H}(\boldsymbol{C}) \le G \end{aligned} \tag{3.12}$$

where $\mathbb{C}^N$ is the N-dimensional complex number space and $\mathcal{H}(\boldsymbol{v})$ denotes the Hamming weight of vector $\boldsymbol{v}$, which is the number of non-zero elements in $\boldsymbol{v}$. Methods to find the solution to the optimization problem in (3.12) are discussed next.

Finding the Optimal Peak Canceling Signal in the TR Method

The time-domain signal of an $J-$times oversampled OFDM symbol can be written as:

$$x[n] = \frac{1}{\sqrt{JN}} \sum_{k=-\frac{N}{2}}^{\frac{N}{2}-1} X_k \mathrm{e}^{j2\pi kn/JN}, \quad 0 \le n \le NJ-1 \tag{3.13}$$

The oversampled time vector $\boldsymbol{x} = \Big[x[0], x[1], \ldots, x[NJ-1]\Big]^T$ can also be represented using a matrix multiplication

$$\boldsymbol{x} = \boldsymbol{Q}\boldsymbol{X} \tag{3.14}$$

where $\boldsymbol{Q}$ is a $NJ \times NJ$ IDFT matrix, given as:

$$\boldsymbol{Q} = \frac{1}{\sqrt{JN}} \times \begin{bmatrix} 1 & 1 & \ldots & 1 & \ldots & 1 \\ 1 & \mathrm{e}^{j2\pi \frac{1}{NJ}} & \ldots & \mathrm{e}^{j2\pi \frac{k}{NJ}} & \ldots & \mathrm{e}^{j2\pi \frac{(NJ-1)}{NJ}} \\ \vdots & \vdots & \ddots & \vdots & \ddots & \vdots \\ 1 & \mathrm{e}^{j2\pi \frac{(NJ-1)}{NJ}} & \ldots & \mathrm{e}^{j2\pi \frac{(NJ-1)k}{NJ}} & \ldots & \mathrm{e}^{j2\pi \frac{(NJ-1)^2}{NJ}} \end{bmatrix}_{NJ \times NJ} \tag{3.15}$$

In addition, the frequency symbol vector $\boldsymbol{X}$ has only N non-zero elements out of NJ total elements, due to the oversampling operation.

Using (3.14), one has:

$$\boldsymbol{c} = \boldsymbol{Q}\boldsymbol{C}, \text{ or } c[n] = \boldsymbol{q}_n\boldsymbol{C}, \quad 0 \leq n \leq NJ-1. \tag{3.16}$$

where $\boldsymbol{q}_n = \frac{1}{\sqrt{NJ}}\left[1, \mathrm{e}^{j2\pi\frac{n}{NJ}}, \ldots, \mathrm{e}^{j2\pi\frac{n\,(NJ-1)}{NJ}}\right]$ is the nth row of matrix $\boldsymbol{Q}$.

Therefore, Equation (3.12) can be reformulated as:

$$\begin{aligned} \min_{\boldsymbol{C}} \quad & p \\ \text{subject to:} \quad & \max_{0\leq n\leq NJ-1} |x[n] + \boldsymbol{q}_n\boldsymbol{C}|^2 \leq p \end{aligned} \tag{3.17}$$

The above optimization problem is equivalent to:

$$\begin{aligned} \min_{\boldsymbol{C}} \quad & p \\ \text{subject to:} \quad & \left|x[0] + \boldsymbol{q}_0\boldsymbol{C}\right|^2 \leq p \\ & \left|x[1] + \boldsymbol{q}_1\boldsymbol{C}\right|^2 \leq p \\ & \vdots \\ & \left|x[NJ-1] + \boldsymbol{q}_{NJ-1}\boldsymbol{C}\right|^2 \leq p \end{aligned} \tag{3.18}$$

Expanding the square of the absolute value using the identity $|\alpha|^2 = \alpha\,\alpha^*$, where α^* is a complex conjugate of α, results in:

$$\begin{aligned} \min_{\boldsymbol{C}} \quad & p \\ \text{subject to:} \quad & (x[0] + \boldsymbol{q}_0\boldsymbol{C})\,(x[0] + \boldsymbol{q}_0\boldsymbol{C})^* \leq p \\ & (x[1] + \boldsymbol{q}_1\boldsymbol{C})\,(x[1] + \boldsymbol{q}_1\boldsymbol{C})^* \leq p \\ & \vdots \\ & \left(x[NJ-1] + \boldsymbol{q}_{NJ-1}\boldsymbol{C}\right)\left(x[NJ-1] + \boldsymbol{q}_{NJ-1}\boldsymbol{C}\right)^* \leq p \end{aligned} \tag{3.19}$$

The constraints in (3.19) are quadratic so they are convex constraints. Hence, this is an optimization problem which minimizes a linear constraint over an intersection of convex constraints on the variable $\boldsymbol{C}$, which falls into a class of convex optimization called *quadratically constrained quadratic program* (QCQP) [54].

In a simplified case when the transmit signal is a real signal, the QCQP problem simplifies to a *linear program* (LP) problem. Since $x[n]$ is real, the additive signal $c[n]$ must be real,

which means $\boldsymbol{C}$ must satisfy the Hermitian symmetry property ($C_k = C^*_{NJ-k}$). For simplicity, N and G can be assumed to be even without any loss of generality. It means that the reserved tones should be chosen to provide a symmetry property, so only a half number of the reserved tones are actually selected. If $\mathcal{R}_{\frac{1}{2}} = \{i_0, i_1, \ldots, i_{G/2-1}\}$ denotes the set of the first $\frac{G}{2}$ elements in $\mathcal{R}$, the canceling signal can be written as:

$$\begin{aligned} c[n] &= \frac{1}{JN} \sum_{r=0}^{G/2-1} \left(C_m \mathrm{e}^{j2\pi \frac{i_r n}{JN}} + C_m^* \mathrm{e}^{-j2\pi \frac{i_r n}{JN}} \right) \\ &= \frac{1}{JN} \sum_{r=0}^{G/2-1} \left(C_m \mathrm{e}^{j2\pi \frac{i_r n}{JN}} + \left(C_m \mathrm{e}^{j2\pi \frac{i_r n}{JN}} \right)^* \right) \\ &= \frac{2}{JN} \sum_{r=0}^{G/2-1} \left(\Re\{C_m\} \cos\left(2\pi \frac{i_r n}{JN} \right) - \Im\{C_m\} \sin\left(2\pi \frac{i_r n}{JN} \right) \right), \end{aligned} \tag{3.20}$$

which can be compactly expressed as:

$$\boldsymbol{c} = \hat{\boldsymbol{Q}}\, \hat{\boldsymbol{C}}$$

where $\hat{\boldsymbol{C}} = \left[\Re\{C_0\}, \ldots, \Re\{C_{G/2-1}\}, \Im\{C_0\}, \ldots, \Im\{C_{G/2-1}\} \right]^T$ is a length-G column vector, and $\hat{\boldsymbol{Q}}$ is a $NJ \times G$ matrix that includes all the sinusoidal terms in (3.20).

With this notation, the problem in (3.19) for a real baseband signal is equivalently transformed into:

$$\begin{aligned} \min_{\boldsymbol{C}} \quad & p \\ \text{subject to:} \quad & \left| x[0] + \hat{\boldsymbol{q}}_0 \hat{\boldsymbol{C}} \right| \leq p \\ & \left| x[1] + \hat{\boldsymbol{q}}_1 \hat{\boldsymbol{C}} \right| \leq p \\ & \vdots \\ & \left| x[NJ-1] + \hat{\boldsymbol{q}}_{NJ-1} \hat{\boldsymbol{C}} \right| \leq p \end{aligned} \tag{3.21}$$

where $\hat{\boldsymbol{q}}_i$ is the ith row of matrix $\hat{\boldsymbol{Q}}$. The NJ scalar constraints in (3.21) can be rewritten in a vector form as:

$$\begin{aligned} \min_{\boldsymbol{C}} \quad & p \\ \text{subject to:} \quad & \boldsymbol{x} + \hat{\boldsymbol{Q}}\hat{\boldsymbol{C}} \leq p\, \mathbf{1}_{JN} \\ & \boldsymbol{x} + \hat{\boldsymbol{Q}}\hat{\boldsymbol{C}} \geq -p\, \mathbf{1}_{JN} \end{aligned} \tag{3.22}$$

where $\mathbf{1}_{JN}$ is a length-JN vector of all ones.

By grouping the constraints, the optimization problem in (3.22) is equivalent to:

$$\begin{aligned} \min_{\hat{\boldsymbol{C}}} \quad & p \\ \text{subject to:} \quad & \begin{bmatrix} \hat{\boldsymbol{Q}} & -\mathbf{1}_{NJ} \\ \hat{\boldsymbol{Q}} & -\mathbf{1}_{NJ} \end{bmatrix} \begin{bmatrix} \hat{\boldsymbol{C}} \\ p \end{bmatrix} \leq \begin{bmatrix} -\boldsymbol{x} \\ \boldsymbol{x} \end{bmatrix} \end{aligned} \tag{3.23}$$

Let $\boldsymbol{y} = \begin{bmatrix} \hat{\boldsymbol{C}} \\ p \end{bmatrix}$; $\boldsymbol{\alpha} = [\underbrace{0, \ldots, 0}_{JN \text{ zeros}}, 1]$; $\boldsymbol{A} = \begin{bmatrix} \hat{\boldsymbol{Q}} & -\mathbf{1}_{NJ} \\ \hat{\boldsymbol{Q}} & -\mathbf{1}_{NJ} \end{bmatrix}$ and $\boldsymbol{b} = \begin{bmatrix} -\boldsymbol{x} \\ \boldsymbol{x} \end{bmatrix}$, then (3.23) is formulated in a standard LP form as [54]:

$$\begin{aligned} \min_{\boldsymbol{y}} \quad & \boldsymbol{\alpha}\, \boldsymbol{y} \\ \text{subject to:} \quad & \boldsymbol{A}\boldsymbol{y} \leq \boldsymbol{b} \end{aligned} \tag{3.24}$$

The LP problem in (3.24) has $(G+1)$ unknown variables $\{\hat{\boldsymbol{C}}, p\}$ and $2NJ$ inequalities.

The simplification to the LP problem is only effective in the case of real baseband OFDM signals. In a more general case, the authors in [55] propose a method to formulate the TR problem in (3.12) to a *second-order-cone program* (SOCP), which can be solved efficiently using the *interior-point* (IP) method.

3.6 Active Constellation Extension Technique

In *active constellation extension* (ACE) or *active set extension* (ASE) approaches, the modulation constellation over active subcarriers are modified so that the PAPR of the signal formed from the data block is reduced without significantly degrading the BER performance [38,39]. The constellation is extended in a way that the minimum Euclidian distance between any two constellation points does not increase. For example, the shaded areas in Figure 3.10 are the feasible extension regions for the case of QPSK and 16−QAM constellations.

In the extension process, the outer constellation points are dynamically relocated toward the outside of the original constellation. For QPSK, all four constellation points can be freely chosen in the shaded areas, which guarantees that the minimum Euclidian distance of the original constellation does not increase. Because the increase of average power due to modification of the constellation points is fairly small [38], the BER degradation is not

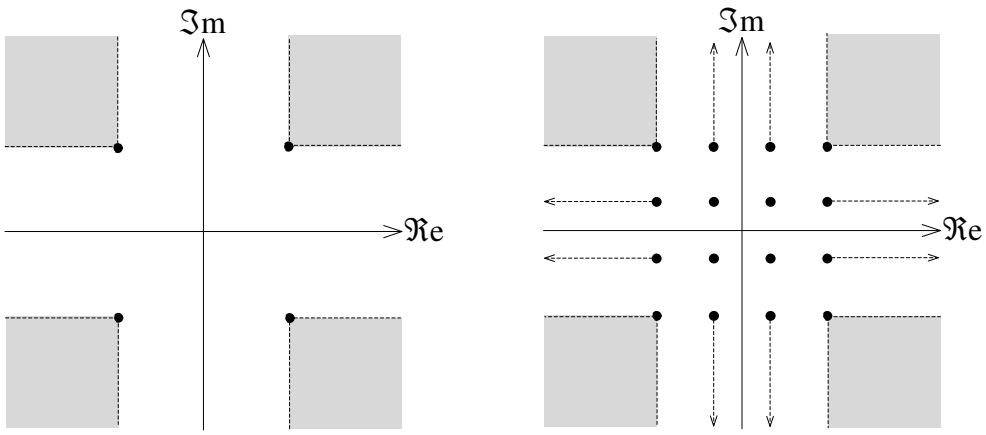

Figure 3.10 Feasible extension regions for QPSK constellation (left) and 16-QAM constellation (right).

significant. In the 16−QAM case, the exterior corner points have their corresponding shaded regions, while the exterior non-corner points are only allowed to move along the dashed lines (as depicted in Figure 3.10). While this approach reduces PAPR without considerable degradation in BER, it's application is limited for the case of using large constellations since the interior points cannot be relocated [2].

3.7 Summary

This chapter reviews different techniques that can be used for PAPR reduction. They can be categorized into two classes, namely signal distortion techniques and signal distortion-less techniques. The signal distortion techniques exploit a number of methods of distorting the signal to fit its dynamic range within some predetermined range with a sacrifice of some distortion in both in-band and out-band spectrum. Although most of the techniques in this category are very efficient in computational cost, their direct application in a complicated OFDM system with high-order QAM constellations becomes impractical due to restrictive requirements of spectral masks imposed by the standards. Because of this, techniques that can reduce PAPR without distorting the signals are of more interest in our research. However, almost all of the distortion-less PAPR reduction techniques require to solve some combinatorial optimization problems, which are not practically solvable because of the exponential-growth

order of the search space for optimum solutions. Thus there is active research to combine the principles of distortion-less techniques with the distortion techniques to create algorithms to reduce PAPR effectively with less computation efforts. The following chapter elaborates on one of the distortion-less techniques, the TR technique, and explores the possibility of combining the TR technique with clipping-and-filtering. It then proposes more efficient PAPR reduction algorithms for OFDM signals built from large QAM constellations.

4. Novel PAPR Reduction Techniques based on Tone Reservation

Tone reservation (TR) is an attractive and widely used method for PAPR reduction of OFDM signals because it does not require transmission of extra side information. This allows changes in the transmitter to be made independently of the receivers. This chapter discusses in more detail TR-based PAPR reduction techniques.

In the previous chapter, the TR problem is discussed in Section 3.5. Its optimal solution can be obtained by solving the quadratic constraints quadratic program (QCQP) for the complex baseband OFDM signal or the linear program for the real baseband OFDM signal. In this chapter, an approach to find peak-reduction signals in an iterative manner, called a gradient-based TR algorithm [36], is first discussed. Then, a clipping-and-filtering TR algorithm, which is a combination of the gradient-based TR algorithm and the clipping-and-filtering principle considered in Section 3.1, is presented.

The last two sections of this chapter propose two new algorithms. The first algorithm is performed in the time domain, whereas the second algorithm is a new clipping-and-filtering method. Both algorithms consist of two stages. The first stage, which is done off-line, creates a set of canceling signals based on the settings of the OFDM system. In particular, these signals are constructed to cancel signals at different levels of maximum instantaneous power that are above a predefined threshold. The second stage, which is online and iterative, reduces the signal peaks by using the canceling signals constructed in the first stage. When the reserved tones are distributed among the data tones, analysis and simulation results show that the proposed algorithms achieve slightly better PAPR reduction performance with significantly less complexity when compared to the conventional algorithms.

4.1 Conventional Gradient-Based TR (GTR) Algorithm

Recall that the optimal peak cancelling signal $c[n]$ is chosen to minimize the peak power of $y[n] = x[n] + c[n]$:

$$\begin{aligned} &\boldsymbol{C} = \arg \min_{\boldsymbol{C} \in \mathbb{C}^{NJ}} \left\{ \max_{0 \le n \le NJ-1} |x[n] + c[n]|^2 \right\} \\ &\text{subject to: } \mathcal{H}(\boldsymbol{C}) \le G, \end{aligned} \tag{4.1}$$

where $\mathbb{C}^{NJ}$ is the NJ-dimensional complex number space and $\mathcal{H}(\boldsymbol{v})$ denotes the Hamming weight of vector $\boldsymbol{v}$, which is the number of non-zero elements in $\boldsymbol{v}$.

As shown in Section 3.5, the optimization problem in (4.1) can be solved for the optimal solution using quadratic programming [54] but with high computational cost, which is not suitable for online processing. Instead of solving for the optimal canceling signal, one could find a canceling signal to bring the peak of $y[n]$ to be very close to some predefined threshold, $\mathcal{T}$. This is explained further below.

Given a threshold $\mathcal{T}$, introduce a clipping function [36]:

$$g_{\mathcal{T}}(\xi) = \begin{cases} \xi, & \text{if } |\xi| \le \mathcal{T} \\ \mathcal{T}\, \mathrm{e}^{j\angle\xi}, & \text{if } |\xi| > \mathcal{T} \end{cases} \tag{4.2}$$

where ξ is a complex variable. By applying the clipping function to $y[n]$, the problem in (4.1) is transformed into the following problem:

$$\begin{aligned} &\boldsymbol{C} = \arg \min_{\boldsymbol{C} \in \mathbb{C}^{NJ}} \left\{ \sum_{n=0}^{NJ-1} |x[n] + c[n] - g_{\mathcal{T}}\left(x[n] + c[n]\right)|^2 \right\} \\ &\text{subject to: } \mathcal{H}(\boldsymbol{C}) \le G. \end{aligned} \tag{4.3}$$

Let $\boldsymbol{f} = [f[0], \ldots, f[NJ-1]]$ be the residual signal after applying the clipping operation on $y[n]$. That is,

$$f[n] = y[n] - g_{\mathcal{T}}(y[n]) = x[n] + c[n] - g_{\mathcal{T}}\left(x[n] + c[n]\right). \tag{4.4}$$

The optimization problem in (4.3) tries to find $\boldsymbol{C}$ to minimize the power of $\boldsymbol{f}$. For this reason, $\boldsymbol{f}$ is also called the *clipping noise* associated with the signal $\boldsymbol{y}$, and the optimum $\boldsymbol{C}$ helps to create a signal with minimal level of this noise.

Note that $\boldsymbol{C}$ has only G non-zero elements with indices $i_0, \ldots, i_{G-1}$, which are also indices of reservation tones in $\mathcal{R}$. Define $\hat{\boldsymbol{C}} = [C[i_0], \ldots, C[i_{G-1}]]$ as a *coefficient vector* of a selected $\mathcal{R}$. One has:

$$\boldsymbol{c} = \boldsymbol{Q}\boldsymbol{C} = \boldsymbol{Q}_{\mathcal{R}}\hat{\boldsymbol{C}}; \quad c[n] = \boldsymbol{q}_n\boldsymbol{C} = \hat{\boldsymbol{q}}_n\hat{\boldsymbol{C}}, \tag{4.5}$$

where $0 \leq n \leq NJ-1$; $\boldsymbol{Q}_{\mathcal{R}}$ is a submatrix obtained from $\boldsymbol{Q}$ by keeping only columns that are defined in $\mathcal{R}$, and $\hat{\boldsymbol{q}}_n$ is the nth row of $\boldsymbol{Q}_{\mathcal{R}}$. The matrix $\boldsymbol{Q}_{\mathcal{R}}$ has dimensions $NJ \times G$ and it is given by:

$$\boldsymbol{Q}_{\mathcal{R}} = \frac{1}{\sqrt{JN}} \times \begin{bmatrix} 1 & 1 & \ldots & 1 \\ \mathrm{e}^{j2\pi\frac{i_0}{NJ}} & \mathrm{e}^{j2\pi\frac{i_1}{NJ}} & \ldots & \mathrm{e}^{j2\pi\frac{i_{G-1}}{NJ}} \\ \vdots & \vdots & \ddots & \vdots \\ \mathrm{e}^{j2\pi\frac{(NJ-1)i_0}{NJ}} & \mathrm{e}^{j2\pi\frac{(NJ-1)i_1}{NJ}} & \ldots & \mathrm{e}^{j2\pi\frac{(NJ-1)i_{G-1}}{NJ}} \end{bmatrix}_{NJ\times G}. \tag{4.6}$$

Using (4.2), the objective function in (4.3) can be written as:

$$\mathcal{N}(\hat{\boldsymbol{C}}) = \sum_{n\in\mathcal{S}} |x[n] + c[n] - \mathcal{T}\mathrm{e}^{j\angle(x[n]+c[n])}|^2 = \sum_{n\in\mathcal{S}} |x[n] + \hat{\boldsymbol{q}}_n\hat{\boldsymbol{C}} - \mathcal{T}\mathrm{e}^{j\angle\left(x[n]+\hat{\boldsymbol{q}}_n\hat{\boldsymbol{C}}\right)}|^2, \tag{4.7}$$

where $\boldsymbol{q}_n$ is the nth row of matrix $\boldsymbol{Q}$ as defined in (3.16) and $\mathcal{S}$ is the set of indices of those samples in $\boldsymbol{x} + \boldsymbol{c}$ having their magnitudes larger than $\mathcal{T}$. That is:

$$\mathcal{S} = \{n \ : \ |x[n] + c[n]| \geq \mathcal{T}\}.$$

The optimization problem in (4.3) thus can be rewritten as:

$$\boldsymbol{C} \equiv (\mathcal{R}, \hat{\boldsymbol{C}}) = \arg\min_{\mathcal{R}\in\Phi^G} \left\{ \min_{\hat{\boldsymbol{C}}\in\mathbb{C}^G} \left\{ \mathcal{N}\left(\hat{\boldsymbol{C}}\right) \right\} \right\}, \tag{4.8}$$

where $\Phi^G = \{0, \ldots, NJ-1\}^G$ is a $G-$dimensional integer number space. Equation (4.8) means that the solution to the problem in (4.3) can be derived in two steps [37]. The first step finds the best reservation tone set $\mathcal{R}$. Finding the reservation tone set which could provide the best peak reduction performance belongs to a class of combinatorial NP-hard optimization problems [37]. As such, only heuristic search for a near optimal solution is practical. Some well known techniques shall be discussed after the next subsection which discusses the second step. This step searches for the best coefficient vector $\hat{\boldsymbol{C}}$ with a given set $\mathcal{R}$ to obtain the best peak reduction performance.

4.1.1 Gradient Search for the Coefficient Vector

The coefficient vector $\hat{\boldsymbol{C}}$ that minimizes the objective function in (4.8) can be found using a gradient or steepest-decent method. Taking the gradient of $\mathcal{N}(\hat{\boldsymbol{C}})$ with respect to $\hat{\boldsymbol{C}}$ leads to [37]:

$$\nabla_{\hat{\boldsymbol{C}}}(\mathcal{N}) = 2\sum_{n\in\mathcal{S}}\left(x[n] + \hat{\boldsymbol{q}}_n\hat{\boldsymbol{C}} - \mathcal{T}\mathrm{e}^{j\angle\left(x[n]+\hat{\boldsymbol{q}}_n\hat{\boldsymbol{C}}\right)}\right)(\hat{\boldsymbol{q}}_n^*) \tag{4.9}$$

where $\hat{\boldsymbol{q}}_n^*$ is a complex conjugate vector of $\hat{\boldsymbol{q}}_n$.

The quadratic form of $\mathcal{N}(\hat{\boldsymbol{C}})$ makes it a complex multivariate function. The gradient at a specific point indicates the direction that the function would increase. Hence, based on the steepest-decent principle [54], the optimum $\hat{\boldsymbol{C}}$ can be approximately found by an iterative process. The process initializes with an initial value of $\hat{\boldsymbol{C}}_0 = \mathbf{0}_G$, where $\mathbf{0}_G$ is an length-G vector of all zeros. The frequency vector of the canceling vector is then constructed iteratively by:

$$\begin{aligned}\hat{\boldsymbol{C}}_{k+1} &= \hat{\boldsymbol{C}}_k - \frac{\lambda}{2}\nabla_{\hat{\boldsymbol{C}}_k}(\mathcal{N}) \\ &= \hat{\boldsymbol{C}}_k - \lambda\sum_{n\in\mathcal{S}_k}\left(x[n] + c_k[n] - \mathcal{T}\mathrm{e}^{j\angle(x[n]+c_k[n])}\right)(\hat{\boldsymbol{q}}_n^*)\end{aligned} \tag{4.10}$$

where λ is a step-size [36]; $c_k[n] = \hat{\boldsymbol{q}}_n\hat{\boldsymbol{C}}$ and

$$\mathcal{S}_k = \{n : |x[n] + c_k[n] \geq \mathcal{T}\} \tag{4.11}$$

is a set of indices of those samples in $(\boldsymbol{x} + \boldsymbol{c}_k)$ having their magnitudes larger than $\mathcal{T}$.

Multiplying both sides of (4.10) with $\boldsymbol{Q}_{\mathcal{R}}$ gives:

$$\boldsymbol{Q}_{\mathcal{R}}\hat{\boldsymbol{C}}_{k+1} = \boldsymbol{Q}_{\mathcal{R}}\hat{\boldsymbol{C}}_k - \lambda\sum_{n\in\mathcal{S}_k}\left(x[n] + c_k[n] - \mathcal{T}\mathrm{e}^{j\angle(x[n]+c_k[n])}\right)(\boldsymbol{Q}_{\mathcal{R}}\hat{\boldsymbol{q}}_n^*). \tag{4.12}$$

Let $\boldsymbol{c}_k = \boldsymbol{Q}_{\mathcal{R}}\hat{\boldsymbol{C}}_{k+1} = [c_k[0], \ldots, c_k[NJ-1]]$ be the length-NJ vector representing the peak canceling signal in the time domain at the kth iteration. Then (4.12) is equivalent to:

$$\boldsymbol{c}_{k+1} = \boldsymbol{c}_k - \lambda\sum_{n\in\mathcal{S}_k}\left(x[n] + c_k[n] - \mathcal{T}\mathrm{e}^{j\angle(x[n]+c_k[n])}\right)(\boldsymbol{Q}_{\mathcal{R}}\hat{\boldsymbol{q}}_n^*) \tag{4.13}$$

The term $\boldsymbol{Q}_{\mathcal{R}}\hat{\boldsymbol{q}}_n^*$ in (4.13) is a length-NJ vector which depends on the reservation tone set $\mathcal{R}$ and the sample index n.

From Equation (4.13), one has:

$$\begin{aligned}\boldsymbol{Q}_{\mathcal{R}}\hat{\boldsymbol{q}}_n^* &= \frac{1}{JN}\times\begin{bmatrix} 1 & 1 & \dots & 1 \\ \mathrm{e}^{j\frac{2\pi i_0}{NJ}} & \mathrm{e}^{j\frac{2\pi i_1}{NJ}} & \dots & \mathrm{e}^{j\frac{2\pi i_{G-1}}{NJ}} \\ \vdots & \vdots & \ddots & \vdots \\ \mathrm{e}^{j\frac{2\pi(NJ-1)i_0}{NJ}} & \mathrm{e}^{j\frac{2\pi(NJ-1)i_1}{NJ}} & \dots & \mathrm{e}^{j\frac{2\pi(NJ-1)i_{G-1}}{NJ}} \end{bmatrix}_{NJ\times G}\begin{bmatrix} \mathrm{e}^{-j2\pi\frac{ni_0}{NJ}} \\ \mathrm{e}^{-j2\pi\frac{ni_1}{NJ}} \\ \vdots \\ \mathrm{e}^{-j2\pi\frac{ni_{G-1}}{NJ}} \end{bmatrix}_{G\times 1} \\ &= \frac{1}{JN}\times\begin{bmatrix} \sum\limits_{i\in\mathcal{R}}\mathrm{e}^{j2\pi\frac{i(0-n)}{NJ}} \\ \sum\limits_{i\in\mathcal{R}}\mathrm{e}^{j2\pi\frac{i(1-n)}{NJ}} \\ \sum\limits_{i\in\mathcal{R}}\mathrm{e}^{j2\pi\frac{i(2-n)}{NJ}} \\ \vdots \\ \sum\limits_{i\in\mathcal{R}}\mathrm{e}^{j2\pi\frac{i[(NJ-1)-n]}{NJ}} \end{bmatrix}_{NJ\times 1}\end{aligned} \tag{4.14}$$

It can be seen easily that:

$$\boldsymbol{Q}_{\mathcal{R}}\hat{\boldsymbol{q}}_n^* = \circlearrowleft_{-n}\left(\boldsymbol{Q}_{\mathcal{R}}\hat{\boldsymbol{q}}_0^*\right) \tag{4.15}$$

where the operation $\circlearrowleft_i(\boldsymbol{v})$ represents a circular shift of a time vector $\boldsymbol{v}$ by i samples to the right.

Define an length-NJ vector $\boldsymbol{k} = [k[0], \dots, k[NJ-1]]^T$ as:

$$\boldsymbol{k} = \frac{JN}{|\mathcal{R}|}\boldsymbol{Q}_{\mathcal{R}}\hat{\boldsymbol{q}}_0^* \tag{4.16}$$

where $|\mathcal{R}|$ is the cardinality of set $\mathcal{R}$. The vector $\boldsymbol{k}$ is called a *kernel* [36], whose values only depend on the tone reservation set $\mathcal{R}$. It can be shown that $\boldsymbol{k}$ can be obtained by setting the magnitudes of the reserved tones to 1 and then performing an *inverse discrete Fourier transform* (IDFT) [36]. That is:

$$k[n] = \frac{1}{|\mathcal{R}|}\sum_{\ell=0}^{NJ-1} p[\ell]\mathrm{e}^{j2\pi\frac{n\ell}{NJ}},\ 0\le n\le NJ-1, \tag{4.17}$$

where

$$p[\ell] = \begin{cases} 1, & \text{if } \ell\in\mathcal{R} \\ 0, & \text{otherwise} \end{cases}. \tag{4.18}$$

The kernel has its peak magnitude sample at 0 index, which means $k[0] = 1$ and

$$|k[n]| = \frac{1}{|\mathcal{R}|}\left|\sum_{\ell=0}^{NJ-1} p[\ell]\mathrm{e}^{j2\pi\frac{n\ell}{NJ}}\right| \leq \frac{1}{|\mathcal{R}|}\left|\sum_{\ell=0}^{NJ-1} p[\ell]\right| = \frac{|\mathcal{R}|}{|\mathcal{R}|} = 1 \tag{4.19}$$

where $0 \leq n \leq NJ-1$. Examples of kernel signals for different values of G, i.e., different numbers of reservation tones, are given in Figures 4.1 and 4.2.

It is important to note that the magnitudes of the kernel signal only depend on the relative locations of its tones. The relative locations are defined by the differences between the tone indices. If two sets have the same relative locations, the values of tone indices in any set can be obtained from the values of tone indices in the other set by a circular shift. As an example, two sets having the same relative locations can be represented as $\mathcal{R}_1 = \{i_0, i_1, \ldots, i_{G-1}\}$ and $\mathcal{R}_2 = \{(\zeta + i_0), (\zeta + i_1), \ldots, (\zeta + i_{G-1})\}$, where ζ represents the number of shifted locations. Then their corresponding kernel signals, $\boldsymbol{k}_1$ and $\boldsymbol{k}_2$, respectively have the same magnitude for every sample. That is:

$$k_2[n] = \frac{1}{G}\sum_{i\in\mathcal{R}_2} \mathrm{e}^{j2\pi\frac{ni}{NJ}} = \frac{1}{G}\sum_{i\in\mathcal{R}_1} \mathrm{e}^{j2\pi\frac{n(i+\zeta)}{NJ}} = \mathrm{e}^{j2\pi\frac{n\zeta}{NJ}}\frac{1}{G}\sum_{i\in\mathcal{R}_2} \mathrm{e}^{j2\pi\frac{ni}{NJ}} = \mathrm{e}^{j2\pi\frac{n\zeta}{NJ}}\, k_1[n]$$

or $|k_1[n]| = |k_2[n]|$ for $0 \leq n \leq NJ-1$.

Next, define $\alpha_{k,i}$ as:

$$\alpha_{k,i} = \left(|x[i] + c_k[i]| - \mathcal{T}\right)\mathrm{e}^{j\angle(x[i]+c_k[i])} \tag{4.20}$$

Equation (4.13) hence can be rewritten as:

$$\boldsymbol{c}_{k+1} = \boldsymbol{c}_k - \gamma\sum_{n\in\mathcal{S}_k} \alpha_{k,n}\circlearrowleft_n(\boldsymbol{k}) \tag{4.21}$$

where $\gamma = \frac{\lambda JN}{|\mathcal{R}|}$. The peak reduced signal after performing k iterations is therefore:

$$\boldsymbol{y}_k = \boldsymbol{x} + \boldsymbol{c}_k \tag{4.22}$$

For illustration, a single step of peak reduction using a peak cancelling signal generated from a kernel signal is shown in Figure 4.3. To reduce a signal peak, all samples neighbouring the peak with magnitudes exceeding threshold $\mathcal{T}$ are determined. For each of these samples,

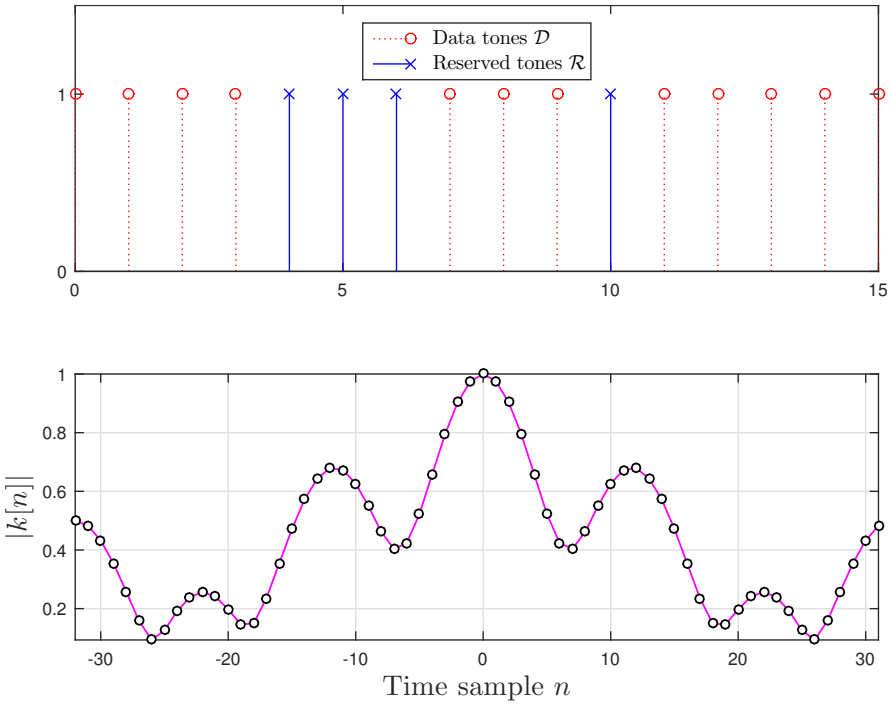

Figure 4.1 An example of a kernel signal with $N = 16, J = 4, G = 4$.

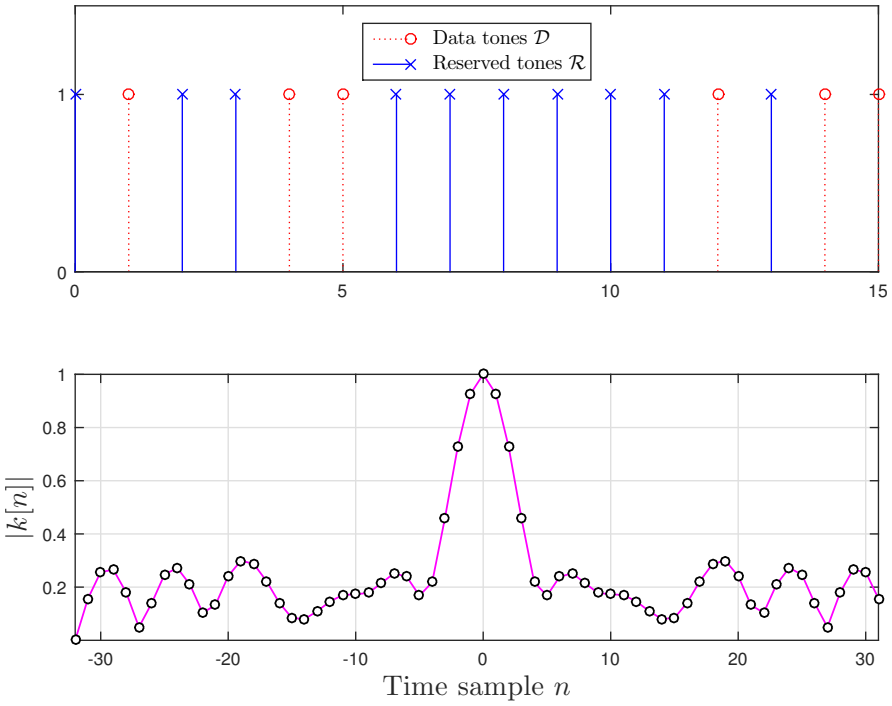

Figure 4.2 An example of a kernel signal with $N = 16, J = 4, G = 10$.

a sub-canceling signal is formed by cyclically shifting the kernel to align with the sample index and scaled with some appropriate factor. The peak cancelling signal is then made by

adding all these sub-canceling signals in the time domain. Since this process only cares about the samples around the peak, it can suppress the selected peak as well as its surrounding samples but does not guarantee that other samples of the signal after this addition have their magnitudes below $\mathcal{T}$. It is possible that after adding with the canceling signal, the resulting signal has new peaks. This is often referred to as *peak regrowth* [2], which requires extra steps of the peak reduction algorithm.

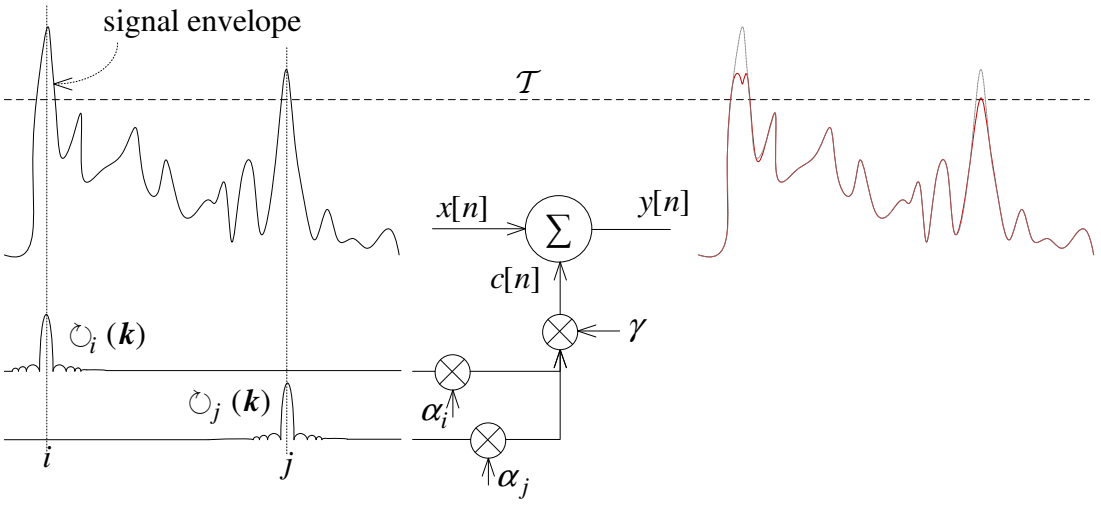

Figure 4.3 Peak reduction using kernel signals.

The number of iterations required for peak reduction is therefore determined by the amount of peak regrowth occurs after each step of the algorithm. If the peaks regrow more often after each iteration, the algorithm would *diverge*. In a diverged state, the complexity of the GTR algorithm grows after each iteration due to the increase in the number of peaks and accordingly the number of samples above the threshold. On the contrary, the algorithm is in a *converged* state when the amount of peak regrowth is reduced after each application of the algorithm.

There are two factors that affect the convergence rate of the GTR algorithm, which are the kernel signal and the scaling factors [2]. A number of proposals thus have been suggested in the literature to either optimize the kernel signal for better peak reduction performance, or adaptively change the scaling factors so that the peak regrowth would be less likely to occur [56–60]. The following discussions are dedicated to some well known methods to

construct the kernel signal, whereas Section 4.2 presents a conventional approach that finds the optimal value of the scaling factors after each iteration of the peak reduction algorithm.

Ideally, if the kernel signal is an impulse, the addition with the kernel signal only affects the sample that it aligns to without modifying the neighbouring samples. This results in no peak regrowth after each iteration of the algorithm. However this type of kernel signal occupies the whole spectrum, which is not acceptable. Therefore, a more practical choice is to select kernel signals whose secondary peaks or side-lobes are minimized.

4.1.2 Search for the Kernel Signal

Since the kernel signal is defined by the set of reservation tones, a search for a suitable kernel signal is thus equivalent to a search for a suitable set $\mathcal{R}$. The objective of finding an optimal set $\mathcal{R}$ can be expressed as [37]:

$$\mathcal{R}^{\text{opt}} = \arg \min_{\mathcal{R} \in \Phi^G} \Big\{ |k[J]|, |k[J+1]|, \ldots, |k[J(N-1)]| \Big\} \tag{4.23}$$

where $\mathcal{R} = \{i_0, i_1, \ldots, i_{G-1}\}$ and Φ^G is a G-dimensional integer number space.

The problem in (4.23) is an NP-hard optimization problem [37, 54], which is practically unsolvable. The total number of possible outcomes for $\mathcal{R}$ is G^{NJ}, and is extremely large for an exhaustive search, even for a small number of reserved tones. Because of this, a number of different heuristical search techniques have been proposed to find a near optimal set $\mathcal{R}$. Some well known techniques are: using kernel signal variance [61], using a genetic algorithm [62], using a probabilistic search [63], or generating tone sets from sequences with good correlation properties [2].

Simple Selection Methods [37]

Before discussing some heuristically generated kernels or reservation sets $\mathcal{R}$, it is worthwhile to mention some simple selection methods. The easiest way is to pick a set of consecutive tones, which occupy a contiguous region in the spectrum. By adding a number of consecutive frequency tones, the kernel signal has a shape of a *sinc* function, whose main lobe's width is determined by the width of the selected region. To make the main lobe sharper in the time domain, a bigger region of tones is required, which is usually prohibited

by the standards.

Another method is to select equally-spaced tones, which is equivalent to zero-padding a set of consecutive tones. A kernel constructed from an equally spaced tones has a sharper lobe when compared to the kernel built from consecutive tones. However, multiple peaks are generated in the time domain. Thus, such a kernel is not recommended since the addition of the kernel with the original OFDM signal affects not only the peak-magnitude sample but also those samples located at secondary peaks.

The most widely-used method is to select G reserved tones in a random manner. By randomly spreading the reservation tones amongst the data tones, the obtained kernel generally does not exhibit high secondary peaks and has a smaller main lobe width when compared to the case of using consecutive tones.

Some example kernels developed from three sets of reservation tones namely, a set of randomly selected tones, a set of equally spaced tones, and a set of contiguous tones, are shown in Figure 4.4. Notice that the kernel generated using equally-spaced tones has multiple peaks. Figure 4.5 shows a comparison of PAPR reduction using these reservation tones with the conventional GTR algorithm. It can be seen that using randomized reservation tones provides the best peak reduction performance.

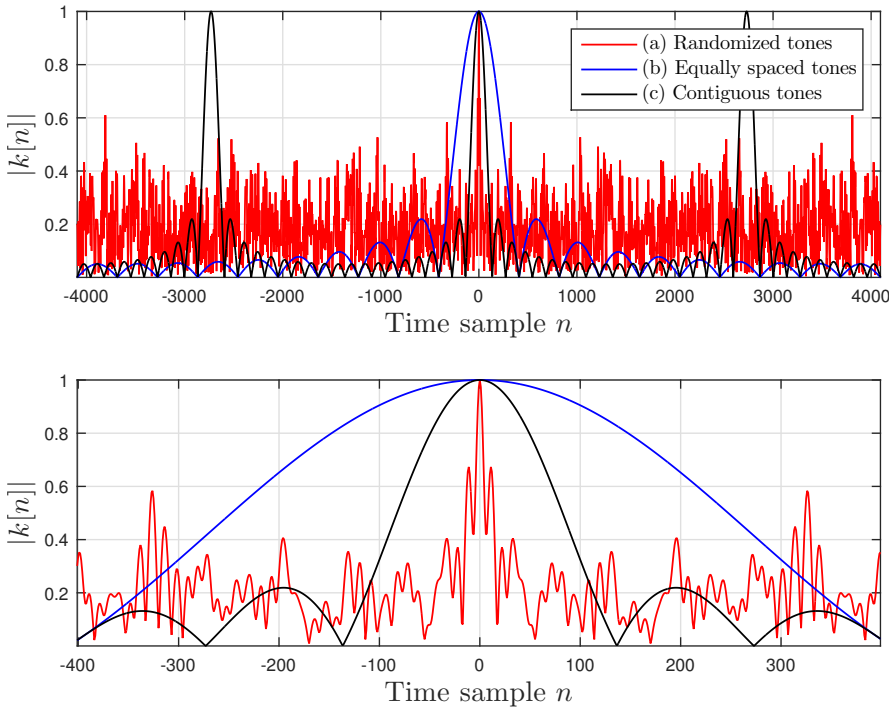

Figure 4.4 Comparison of kernel signals generated from different reservation tone sets with $N = 1024, J = 8, G = 20$: (a) randomized tones, (b) equally spaced tones, (c) contiguous tones.

Kernel Variance Based Search [61]

The authors in [61] propose a simple heuristical search method to find a near optimum kernel based on the relationship between the secondary peaks and variance of the kernel. Numerical results in [61] reveal that the time-domain kernels having the same variance can have various secondary peaks and the values of the secondary peaks statistically tend to decrease as the variance decreases. For completeness, a detailed derivation of this method can be found in Appendix 5.2.

In summary, the kernel variance is given by:

$$\sigma^2 = \frac{8}{NJG^2} \sum_{\tau=1}^{N-1} R_\tau^2 \tag{4.24}$$

where R_τ denotes the *aperiodic autocorrelation function (APCF)* of the sequence $p[\ell]$ defined

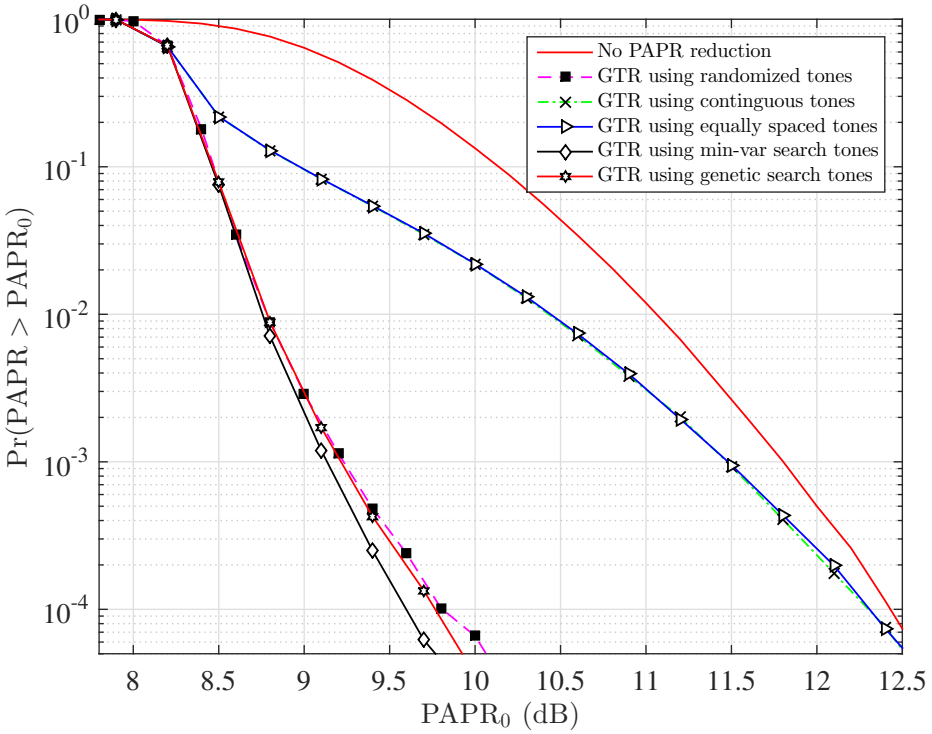

Figure 4.5 Comparison of PAPR reduction using the conventional GTR algorithm with $N = 1024, J = 8, \mathcal{T} = 8$dB for different sets of reservation tones: (a) randomized tones, (b) equally-spaced tones, (c) contiguous tones, (d) variance-based search tones, (e) genetic search tones.

in (4.18). It is given as:

$$R_\tau = \sum_{m=0}^{NJ-1-\tau} p[m]p[m+\tau] \tag{4.25}$$

where $0 \leq \tau \leq NJ - 1$.

Note from (4.25) that R_τ is calculated by multiplying two binary sequences. Therefore, the kernel variance given in (4.24) can be effectively implemented using logical ANDs.

A kernel variance based search algorithm to find a near optimal set $\mathcal{R}$ is outlined next [61].

Kernel Variance Based Search

1. Population generation: Generate a sufficient large number of sets with G tones, calculate the corresponding kernel variances of them using (4.24), and sort them in an increasing order.

2. Extraction of good candidates: Select a small percentage (around 1% [61]) of the generated sets having smallest variance values, which is denoted as Φ_σ.

3. Search for minimal secondary peaks: Choose a set from those selected sets that gives the kernel with the smallest level of secondary peaks, that is:

$$\mathcal{R}_\sigma = \arg \min_{\mathcal{R} \in \Phi_\sigma} \Big\{ |k[J]|, |k[J+1]|, \ldots, |k[J(N-1)]| \Big\}. \tag{4.26}$$

Genetic Based Kernel Search [62]

The idea basically is to create a search scheme resembling the principles of biological evolution observed in nature. The algorithm, so called a *genetic algorithm*, is proposed in [62]. Its detailed description is given in Appendix 5.2. In summary, the search procedure consists of four steps as outlined next.

Genetic Based Kernel Search

1. Parent population generation: A small number of sequences $p[\ell]$ is randomly generated to make a set of parent sequences.

2. Ranking parent sequences: Corresponding kernels are generated from the parent sequences, and ranked by their merit factors, which measure levels of secondary magnitude peaks.

3. Crossover and mutate: There are two processes in this step. The first process, called a *crossover*, makes every two parent sequences exchange parts of their bodies to make two new sequences, which are then called offspring sequences. The second process is to mutate the offsping sequences by randomly adding, inserting, deleting, switching some locations in the offspring sequences.

4. Ranking offspring sequences: After the third step, the population grows bigger as more offsping sequences are generated. Their corresponding kernels are generated, and ranked based on their merit factors. Only the sequences having the highest merit factors are kept to become the next parent sequences. The search then continues again with Step 3 until the maximum number of iterations N_{it} is reached.

It is shown in [62] that the genetic based search provides the same kernel performance as the kernel from variance-based search while being simpler in implementation.

Figure 4.6 shows a comparison in the time domain between the kernel generated using the same randomized tone set as in Figure 4.4 and the kernels generated from two sets of tones found with the variance-based and genetic approaches. In the variance-based search, 10^4 random sets with $G = 20$ tones are generated and ranked. Of which, only 20 sets with the highest ranking factors are selected to search for the lowest side-lobe level (see (4.26)). On the other hand, for the genetic search, the initial population size of parent sequences was selected to be $N_{\wp} = 30$, the number of revolutions (i.e., iterations) was $N_{\text{it}} = 10$, and the crossing rate was $\epsilon = 0.8$ (see Appendix 5.2 for explanations of these numbers).

CCDF curves of PAPR reduction performance obtained using variance-based search and genetic-based search kernels are also plotted in Figure 4.5. It can be seen that an improvement of 0.5 dB of PAPR reduction can be achieved at the probability of 10^{-4} by using a kernel from the variance-based search when compared to the performance of using only a randomized kernel. Note that the kernel selection is performed offline. So a complicated search for a good kernel can be conducted without affecting the processing costs of the online peak reduction algorithms.

4.1.3 Conventional GTR Algorithm

In summary, the so-called *gradient-based tone reservation* (GTR) algorithm outlined next consists of two parts. The first part is initialization, which is typically executed once. The second part, which is a run-time part, is executed online that uses the signal constructed from the first part to iteratively reduce the signal peaks. The process stops when either a maximum

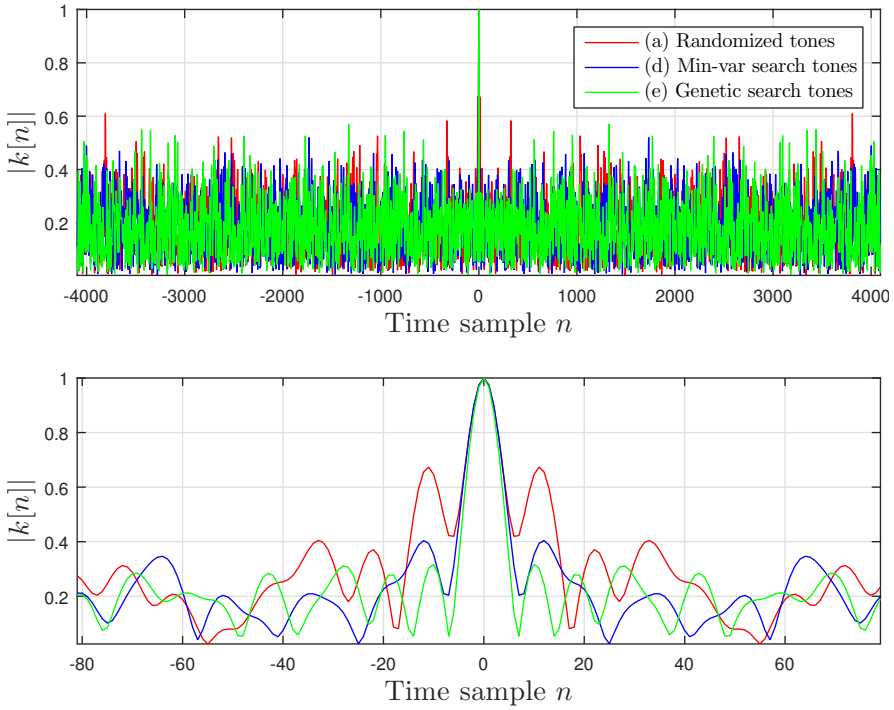

Figure 4.6 Comparison of kernel signals generated from different reservation tone sets with $N = 1024, J = 8, G = 20$: (a) randomized tones, (d) variance-based search tones, (e) genetic search tones.

number of iterations is reached or no peak above $\mathcal{T}$ in $\boldsymbol{y}_k$ is found, i.e., $\max|\boldsymbol{y}_k| < \mathcal{T}$.

GTR Initialization Phase

(i) THRESHOLD SELECTION: Select the target PAPR level or equivalently the desired magnitude threshold $\mathcal{T}$. The target PAPR is largely dependent on the required transmit power [2].

(ii) $\mathcal{R}$ SELECTION: Choose the set of reserved tones $\mathcal{R}$ in accordance with data transmission tones $\mathcal{D}$.

(iii) KERNEL GENERATION: Generate a kernel vector $\boldsymbol{k}$ using (4.17).

GTR Run-Time Phase

(i) INPUT: Symbol vector $\boldsymbol{x}$; Kernel vector $\boldsymbol{k}$; Threshold $\mathcal{T}$; Number of iterations N_{it}.

(ii) INITIALIZATION:

- Loop variable $k = 1$; $\boldsymbol{c}_k = 0$.
- Fix a constant γ.

(iii) LOOP_BEGIN:

- Determine the set of all samples whose magnitudes are larger than $\mathcal{T}$ as defined in (4.11).
- Update $\boldsymbol{c}_{k+1}$ using (4.20) and (4.21).

(iv) LOOP_END:

- IF $(k > N_{\text{it}})$ RETURN $\boldsymbol{y}_{k+1} = \boldsymbol{c}_{k+1} + \boldsymbol{x}$
- ELSEIF $\max |\boldsymbol{y}_{k+1}| \leq \mathcal{T}$ RETURN $\boldsymbol{y}_{k+1}$
- ELSE $k = k + 1$, jump LOOP_BEGIN

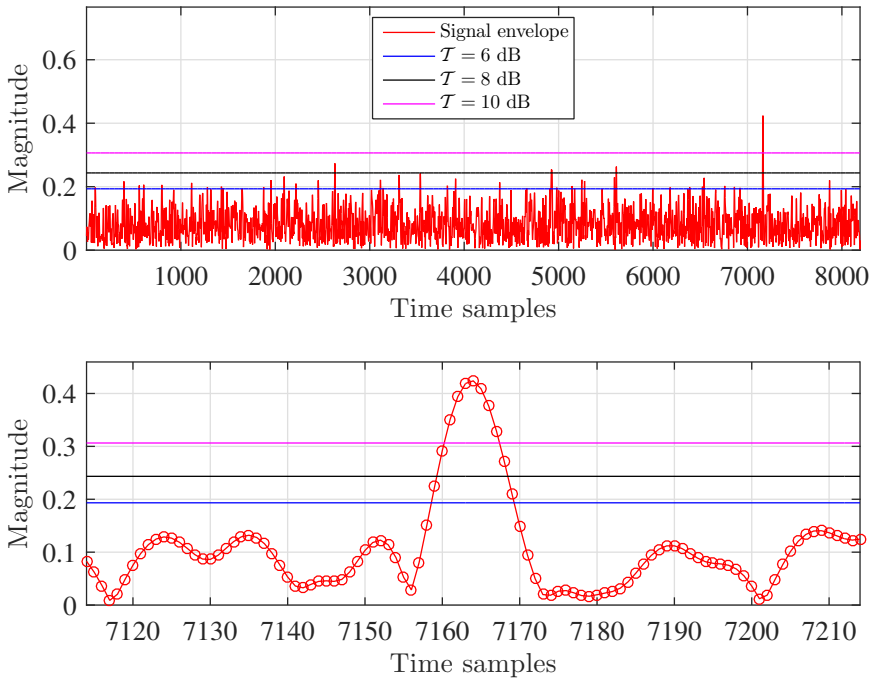

Figure 4.7 A time-domain view of an OFDM symbol ($N = 1024, J = 8$) with different levels of threshold: $\mathcal{T} = 6$, 8 and 10 dB.

Complexity Analysis

The GTR algorithm works with time-domain samples and utilizes a large number of multiplications and additions per iteration. The calculation of $\alpha_{k,i}$ needs $2|\mathcal{S}_k|$ real multiplications (see (4.11)). The scaling with $\alpha_{k,i}$ and γ in (4.13) requires additional $4|\mathcal{S}_k|JN+4JN$ complex multiplications. So in total, the number of multiplications per iteration of the GTR algorithm is $4|\mathcal{S}_k|JN+2|\mathcal{S}_k|+4JN$. The number of additions required by the GTR algorithm is $|\mathcal{S}_k|JN+1$ for each iteration, which is in the same order as the number of multiplications. Moreover, it should be pointed out that γ is defined as a constant in [36, 37] and how to properly choose its value is not thoroughly studied in the literature. A large value of γ could cause the algorithm not to converge as the set $\mathcal{S}_k$ grows larger after each iteration, whereas a small value of γ makes the algorithm to converge slowly.

CCDF curves showing the PAPR reduction performance of the GTR algorithm using randomized sets of reservation tones for different target PAPR levels are shown in Figures 4.8 to 4.13. In each simulation, 10^6 OFDM symbols are generated using 1024-QAM constellation, 1024-point IFFT block ($N = 1024$), and an oversampling factor $J = 8$. Two different numbers of reserved tones are simulated and all of them are generated randomly for simplicity. The first case considers $G = 50$ tones, which are approximately 5% of the available tones, making the number of data tones to be $N-G = 1024-50 = 974$. The second case considers $G = 100$ tones and the corresponding number of data tones is $N - G = 1024 - 100 = 924$.

The sharpness of CCDF curves is strongly affected by the target PAPR level, the value of γ and the number of reservation tones used. A lower threshold of the target PAPR causes the algorithm to run significantly slower as the number of samples crossing $\mathcal{T}$ is considerably larger[1]. Figure 4.7 shows the time-domain plot of an example OFDM symbol with different levels of $\mathcal{T}$ measured in dB with respect to the average symbol power. It can be seen that with a lower threshold, more peaks have crossed the threshold as well as there is a larger number of over-threshold samples, resulting in a bigger set $\mathcal{S}_k$ at the kth iteration of the PAPR reduction loop in the conventional GTR algorithm. This slows down the processing

[1]This can be shown by the level-crossing theory, whose explanation is out of the scope of this thesis. Interested readers can refer to [64] and [65] for more information.

since more cyclic shifting needs to be performed and a larger number of kernels are used to cancel peaks crossing the threshold. This also means that larger numbers of multiplications and additions are required.

With a target PAPR of 6 dB and $G = 50$ tones, the best peak performance is at $\gamma = 0.15$. On the other hand, with $G = 100$, the best performance corresponds to $\gamma = 0.2$ or $\gamma = 0.25$. In addition, in both cases, using the largest values of γ, that is $\gamma = 0.5$ and $\gamma = 1$, leads to the poorest reduction performance. Moreover, although targeting at a clipping level of 6 dB, at the probability of 10^{-4}, the PAPR level can only be reduced to around 9 dB and 8.3 dB by using 5% and 10% of available tones, respectively. This is almost the same performance by setting the target threshold at 8 dB as shown in Figures 4.10 and 4.11. As the target threshold increases, using a bigger value of γ provides a better peak reduction performance after 2 iterations. At $\mathcal{T} = 10$ dB, $\gamma = 1$ appears to be the best scaling factor. Moreover, Figures 4.12 and 4.13 reveal that at this high level of $\mathcal{T}$, using a larger number of reserved tones shows no significant increase in PAPR reduction performance.

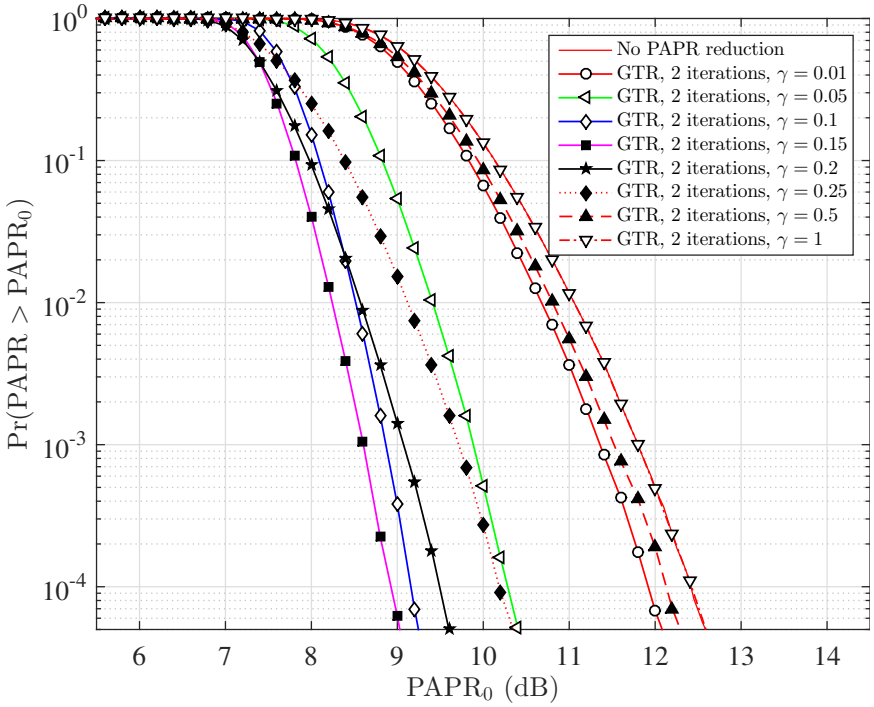

Figure 4.8 Comparison of PAPR reduction of the GTR algorithm using a randomized set of $G = 50$ tones ($G/N \approx 5\%$) with a target PAPR of $\mathcal{T} = 6$ dB.

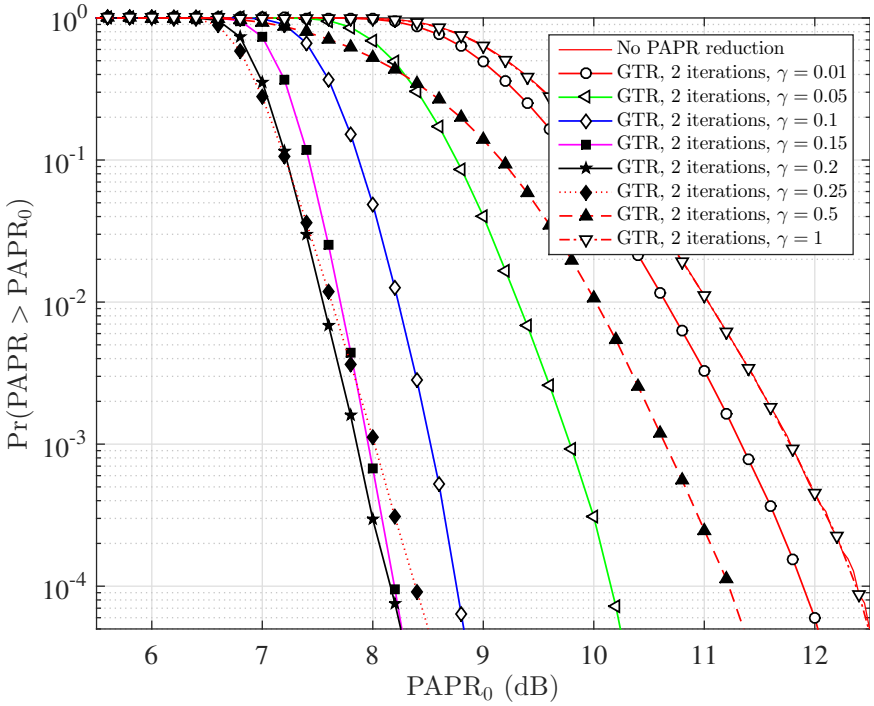

Figure 4.9 Comparison of PAPR reduction of the GTR algorithm using a randomized set of $G = 100$ tones ($G/N \approx 10\%$) with a target PAPR of $\mathcal{T} = 6$ dB.

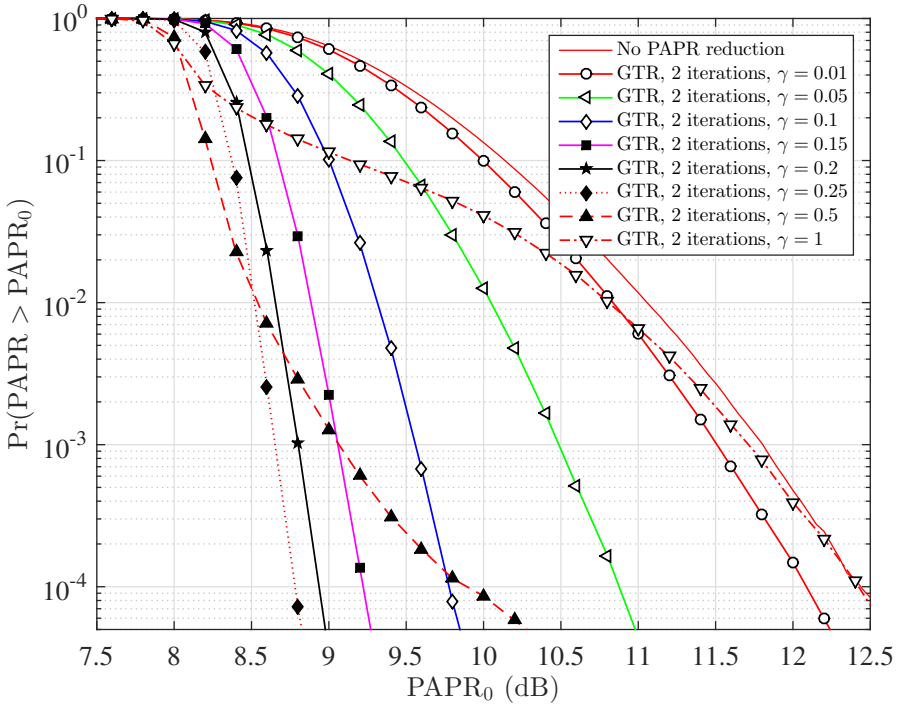

Figure 4.10 Comparison of PAPR reduction of the GTR algorithm using a randomized set of $G = 50$ tones ($G/N \approx 5\%$) with a target PAPR of $\mathcal{T} = 8$ dB.

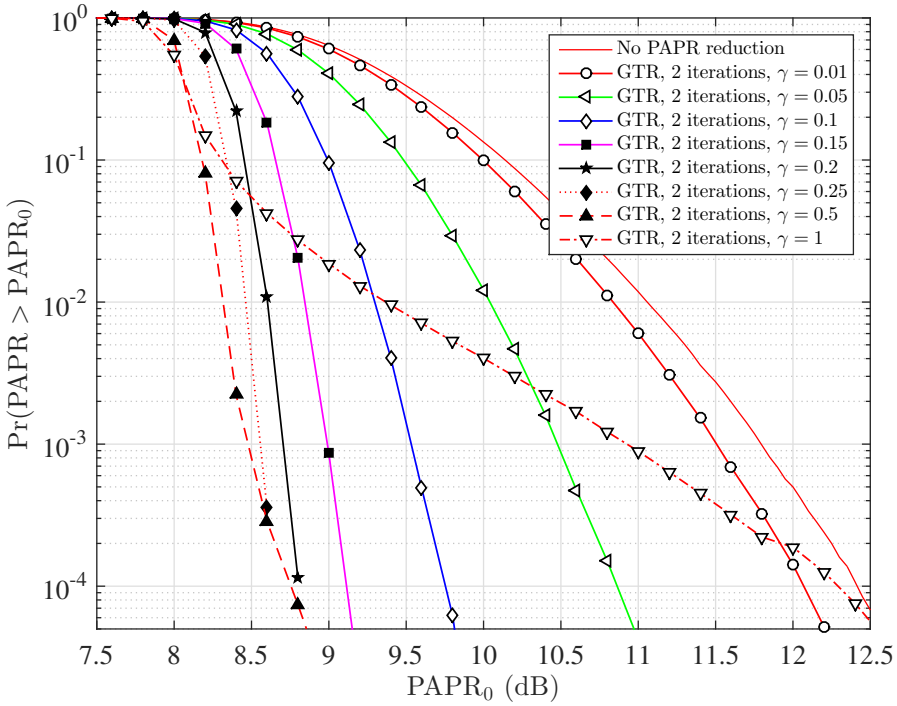

Figure 4.11 Comparison of PAPR reduction of the GTR algorithm using a randomized set of $G = 100$ tones ($G/N \approx 10\%$) with a target PAPR of $\mathcal{T} = 8$ dB.

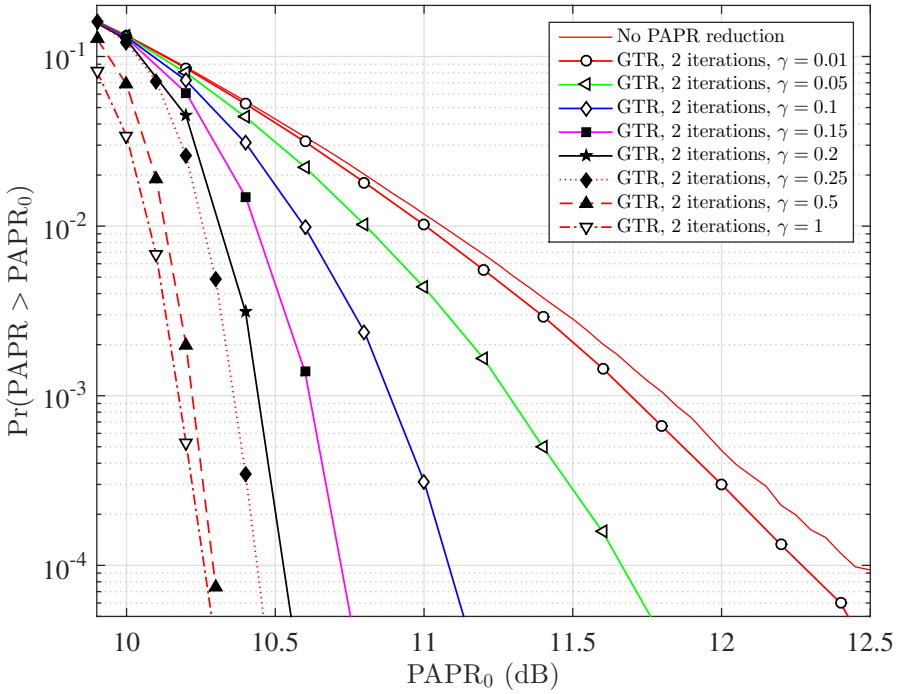

Figure 4.12 Comparison of PAPR reduction of the GTR algorithm using a randomized set of $G = 50$ tones ($G/N \approx 5\%$) with a target PAPR of $\mathcal{T} = 10$ dB.

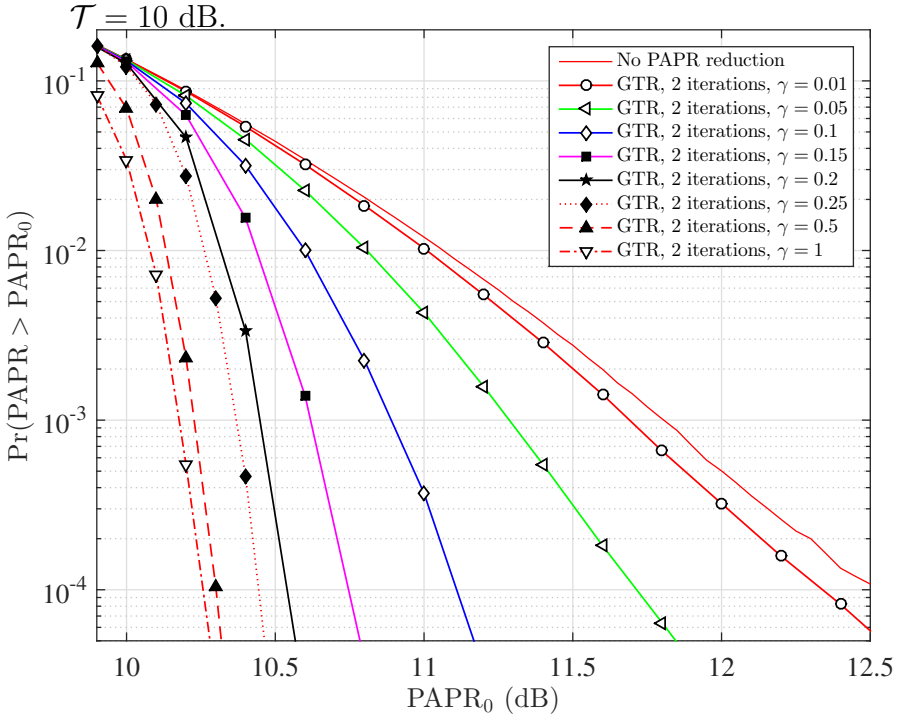

Figure 4.13 Comparison of PAPR reduction of the GTR algorithm using a randomized set of $G = 100$ tones ($G/N \approx 10\%$) with a target PAPR of $\mathcal{T} = 10$ dB.

4.2 Conventional Clipping-And-Filtering TR (CFTR) Algorithms

The high complexity of the GTR algorithm could be reduced by applying clipping-and-filtering the clipping noise defined in (4.4). Filtering the clipping noise, however, might cause distortions to the data tones. Thus, filtering is implemented so that only the frequency portion of the clipping noise that corresponds to locations of the reserved tones is kept. That is, the filter is defined as:

$$H(\mathrm{e}^{j\omega}) = \begin{cases} 1, & \text{if } \omega \in \mathcal{R} \\ 0, & \text{otherwise.} \end{cases} \tag{4.27}$$

In other words, the filtering operation in (4.27) is simply a projection on the reserved tone set. Hence, a signal obtained after filtering the clipping noise is:

$$\boldsymbol{c} = \mathcal{F}^{-1}\left\{H\left(\mathcal{F}\{\boldsymbol{f}\}\right)\right\}, \tag{4.28}$$

where $\mathcal{F}$ denotes the discrete Fourier transform (DFT) and $\mathcal{F}^{-1}$ is the inverse DFT (IDFT). The canceling vector $\boldsymbol{c}$ is then scaled by a factor β to further suppress the peak of the resulting signal [51, 62]. That is,

$$\boldsymbol{y} = \boldsymbol{x} - \beta\boldsymbol{c}. \tag{4.29}$$

The factor β is chosen to minimize the mean squared error between the canceling signal and clipping noise:

$$\beta = \arg\min_{\beta} \sum_{n\in\mathcal{S}} |f[n] - \beta c[n]|^2 \tag{4.30}$$

where $\mathcal{S}$ represents the set of the peak samples. Two methods of selecting this set which are proposed in [51] and [62] are:

$$\begin{aligned} \mathcal{S}_{\,[51]} &= \{n : |x[n]| > \mathcal{T}\}, \\ \mathcal{S}_{\,[62]} &= \{n : (|x[n]| > |x[n-1]|);\ (|x[n]| > x[n+1]|\}, \end{aligned} \tag{4.31}$$

where $0 \le n \le NJ - 1$. In other words, $\mathcal{S}_{\,[51]}$ defines the set of over-threshold samples, whereas $\mathcal{S}_{\,[62]}$ denotes the set of all local peak magnitude samples. In this thesis, $\mathcal{S}_{\,[51]}$ is used since it resembles the set $\mathcal{S}_k$ used in the GTR algorithm discussed previously in (4.11).

A solution to the problem in (4.30) is given by [51]:

$$\beta = \frac{\Re\left[\sum\limits_{n\in\mathcal{S}} f[n]c^*[n]\right]}{\sum\limits_{n\in\mathcal{S}} |c[n]|^2}, \tag{4.32}$$

where $c^*[n]$ is a complex conjugate of $c[n]$. It is pointed out that, due to the effect of the filter $H(\mathrm{e}^{j\omega})$, the peak of the signal after the filter regrows significantly. As a consequence, multiple iterations of the clipping-and-filtering are required to obtain satisfactory PAPR reduction. The algorithm is illustrated in Figure 4.14.

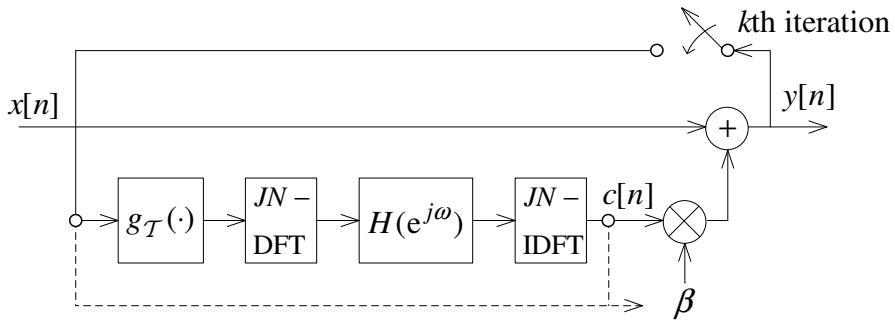

Figure 4.14 Conventional clipping-and-filtering TR algorithm.

For completeness, the CFTR algorithm in run-time is described in the following.

CFTR Run-Time

(i) INPUT: Symbol vector $\boldsymbol{x}$; Kernel vector $\boldsymbol{k}$; Threshold $\mathcal{T}$; Number of iterations N_{it}.

(ii) INITIALIZATION:

- Loop variable $k = 1$; $\boldsymbol{c}_k = 0$.
- Fix a constant γ.

(iii) LOOP_BEGIN:

- Find the clipping noise by

$$\boldsymbol{f}_k = \boldsymbol{y}_k - g_{\mathcal{T}}(\boldsymbol{y}_k) \tag{4.33}$$

where $g_{\mathcal{T}}(\cdot)$ is defined in (4.2).

- Construct the canceling signal

$$\boldsymbol{c}_k = \mathcal{F}^{-1}\left\{H\left(\mathcal{F}\{\boldsymbol{f}_k\}\right)\right\} \tag{4.34}$$

  using $H(\cdot)$ in (4.27).

- Construct the set $\mathcal{S}_k$ as in (4.11).

- Calculate the scaling factor

$$\beta_k = \frac{\Re\left[\sum\limits_{n\in\mathcal{S}_k} f_k[n]c_k^*[n]\right]}{\sum\limits_{n\in\mathcal{S}_k}|c_k[n]|^2}$$

- Update the peak reduced signal

$$\boldsymbol{y}_{k+1} = \boldsymbol{x} - \beta_k \boldsymbol{c}_k \tag{4.35}$$

(iv) Loop_End:

- If $(k > N_{\text{it}})$ return $\boldsymbol{y}_{k+1}$
- Elseif $\max|\boldsymbol{y}_{k+1}| \leq \mathcal{T}$ return $\boldsymbol{y}_{k+1}$
- Else $k = k+1$, jump Loop_Begin

Complexity Analysis

The complexity of the CFTR algorithm depends mainly on the $JN-$point DFT/IDFT pair and weighting the canceling signal in (4.29). The former can be efficiently implemented by FFT/IFFT, which has a complexity of $\mathcal{O}(JN\log(JN))$. The latter needs $4|\mathcal{S}|$ real multiplications, one real division for the calculation of β in (4.32) and $2JN$ real multiplications to scale the time vector $\boldsymbol{c}$. In total, per iteration, the CFTR algorithm requires 1 real division and $(\mathcal{M}_{\text{DFT}} + \mathcal{M}_{\text{IDFT}} + 4|\mathcal{S}| + 2JN)$ multiplications, with $\mathcal{M}_{\text{DFT}}, \mathcal{M}_{\text{IDFT}}$ multiplications are used in the DFT/IDFT blocks.

The CFTR algorithm can be equivalently transformed into the conventional GTR algorithm. The derivation in Appendix 5.2 shows that β_k (in (4.35) acts equivalently as an adaptive scaling factor γ as in (4.21) of the conventional GTR algorithm. Utilizing a pair

of DFT/IDFT, the CFTR algorithm helps to reduce the complexity of the GTR algorithm. However, its complexity is still too high and can be further reduced.

The simulation results that compare the performance of the conventional CFTR with the conventional GTR algorithm are provided in Section 4.5.

The following two sections propose two new PAPR reduction algorithms. The first algorithm works in the time domain, aiming to improve the performance of the GTR algorithm. The second algorithm is performed in the frequency domain to reduce the complexity of the CFTR algorithm.

4.3 Proposed Time-Domain Algorithm

The main idea of the proposed time-domain algorithm is to create a database of canceling signals for different levels of peak magnitudes, then reuse them to reduce the peaks of symbols having similar magnitudes. This is done in two stages. The first stage is called a learning stage, which initializes a set of peak-reduction signals corresponding to clipping noise of different maximum magnitudes. The second stage is an online process, which combines the conventional TR and some pre-processing steps using the canceling signals developed in the first stage.

Provided that $\mathcal{T}$ is large enough, the authors in [64] show that the clipping noise defined in (4.4) can be approximated by a sum of constant-phase parabolic pulses and each pulse has one local minimum or maximum. As an example, Figure 4.15 plots a symbol having one dominant peak above $\mathcal{T}$ and its corresponding clipping noise. In order to effectively reduce this peak, the most effective signal $\boldsymbol{c}$ should be the one that closely resembles the inverse of the clipping pulse. Due to the property of having a constant phase around over-threshold samples, the signal $\boldsymbol{c}$ can be reused to cancel other clipping pulses with similar levels by cyclic-shifting it to align with the pulse location and phase shifting with an appropriate amount. Since cyclic-shifting a signal in the time domain does not change its frequency components, the newly shifted time signal still contains only those tones which are reserved for peak reduction.

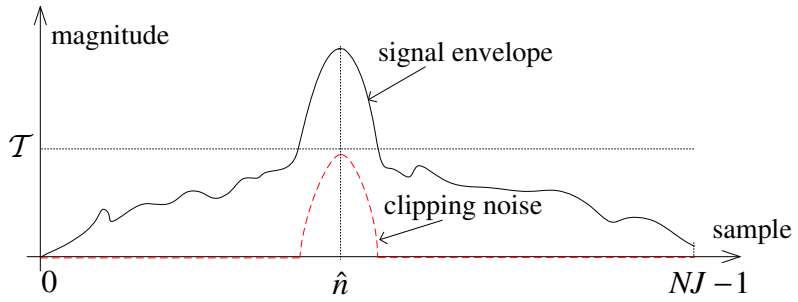

Figure 4.15 Example of a single clipping pulse.

Stage 1 – Learning

Given $\mathcal{T}$, a set of possible levels of peak magnitude is formed as:

$$\mathcal{L}_{\mathcal{T}} = \Big\{ \mathcal{T}_i = \mathcal{T} + i\delta_{\mathcal{T}},\ 1 \le i \le q,\ \delta_{\mathcal{T}} > 0 \Big\}, \tag{4.36}$$

where $\delta_{\mathcal{T}}$ is the step size and $\mathcal{T}_q$ is the maximum peak amplitude. A large number of randomized OFDM symbols is then generated and their peak amplitudes are recorded and classified into q sets:

$$\mathcal{B}_i = \{ \boldsymbol{x} \ : \mathcal{T}_i \le \max|\boldsymbol{x}| \le \mathcal{T}_{i+1} \},\ i = 1, \ldots, q. \tag{4.37}$$

For each set in (4.37), a reference signal is constructed as:

$$\hat{\boldsymbol{x}}_i = \frac{1}{|\mathcal{B}_i|} \sum_{\boldsymbol{x} \in \mathcal{B}_i} \circlearrowleft_{-\hat{n}} \left(\boldsymbol{x}\, \mathrm{e}^{-j\angle x[\hat{n}]} \right), \tag{4.38}$$

where $x[\hat{n}]$ is the sample of $\boldsymbol{x}$ having the maximum magnitude, and $|\mathcal{B}_i|$ is the number of elements in the set $\mathcal{B}_i$.

The reference signal in (4.38) is obtained in three steps. The first step cancels the phase of the highest peak sample. Second, the time samples are cyclically shifted to the original time index. After this, the OFDM symbols in $\mathcal{B}_i$ are all aligned at 0 index, with roughly zero phase for samples around the zero index, and uncorrelated phases for other samples. This makes their sum in the third step to have a high ratio between its major lobe and side lobes. Moreover, the reference signal still has the same frequency tones as the OFDM symbols since averaging and phase shifting do not introduce any new frequency.

For each reference signal, the corresponding peak canceling signal is found to reduce its peak below $\mathcal{T}$. This can be achieved by applying the conventional TR technique to produce:

$$\hat{\boldsymbol{c}}_{\mathcal{T},i} \leftarrow \mathrm{TR}\left(\hat{\boldsymbol{x}}_i, \boldsymbol{k}, \mathcal{T}\right). \tag{4.39}$$

The first stage finishes by finding a set of peak canceling signals

$$\mathcal{C}_{\mathcal{T}} = \{\hat{\boldsymbol{c}}_{\mathcal{T},1}, \ldots, \hat{\boldsymbol{c}}_{\mathcal{T},q}\}. \tag{4.40}$$

Theoretically, the value of q can be very large depending on peak magnitudes of OFDM symbols. Recall (see Figure 2.17) that the probability of an OFDM symbol having a higher value of peak magnitude gets smaller. This means that it likely requires a long time to generate symbols with magnitudes near the peak. Therefore, in practice q can be chosen as some reasonable value so that the set $\mathcal{C}_{\mathcal{T}}$ of peak canceling signals is created when a maximum number of randomly-generated OFDM symbols is reached (for example, 10^6 symbols). In the second stage discussed below, when an OFDM symbol having a magnitude higher than $\mathcal{T}_q$ is found, the set $\mathcal{C}_{\mathcal{T}}$ is updated accordingly. This explains the reason that the first stage is called a "learning" stage.

Stage 2 – Peak-Reduction Loop

The second stage reduces the peak for each OFDM symbol iteratively. At the kth step of the algorithm, the residual signal vector $\boldsymbol{f}_k = \boldsymbol{x} + \boldsymbol{c}_k - g_{\mathcal{T}}(\boldsymbol{x} + \boldsymbol{c}_k)$ is approximated by P_k clipping pulses:

$$\boldsymbol{f}_k \approx \sum_{i=1}^{P_k} \boldsymbol{f}_{k,i}, \tag{4.41}$$

where $\boldsymbol{f}_{k,i}$ is the ith pulse.

Each clipping pulse has a maximum peak magnitude sample, which is the set of peak samples in $\boldsymbol{f}_k$ (as illustrated in Figure 4.16):

$$\mathfrak{P}_k = \{\hat{n} \ : \ |f_k[\hat{n}]| \geq \max\left(|f_k[\hat{n}-1]|, |f_k[\hat{n}+1]|\right)\}. \tag{4.42}$$

The number of clipping pulses is equal to the number of elements in this set, that is $|\mathfrak{P}_k| = P_k$. For each clipping pulse $\boldsymbol{f}_{k,i}$, which has the peak magnitude sample at $\hat{n}_i \in \mathfrak{P}_k$, a

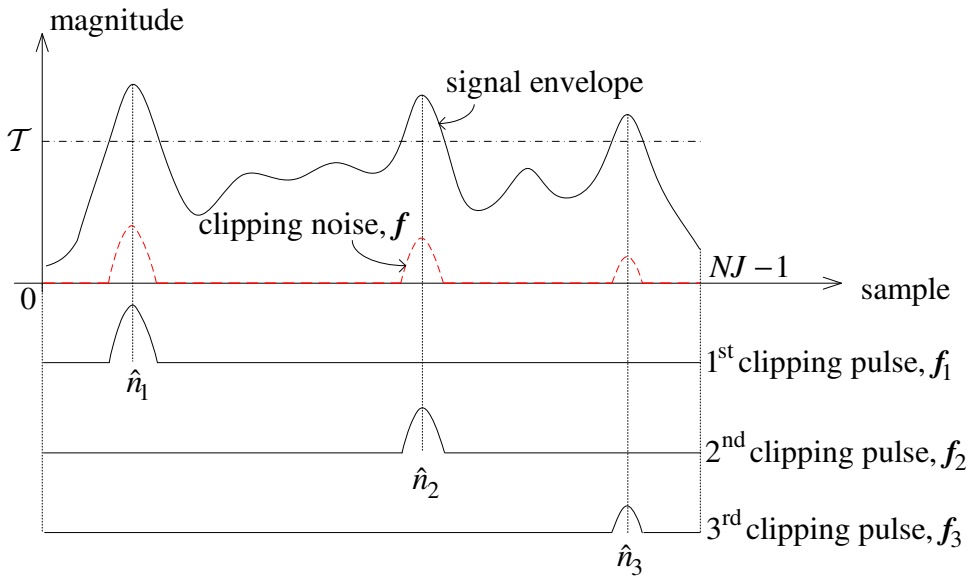

Figure 4.16 Example of multiple clipping pulses.

corresponding level index of the ith pulse is found by:

$$\ell_{k,i} = \min\left(\left\lfloor \frac{\max|\boldsymbol{f}_{k,i}|}{\delta_{\mathcal{T}}} \right\rfloor, q\right). \tag{4.43}$$

Since

$$\max|\boldsymbol{f}_{k,i}| = |f_{k,i}[\hat{n}_i]| = |f_k[\hat{n}_i]|,$$

equation (4.43) can be simplified to:

$$\ell_{k,i} = \min\left(\left\lfloor \frac{|f_k[\hat{n}_i]|}{\delta_{\mathcal{T}}} \right\rfloor, q\right). \tag{4.44}$$

Then, a canceling signal for $\boldsymbol{f}_{k,i}$ is obtained by:

$$\hat{\boldsymbol{f}}_{k,i} = \circlearrowright_{\hat{n}_i}\left(\hat{\boldsymbol{c}}_{\mathcal{T},\ell_{k,i}}\, \mathrm{e}^{+j\angle f_{k,i}[\hat{n}_i]}\right) \approx \boldsymbol{f}_{k,i}. \tag{4.45}$$

The canceling signal is then constructed by:

$$\boldsymbol{c}_{k+1} = \boldsymbol{c}_k - \sum_{i=1}^{P_k} \hat{\boldsymbol{f}}_{k,i}. \tag{4.46}$$

The process repeats until either a maximum number of iterations is reached or all the samples in the peak-reduced signal vector are below the threshold $\mathcal{T}$. The proposed time-domain algorithm is illustrated in Figure 4.17.

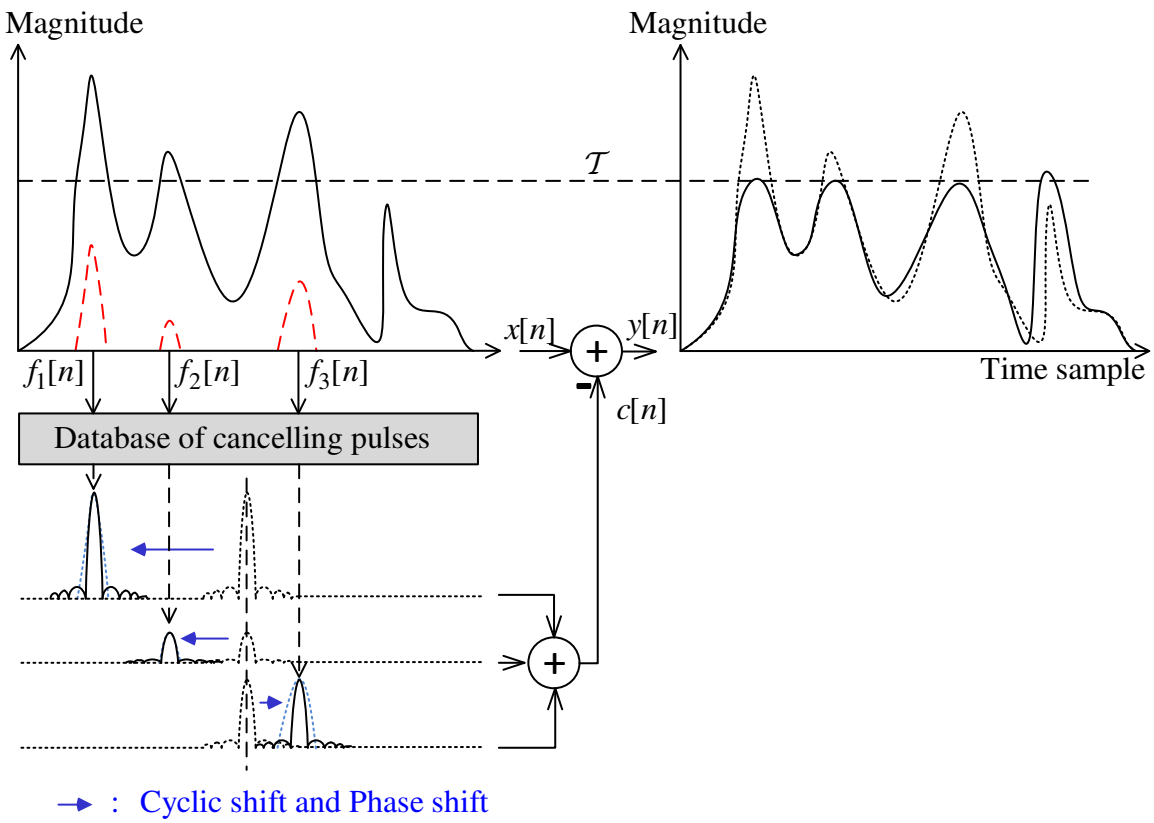

Figure 4.17 Proposed time-domain algorithm.

In summary, the proposed algorithm is outlined below.

Learning Stage

(i) INPUT: Kernel vector $\boldsymbol{k}$; threshold $\mathcal{T}$; set $\mathcal{D}$; set $\mathcal{R}$

(ii) INITIALIZATION:

- Initialize q, resolution $\delta_{\mathcal{T}}$, set $\mathcal{L}_{\mathcal{T}}$ as in (4.36)
- Initialize q sets $\mathcal{B}_1 = \ldots = \mathcal{B}_q = \emptyset$
- Randomly generate a large number of OFDM symbols with data tones $\mathcal{D}$.

(iii) LEARNING:

(a) Classify OFDM symbols into q sets as in (4.37)

(b) Generate reference signals, and their canceling signals using (4.38), (4.39).

(c) After all symbols are tried, RETURN $\mathcal{C}_{\mathcal{T}}$

Peak-Reduction Stage

(i) INPUT: Symbol vector $\boldsymbol{x}$; Kernel vector $\boldsymbol{k}$; Threshold $\mathcal{T}$; Number of iterations N_{it}; Canceling signal set $\mathcal{C}_{\mathcal{T}}$

(ii) INITIALIZATION: Loop variable $k = 1$; $\boldsymbol{c}_k = 0$;

(iii) LOOP_BEGIN:

- Determine the set of peak samples in clipping noise using (4.42)
- Calculate $\boldsymbol{c}_{k+1}$ using (4.44), (4.45) and (4.46)

(iv) LOOP_END:

- IF $(k > N_{\text{it}})$ RETURN $\boldsymbol{y}_{k+1} = \boldsymbol{c}_{k+1} + \boldsymbol{x}$
- ELSE $k = k + 1$, jump LOOP_BEGIN

Complexity Analysis

A single iteration of the proposed algorithm requires $4P_kJN$ real multiplications and $2P_kJN$ additions. Since $P_k \ll |\mathcal{S}_k|$ (see (4.11)), the number of multiplications and additions per iteration of the proposed algorithm are significantly less than the corresponding numbers of the GTR algorithm as discussed in Section 4.1. Moreover, the proposed algorithm does not need to try different values of γ to obtain the optimal amount of peak reduction.

Note that the system complexity grows with the number of iterations. Therefore reducing the number of iterations helps to reduce the cost of the PAPR reduction process. The proposed algorithm helps to transfer most of the computational cost to offline processing steps, which can be regularly updated upon changes in the frequency settings. As can be seen in Section 4.5, the additional step of precalculating the canceling signals makes the proposed algorithm converge in a smaller number of iterations than the conventional GTR algorithm, thereby further reducing the computational cost.

4.4 Proposed Clipping-and-Filtering Algorithm

This section proposes a new clipping-and-filtering algorithm, which uses precalculated canceling signals described in the previous section to establish different gains for reserved tones other than the equal gain for $H(\mathrm{e}^{j\omega})$ in (4.27) as in the conventional CFTR algorithm. This algorithm also has two stages. The first stage calculates the gain coefficients. The second stage is an online process, which iteratively reduces the peak using the precomputed gains.

Recall that the clipping noise $\boldsymbol{f}$ in (4.4) can be approximated by a sum of P_k clipping pulses as $\boldsymbol{f} = \sum_{i=1}^{P_k} \boldsymbol{f}_i$, where $\boldsymbol{f}_i$ is the ith clipping pulse with its maximum magnitude at $\hat{n}_i$. Then the peak canceling signal can be constructed as a combination of different single canceling pulses:

$$\boldsymbol{c} = \sum_{i=1}^{P_k} \boldsymbol{c}_i \tag{4.47}$$

where $\boldsymbol{c}_i$ is the ith canceling pulse, such that $\boldsymbol{c}_i \approx -\boldsymbol{f}_i$ in order to make $\boldsymbol{c} \approx -\boldsymbol{f}$.

Consider two clipping pulses, $\boldsymbol{f}_i$ and $\boldsymbol{f}_j$, having the same peak magnitude at some level, denoted as

$$\ell = \max|\boldsymbol{f}_i| \approx \max|\boldsymbol{f}_j|. \tag{4.48}$$

Because of the property of constant-phase near their maximum, the clipping pulses can be approximated by a cyclic shift with an appropriate amount of phase rotation:

$$\boldsymbol{f}_j \approx \mathrm{e}^{j(\angle f_j[n_j] - \angle f_i[n_i])} \circlearrowleft_{n_j - n_i} (\boldsymbol{f}_i), \tag{4.49}$$

where $f_i[n_i]$ and $f_j[n_j]$ are the samples of $\boldsymbol{f}_i$, and $\boldsymbol{f}_j$ having the maximum magnitudes, respectively. Equation (4.49) suggests that the canceling pulse for $\boldsymbol{f}_j$ can also be derived from the one used to cancel $\boldsymbol{f}_i$, that is:

$$\boldsymbol{c}_j \approx \mathrm{e}^{j(\angle f_j[n_j] - \angle f_i[n_i])} \circlearrowleft_{n_j - n_i} (\boldsymbol{c}_i). \tag{4.50}$$

Let $\boldsymbol{C}_i = [C_i[0], \ldots, C_i[NJ-1]]$ and $\boldsymbol{F}_i = [F_i[0], \ldots, F_i[NJ-1]]$, respectively, be the corresponding frequency vectors of $\boldsymbol{c}_i$ and $\boldsymbol{f}_i$ obtained from DFT operations. Then it follows

from (4.49) that:

$$\begin{aligned} F_j[k] &= \mathcal{F}\{\boldsymbol{f}_j\}|_k; \quad 0 \le k \le NJ-1 \\ &\approx \mathrm{e}^{j(\angle f_j[n_j]-\angle f_i[n_i])}\mathcal{F}\{\circlearrowleft_{n_j-n_i}(\boldsymbol{f}_i)\}|_k \\ &\approx \mathrm{e}^{j(\angle f_j[n_j]-\angle f_i[n_i])}\mathrm{e}^{-j2\pi(n_j-n_i)k/NJ}\mathcal{F}\{\boldsymbol{f}_i\}|_k \\ &\approx \mathrm{e}^{j(\angle f_j[n_j]-\angle f_i[n_i])}\mathrm{e}^{-j2\pi(n_j-n_i)k/NJ}F_i[k]; \end{aligned} \tag{4.51}$$

Similarly, it follows from (4.50) that:

$$C_j[k] \approx \mathrm{e}^{j(\angle f_j[n_j]-\angle f_i[n_i])}\mathrm{e}^{-j2\pi(n_j-n_i)k/NJ}C_i[k], \tag{4.52}$$

where $0 \le k \le NJ-1$. Thus, comparing (4.51) and (4.52) yields:

$$g_\ell[k] = \frac{C_j[k]}{F_j[k]} \approx \frac{C_i[k]}{F_i[k]}; \quad 0 \le k \le NJ-1. \tag{4.53}$$

Equation (4.53) infers that the ratios of the frequency components between the clipping pulses of the same peak magnitudes and their canceling pulses are approximately constant. For each level ℓ, these ratios are defined as a coefficient vector $\boldsymbol{g}_\ell = [g_\ell[0], \ldots, g_\ell[NJ-1]]$. Using such a coefficient vector, the canceling pulse of a clipping pulse $\tilde{\boldsymbol{f}}$ whose peak magnitude is at level ℓ can be obtained by:

$$\tilde{\boldsymbol{c}} = \mathcal{F}^{-1}\{\boldsymbol{g}_\ell \mathcal{F}\{\tilde{\boldsymbol{f}}\}\}. \tag{4.54}$$

Equation (4.54) helps to construct a canceling pulse from the frequency vector of a clipping pulse and the corresponding coefficients. Based on the above analysis, the proposed clipping-and-filtering algorithm is performed in two stages. The first stage, also called a learning stage, initializes a set of coefficient vectors corresponding to different levels of clipping pulses. This stage can be done offline and updated regularly when needed. The second stage is an online process that processes the clipping noise in the frequency domain with the suitable coefficients developed from the first stage to iteratively construct a peak canceling signal.

Learning Stage

This stage has the same steps discussed in Section 4.3. Specifically, the reference signals constructed as in (4.38) are clipped:

$$\hat{\boldsymbol{f}}_{\mathcal{T},i} = \hat{\boldsymbol{x}}_i - g_{\mathcal{T}}(\hat{\boldsymbol{x}}_i) \tag{4.55}$$

Then q coefficient vectors are calculated as:

$$\boldsymbol{g}_{\mathcal{T},i} = \frac{\mathcal{F}\{\hat{\boldsymbol{c}}_{\mathcal{T},i}\}}{\mathcal{F}\{\hat{\boldsymbol{f}}_{\mathcal{T},i}\}} \tag{4.56}$$

where $\hat{\boldsymbol{c}}_{\mathcal{T},i}$ is given by (4.39).

The stage finishes by finding a set of coefficient vectors

$$\mathcal{G}_{\mathcal{T}} = \{\boldsymbol{g}_{\mathcal{T},0}, \ldots, \boldsymbol{g}_{\mathcal{T},q}\} \tag{4.57}$$

Peak-Reduction Stage

The second stage reduces the peak of each symbol iteratively. At the kth iteration, the clipping noise vector $\boldsymbol{f}_k = \boldsymbol{x} + \boldsymbol{c}_k - g_{\mathcal{T}}(\boldsymbol{x} + \boldsymbol{c}_k)$ is also approximated by P_k clipping pulses as in (4.41). For simplicity, only the clipping pulse of highest peak magnitude is selected

$$\tilde{\boldsymbol{f}}_k = \arg \max_{1 \le i \le P_k} |\boldsymbol{f}_{k,i}| \tag{4.58}$$

The corresponding level of $\tilde{\boldsymbol{f}}_k$ is obtained as in (4.43). Then the canceling signal for the next iteration is:

$$\boldsymbol{c}_{k+1} = \mathcal{F}^{-1}\{\boldsymbol{g}_{\ell_k} \mathcal{F}\{\tilde{\boldsymbol{f}}_k\}\} \tag{4.59}$$

The peak-reduction loop is illustrated in Figure 4.18. The leveler block in the figure is to conduct the operation in (4.43). All of the coefficient vectors calculated from the learning stage can be stored in a memory, and a multiplexer (MUX) structure is used to fetch a corresponding coefficient vector at run-time.

Complexity Analysis

The proposed clipping-and-filtering algorithm reduces the computational complexity of the CFTR algorithm. Thanks to the coefficients found in the learning stage, the online

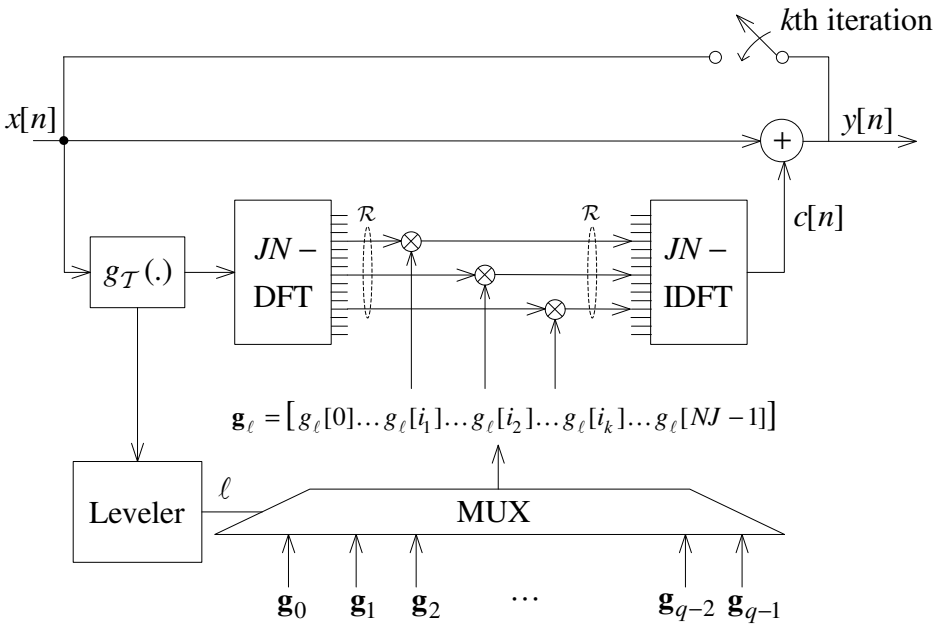

Figure 4.18 Proposed algorithm.

processing stage removes the need for calculating β and scaling the time-domain vector as in the conventional approach. In addition, the division operations are removed from the proposed scheme, and the number of multiplications per iteration is:

$$\mathcal{M}_p = \mathcal{M}_{\text{DFT}} + \mathcal{M}_{\text{IDFT}} + 4|\mathcal{R}| \tag{4.60}$$

where $2|\mathcal{R}|$ multiplications are used to generate the canceling signal in (4.59). Since $|\mathcal{R}| \ll JN$, the complexity of the new clipping-and-filtering algorithm is much smaller than that of the conventional CFTR algorithm (see Section 4.2). Simulation results also reveal that the performance of the proposed algorithm is comparable to that of the conventional CFTR algorithm.

Complexity Comparison of Different PAPR Reduction Algorithms

For ease of reference, Table 4.1 compares the complexity among the two conventional algorithms and the two propose algorithms. Here, the proposed time-domain algorithm and the proposed clipping-and-filtering algorithm are is listed as "Proposed (a)" and "Proposed (b)", respectively. As can be seen, among these algorithms, the conventional GTR algorithm has the highest computational cost in terms of the number of multipliers and additions

Table 4.1 Complexity comparison of different PAPR reduction algorithms.

Algorithms	**# Multipliers**	**# Additions**	**# Divisions**
GTR	$4\|\mathcal{S}_k\|JN + 2\|\mathcal{S}_k\| + 4JN$	$\|\mathcal{S}_k\|JN + 1$	0
CFTR	$\mathcal{M}_{\text{DFT}} + \mathcal{M}_{\text{IDFT}} + 4\|\mathcal{S}_k\| + 2JN$	$\mathcal{O}(JN)$	1
Proposed (a)	$4P_kJN$	$2P_kJN$	0
Proposed (b)	$\mathcal{M}_{\text{DFT}} + \mathcal{M}_{\text{IDFT}} + 4\|\mathcal{R}\|$	$\mathcal{O}(JN)$	0

required per iteration. The conventional CFTR algorithm has a considerably smaller number of multiplications when compared to the conventional GTR algorithm in each iteration, however, one extra division must be performed.

In contrast, the two proposed algorithms do not require any division and use much fewer multiplications per iteration than the conventional algorithms. Such reduction in the complexity is achieved by transferring most of the calculation tasks of calculating canceling signals to the off-line stage. In addition, the DFT/IDFT operations can be very efficiently implemented using FFT/IFFT algorithms. Therefore the proposed CFTR algorithm is very attractive for practical applications.

4.5 Simulation Results of the Proposed Algorithms

In each simulation, 10^6 OFDM symbols are generated using a $1024-$QAM constellation, 1024-point IFFT block ($N = 1024$), and an oversampling factor $J = 8$. Two different sets of reserved tones are simulated in this paper. In the first case, $G = 50$ tones, which is approximately 5% of the available tones, are selected randomly. Hence the number of data tones is $N - G = 1024 - 50 = 974$. The second case considers $G = 100$ tones, which are also randomly selected, and the corresponding number of data tones is $G = 1024 - 100 = 924$. It should be pointed out that practical implementations of PAPR reduction typically select the number of reservation tones to be less than 15% of the available tones [2, 37, 60].

For each of these two cases, two different target PAPR levels and corresponding thresholds $\mathcal{T}$ are tested, namely 8 dB and 10 dB. The learning stage was run over 5×10^5 OFDM symbols.

The quantization level $\delta_{\mathcal{T}}$ was set to provide a resolution of 0.1 dB. This means, for example, in the case of a threshold at 8 dB, $\mathcal{B}_0$ consists of signals with PAPR in the range [8 dB, 8.1 dB], $\mathcal{B}_1$ for the signals with PAPR in [8.1 dB, 8.2 dB] and so on. Extensive testing indicates that this value of $\delta_{\mathcal{T}}$ provides fine enough resolution for the reference signals.

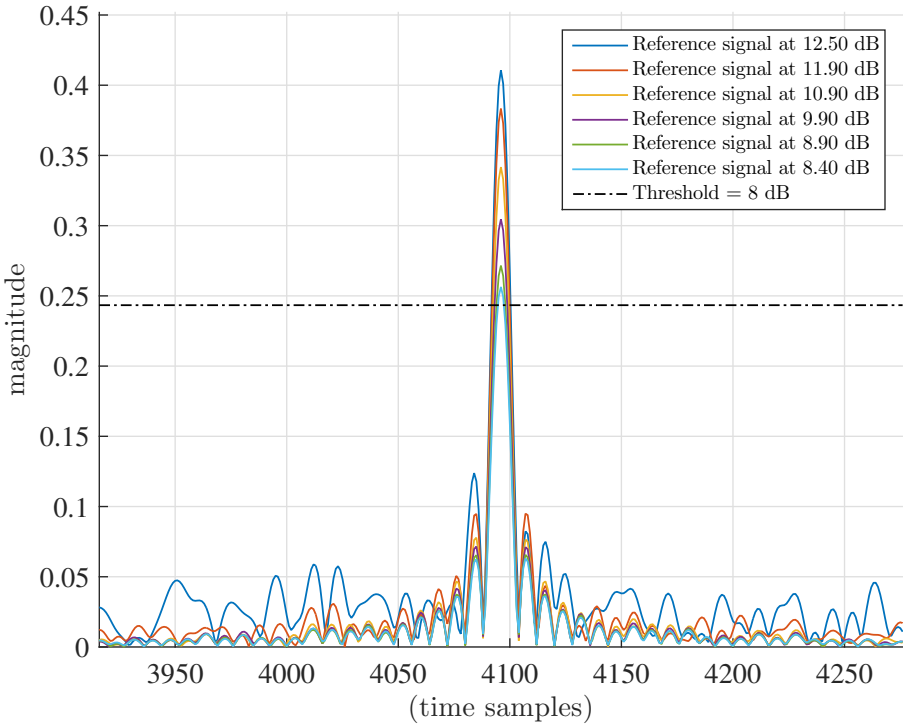

Figure 4.19 Example of reference signals with $G = 100$ reserved tones, and target PAPR of 8 dB (centered at index 4096).

Figure 4.19 shows examples of reference signals of different peak levels. The levels are measured in dB with respect to the average magnitude of OFDM symbols. It is interesting to see that the main lobes of all reference signals have essentially the same width, while the side lobe levels are much smaller when compared to side-lobes of random OFDM signals.

Figure 4.20 presents an example of a reference signal with a maximum magnitude of 10.9 dB, its clipping noise, the corresponding canceling signal and the canceled signal obtained by subtracting the canceling signal from the reference signal.

Figures 4.21 and 4.22 compare the PAPR reduction performance of different algorithms with a target PAPR of 8 dB using 50 and 100 reserved tones, respectively. Similarly,

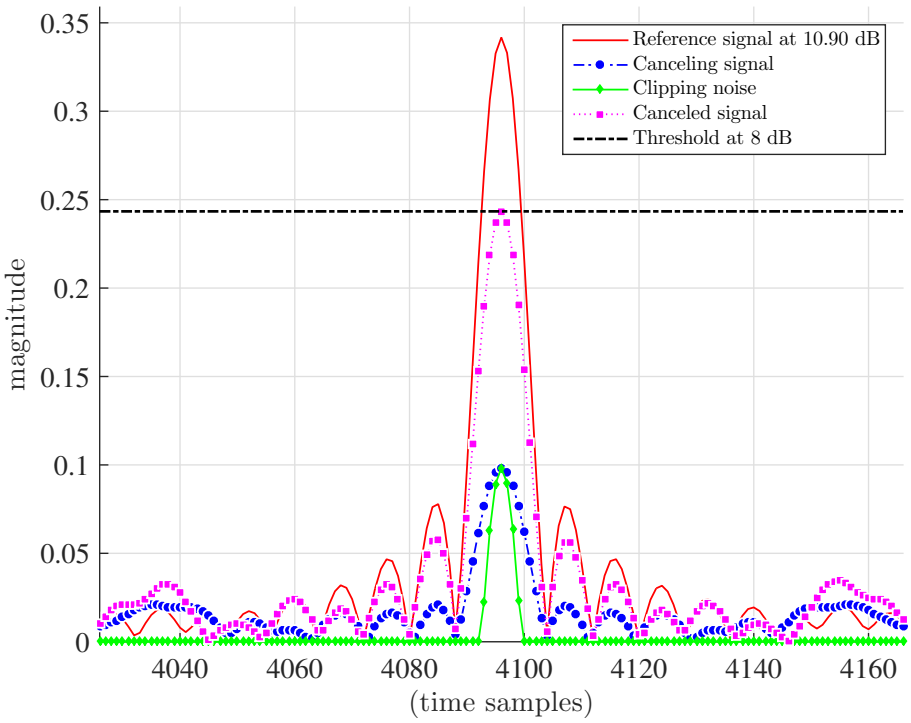

Figure 4.20 Example of a reference signal and its canceling signal with $G = 100$ reserved tones, and target PAPR of 8 dB (centered at index 4096).

Figs. 4.23 and 4.24 report results for a target PAPR of 10 dB. In all cases, the CCDF curves with 1 iteration and 2 iterations of the proposed algorithms are compared against those of the conventional GTR and CFTR algorithms having the same number of iterations. For the conventional GTR algorithm, different values of scaling factor γ are tested: 0.01, 0.05, 0.1, 0.15, 0.2, 0.25, 0.5 and 1. The scaling factor yielding the best peak reduction performance after 2 iterations was selected and indicated in the figure's legend.

Figures 4.21 to 4.24 show that for both $\mathcal{T} = 8$ dB and $\mathcal{T} = 10$ dB, the proposed algorithms generally provide slightly better peak reduction than the conventional algorithms.

In particular, at $\mathcal{T} = 8$ dB and probability of 10^{-4}, the proposed algorithms deliver a PAPR reduction amount of roughly 3.5 dB (12.5 dB when no peak reduction methods are applied down to less than 9 dB), which is similar to that achieved with the conventional algorithms. For the higher threshold of $\mathcal{T} = 10$ dB, the proposed algorithms can provide the same performance with one iteration as the conventional algorithms achieve in two iterations, which is approximately 0.6 dB better than the conventional CFTR achieves in

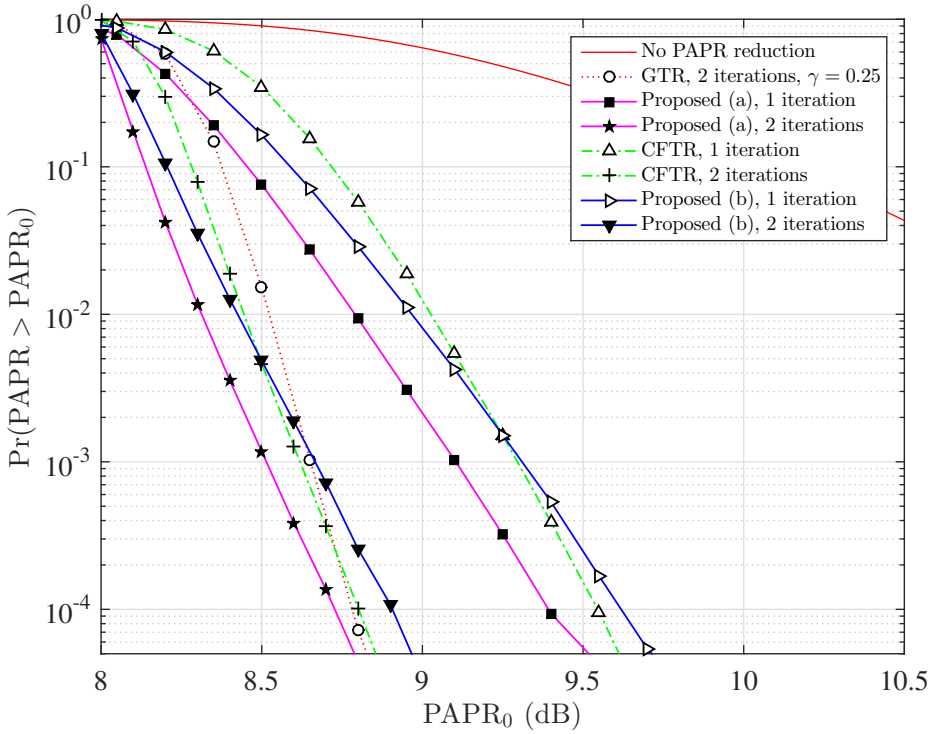

Figure 4.21 Comparison of PAPR reduction for different methods: $G = 50$ random reserved tones with target PAPR, $\mathcal{T} = 8$ dB. "Proposed (a)" is for the proposed time-domain algorithm, "Proposed (b)" is for the proposed clipping and filtering algorithm.

one iteration. Moreover, it should be pointed out that the computational complexity of the proposed algorithms, even when two iterations are used, is still much lower than that of the conventional GTR and CFTR algorithms.

4.6 Summary

The last two sections of the chapter present two novel algorithms for peak reduction of OFDM signals: a time-domain algorithm and a clipping-and-filtering algorithm. Both algorithms efficiently reuse precalculated canceling signals to reduce the computational complexity of the conventional peak reduction algorithms based on the TR principle. The precalculated canceling signals can be updated when different tone sets are selected for data transmission, accommodating many practical applications. Simulation results show that the proposed algorithms achieve slightly better performance than the conventional CFTR and

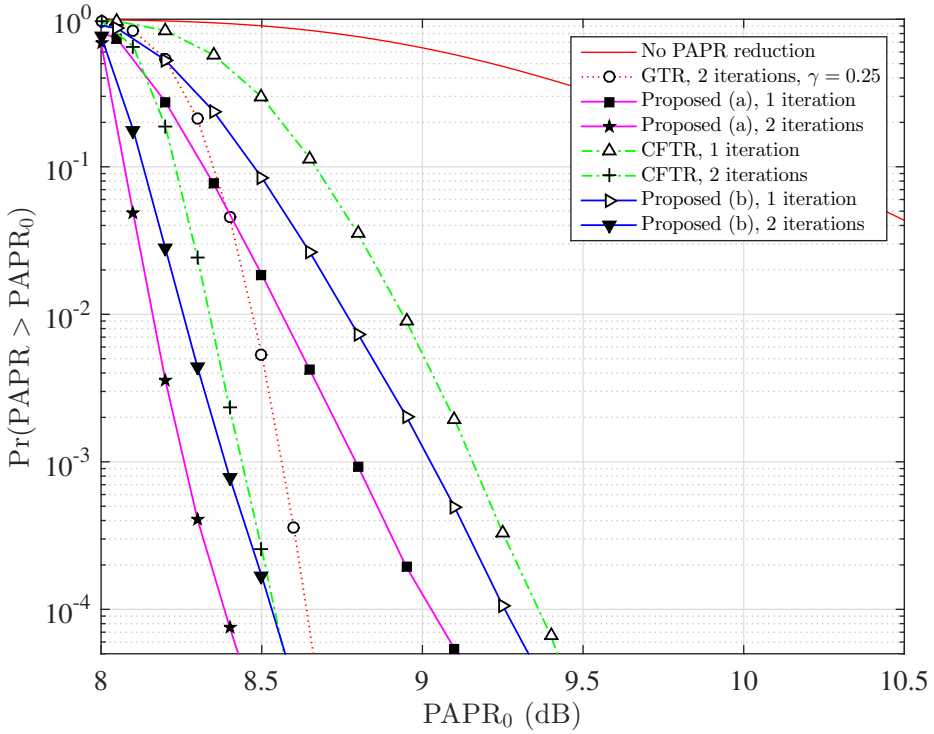

Figure 4.22 Comparison of PAPR reduction for different methods: $G = 100$ random reserved tones with target PAPR, $\mathcal{T} = 8$ dB. "Proposed (a)" is for the proposed time-domain algorithm, "Proposed (b)" is for the proposed clipping and filtering algorithm.

GTR algorithms. Moreover, such performance is achieved with much lower computational complexity when compared to the conventional GTR and CFTR algorithms. Among the algorithms considered, the proposed time-domain GTR algorithm gives the best peak reduction performance but the proposed clipping-and-filtering algorithm requires considerably less number of multiplications per iteration and can be efficiently implemented using FFT/IFFT structure.

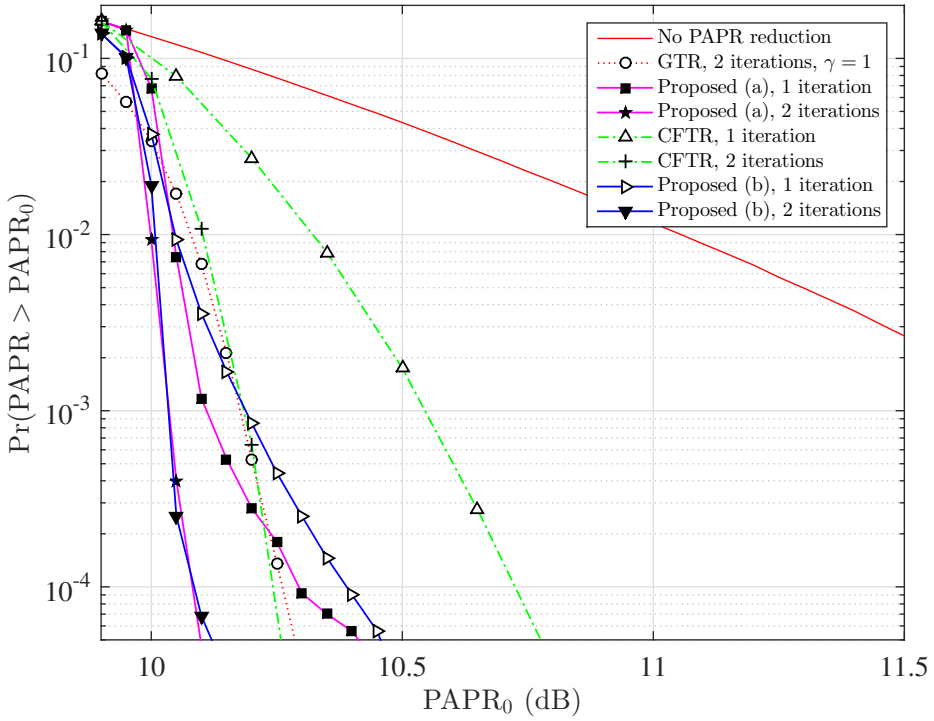

Figure 4.23 Comparison of PAPR reduction for different methods: $G = 50$ random reserved tones with target PAPR, $\mathcal{T} = 10$ dB. "Proposed (a)" is for the proposed time-domain algorithm, "Proposed (b)" is for the proposed clipping and filtering algorithm

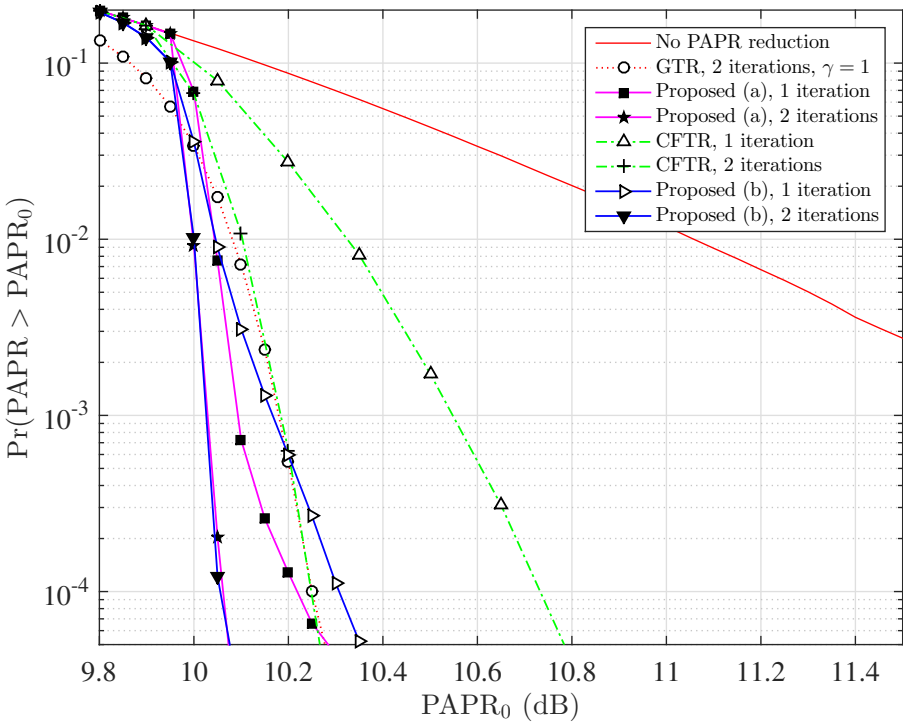

Figure 4.24 Comparison of PAPR reduction for different methods: $G = 100$ random reserved tones with target PAPR, $\mathcal{T} = 10$ dB. "Proposed (a)" is for the proposed time-domain algorithm, "Proposed (b)" is for the proposed clipping and filtering algorithm

5. Summary and Suggestions for Further Studies

5.1 Summary

This thesis has investigated techniques to reduce the PAPR of DOCSIS OFDM downstream signals. To ensure the downward compatibility property of the network where changes in the transmitter's side do not affect the operation at the receivers, the peak reduction is achieved by adding canceling signals, which are constructed by using only reserved subcarriers or tones in the OFDM signal spectrum. As the subcarriers' locations are known in the DOCSIS standards, receivers can agree a priori on reserving some specific tones for the purpose of peak reduction.

The thesis proposes two efficient algorithms based on the TR principle, which do not distort the transmitted data. The first algorithm is performed in the time domain, whereas the second algorithm is a new clipping-and-filtering method. Both techniques use some precalculated canceling signals in order to reduce the peak of OFDM signals and are performed in two stages. The first stage creates a set of canceling signals based on the settings of the OFDM system. In particular, these signals are constructed to cancel signals at different levels of maximum instantaneous power that are above a predefined threshold. The second stage is done online and in an iterative manner, which reduces the signal peaks by adding with the canceling signals constructed in the first stage.

From extensive simulation results, the proposed algorithms can reduce peaks of OFDM signals effectively after two iterations, while the numbers of hardware resources required in terms of multiplications and additions are significantly less than that of the conventional algorithms. Specifically, the two proposed algorithms can provide approximately 3.5 dB

of PAPR reduction with a target PAPR of 8 dB at the probability of 10^{-4}, which meets the objective discussed in Section 1.3. Regarding the complexity comparisons, the number of real multipliers in the kth iteration of the proposed time-domain algorithm is $4P_k$ per sample, and the number of additions is $2P_k$ per sample (as discussed in Section 4.3) where P_k is the number of clipping pulses of the OFDM signal from the previous iteration. As a reference, the required number of multipliers in the conventional gradient-based TR (GTR) algorithm is $4(|\mathcal{S}_k|+1)+(2|\mathcal{S}_k|/JN)$ per sample, where $|S_k|$ is the number of samples in those clipping pulses occurred in the OFDM signal from the previous iteration. Since $P_k << |\mathcal{S}_k|$, especially when the high value of oversampling factor J is used, the conventional approach is certainly much more complicated. Additionally, the conventional GTR must use a scaling factor whose optimal value is not well defined theoretically at run-time which affects the peak reduction performance and might cause the algorithm to diverge. This phenomenon does not happen with the proposed time-domain algorithm where no scaling factor is needed in the online processing stage.

The frequency-domain algorithm offers even a smaller number of multiplications by utilizing a pair of DFT/IDFT blocks. The number of real multipliers required in each iteration of the algorithm is $4G/NJ + \left(\mathcal{M}_{\text{DFT/IDFT}}/NJ\right)$ (see Equation (4.60)) per sample, where G/NJ is actually the ratio between number of reservation tones and the total number of tones available, and $\mathcal{M}_{\text{DFT/IDFT}}$ denotes the number of multipliers used by the DFT/IDFT block. These figures are much smaller than those required in the conventional clipping-and-filtering algorithm which also makes use of DFT/IDFT blocks. As the number of reservation tones is pre-selected in the off-line stage, the number of multipliers for the on-line stage is bounded and does not depend on the time-domain OFDM signals. This feature benefits the real-time processing of the signal where the processing time for each OFDM symbol must be limited.

5.2 Suggestions for Further Studies

The thesis has successfully demonstrated proof-of-concept techniques for PAPR reduction of OFDM signals. While conducting the research works, there is a number of issues that are

worthwhile to investigate further. These issues are elaborated below.

Given the significant reduction of hardware resources, the proposed algorithms are promising to be realized in FPGA devices. Both algorithms are performed in two separate stages, namely an offline stage and online stage. The offline stage can be implemented in a computer to generate all the reference signals, peak cancelling signals and coefficient vectors. Such data then can then be loaded onto a FPGA device in the online stage. A number of implementation techniques can be applied when realizing the peak reduction algorithms in an FPGA, which is worthwhile to investigate further.

The thesis reports extensive simulation results for the case of using a randomized tone set for PAPR reduction. Since the locations of the tones are clearly specified in the standard [4], they can be made known to all the receivers on the network so that they do not use these tones for data transmission. However, it would be more preferable in practice if the reserved tones are limited to be within some frequency regions. The DOCSIS network originally consists of multiple video broadcasting channels where each of them is modulated using SC-QAM with a bandwidth of 6 MHz each. Consequently, the 6 MHz bandwidth is typically considered as a region of one single video channel in DOCSIS standards [4], whereas an OFDM channel is often referred to as a region of a number of video channels resided side-by-side. Therefore more research work is needed to find out if the reserved tones can be limited to be within one or multiple 6 MHz regions.

The TR principle is followed in the proposed techniques as the way to generate peak cancelling signals which use tones totally separated from the data transmission tones. The reason for this is to facilitate the receiver to easily remove the added signal before recovering the original transmit signal. Another possibility of enabling the separation between the peak cancelling signals and the original signals is by power level. That is to say the peak cancelling signals can be generated from the same spectrum region as the data tones but with much lower powers when compared to the original signals. The peak cancelling signals are not confined to only tones specified by the system. Instead, they can make use of any frequency within the spectrum used for data transmission as long as the power allocated for these frequencies are well under the power of the data tones. This makes the original signal

slightly distorted where the distortion level is kept minimal in such a way that it would not affect the detection performance of data tones. It would be an interesting research problem to see if it is possible to generate this type of peak canceling signals and how well they perform.

In practical scenarios of DOCSIS 3.1, there are multiple OFDM channels modulated at different carrier frequencies as well as a number of SC-QAM channels located in the lower frequency regions, which in combination occupy the whole spectrum from 108 MHz to 1218 MHz [4]. These OFDM channels can have the same number of IFFT bins, however with different lengths of cyclic prefixes and roll-off periods. This makes their symbol alignments asynchronous in the time domain. Since the PAPR in (3.11) is defined in a symbol-wise manner, it is not applicable to the case of a composite signal that is a combination of asynchronous OFDM symbols. The composite signal would exhibit peaks at different sample times not being constrained to any specific OFDM symbol duration. Therefore, the definition of *instantaneous power to average power ratio* (IAPR) is more appropriate [66–68] to measure the dynamic range of the composite signal. As a number of OFDM channels are combined together, the oversampling factor required is considerably larger than 4, making the realization of the dynamic reduction techniques more difficult due to a large number of samples involved in the calculation. Due to the asynchronous alignment among symbols from different OFDM channels, the PAPR reduction techniques that reduce peaks in a symbol-wise manner would need to be modified or adapted. As such, more investigation should be conducted to obtain effective dynamic range reduction techniques for the case of multiple asynchronous OFDM channels.

Finally, regarding the PAPR reduced OFDM signal, more peaks will appear near the predefined target PAPR. When this signal is amplified, the HPA's IBO can be released by the amount of PAPR reduction achieved. This means that the HPA is forced to operate at the saturation point more often. Consequently, this would produce more non-linear distortion when compared to the case of amplifying the original OFDM signal. Signal pre-distortion methods can be applied to address the increase in non-linear distortion. Before the signal gets amplified, pre-distortion methods try to distort the signal in a way that when the

signal gets amplified, the combination of amplification and pre-distortion results in a more linear amplification when compared to the amplification alone. It is an interesting research problem to find signals that serve as peak cancelling signals of the OFDM signals as well as pre-distorting signals to decrease the HPA nonlinearity.

Appendix A. Derivation of Kernel Signal Variance

The power sequence of the kernel signal has a special relationship to the correlation of the set $\mathcal{R}$, which is shown as follows:

$$
\begin{aligned}
|k[n]|^2 &= k[n]k^*[n] \\
&= \frac{1}{|\mathcal{R}|^2} \sum_{m=0}^{NJ-1} p[m] \mathrm{e}^{+j\frac{2\pi}{NJ}nm} \sum_{\ell=0}^{NJ-1} p[\ell] \mathrm{e}^{-j\frac{2\pi}{NJ}n\ell} \\
&= \frac{1}{|\mathcal{R}|^2} \left(\underbrace{\sum_{m=0}^{NJ-1} p[m]}_{|\mathcal{R}|} + \sum_{\substack{m\neq\ell \\ m,\ell=0}}^{NJ-1} p[m]p[\ell] \mathrm{e}^{+j\frac{2\pi}{NJ}n(m-\ell)} \right) \\
&= \frac{1}{|\mathcal{R}|} + \frac{1}{|\mathcal{R}|^2} \sum_{\substack{m>\ell \\ m,\ell=0}}^{NJ-1} p[m]p[\ell] \left(\mathrm{e}^{+j\frac{2\pi}{NJ}n(m-\ell)} + \mathrm{e}^{+j\frac{2\pi}{NJ}n(\ell-m)} \right) \\
&= \frac{1}{|\mathcal{R}|} + \frac{2}{|\mathcal{R}|^2} \sum_{\substack{m>\ell \\ m,\ell=0}}^{NJ-1} p[m]p[\ell] \cos\left[\frac{2\pi}{NJ} n(m-\ell) \right] \\
&= \frac{1}{|\mathcal{R}|} + \frac{2}{|\mathcal{R}|^2} \sum_{\tau=1}^{NJ-1} \cos\left[\frac{2\pi n\tau}{NJ} \right] \underbrace{\sum_{m=0}^{NJ-1-\tau} p[m]p[m+\tau]}_{R_\tau} \\
&= \frac{1}{|\mathcal{R}|} + \frac{2}{|\mathcal{R}|^2} \sum_{\tau=1}^{NJ-1} R_\tau \cos\left[\frac{2\pi n\tau}{NJ} \right],
\end{aligned}
\tag{A.1}
$$

where x^* denotes the complex conjugate of x and $1 \leq n \leq NJ-1$. The *aperiodic autocorrelation function (APCF)* of sequence $p[m]$ is

$$
R_\tau = \sum_{m=0}^{NJ-1-\tau} p[m]p[m+\tau], \tag{A.2}
$$

where $0 \leq \tau \leq NJ-1$. Since $\mathcal{R}$ is a subset of $\Phi = \{0, \ldots, N-1\}$, so $R_\tau = 0$ for $\tau \geq N$ and Equation (A.1) can be rewritten as:

$$
|k[n]|^2 = \frac{1}{|\mathcal{R}|} + \frac{2}{|\mathcal{R}|^2} \sum_{\tau=1}^{N-1} R_\tau \cos\left[\frac{2\pi n\tau}{NJ} \right], \quad 1 \leq n \leq NJ-1. \tag{A.3}
$$

From (4.17), $k[n]$ can be calculated by performing the IDFT on sequence $\boldsymbol{p} = [p[0], \ldots, p[NJ-1]]$. That is:

$$k[n] = \frac{\sqrt{NJ}}{|\mathcal{R}|}\left(\frac{1}{\sqrt{NJ}}\sum_{m=0}^{NJ-1} p[m]\mathrm{e}^{j2\pi\frac{nm}{NJ}}\right) = \frac{\sqrt{NJ}}{|\mathcal{R}|}\,\mathcal{F}^{-1}\{\boldsymbol{p}\}|_n. \tag{A.4}$$

Using the Parseval's theorem, the average power of $|k[n]|$ is given by:

$$\mu = E\left\{|k[n]|^2\right\} = \frac{1}{NJ}\sum_{n=0}^{NJ-1}|k[n]|^2 = \frac{1}{|\mathcal{R}|^2}\sum_{m=0}^{NJ-1} p[m]^2 = \frac{1}{|\mathcal{R}|}. \tag{A.5}$$

Thus the variance of $k[n]$ is:

$$\begin{aligned}\sigma^2 &= E\left\{(|k[n]|^2-\mu)^2\right\} = E\left\{\left(|k[n]|^2 - \frac{1}{|\mathcal{R}|}\right)^2\right\} \\ &= E\left\{\left(\frac{2}{|\mathcal{R}|^2}\sum_{\tau=1}^{N-1} R_\tau\cos\left[\frac{2\pi n\tau}{NJ}\right]\right)^2\right\} = \frac{4}{NJ|\mathcal{R}|^2}E\left\{\left(\sum_{\tau=1}^{N-1} R_\tau\cos\left[\frac{2\pi n\tau}{NJ}\right]\right)^2\right\}.\end{aligned} \tag{A.6}$$

Because

$$\begin{aligned}\left(\sum_{\tau=1}^{N-1} R_\tau\cos\left[\frac{2\pi n\tau}{NJ}\right]\right)^2 &= \sum_{\tau=1}^{N-1} R_\tau^2\cos\left[\frac{2\pi n\tau}{NJ}\right]^2 + 2\sum_{\substack{\ell,k=1\\ \ell\neq k}}^{NJ-1} R_\ell R_k\cos\left[\frac{2\pi n\ell}{NJ}\right]\cos\left[\frac{2\pi nk}{NJ}\right] \\ &= 2\sum_{\tau=1}^{N-1} R_\tau^2\left(1+\cos\left[\frac{2\pi 2n\tau}{NJ}\right]\right) + \\ &\sum_{\substack{\ell,k=1\\ \ell\neq k}}^{N-1} R_\ell R_k\left\{\cos\left[\frac{2\pi n(\ell+k)}{NJ}\right] + \cos\left[\frac{2\pi n(\ell-k)}{NJ}\right]\right\},\end{aligned}$$

it follows that:

$$\begin{aligned}\sigma^2 =& \frac{8}{NJ|\mathcal{R}|^2}\sum_{\tau=1}^{N-1} R_\tau^2 E\left\{1+\cos\left[\frac{2\pi 2n\tau}{NJ}\right]\right\} + \\ & \frac{4}{NJ|\mathcal{R}|^2}\sum_{\substack{\ell,k=1\\ \ell\neq k}}^{N-1} R_\ell R_k E\left\{\cos\left[\frac{2\pi n(\ell+k)}{NJ}\right] + \cos\left[\frac{2\pi n(\ell-k)}{NJ}\right]\right\}.\end{aligned}$$

It is easily seen that, for any $0 < k \leq NJ-1$, one has:

$$E\left\{\cos\left[2\pi\frac{kn}{NJ}\right]\right\} = \frac{1}{NJ}\sum_{n=0}^{NJ-1}\cos\left[2\pi\frac{kn}{NJ}\right] = \frac{1}{2NJ}\sum_{n=0}^{NJ-1}\left[\mathrm{e}^{+j2\pi\frac{kn}{NJ}} + \mathrm{e}^{-j2\pi\frac{kn}{NJ}}\right] = 0.$$

In the same manner,

$$E\left\{\cos\left[\frac{2\pi n(\ell+k)}{NJ}\right]\right\} = 0 \text{ for } \ell + k \neq NJ;\ \ell, k < NJ$$
$$E\left\{\cos\left[\frac{2\pi n(\ell-k)}{NJ}\right]\right\} = 0 \text{ for } \ell \neq k;\ \ell, k < NJ$$

Using the above results, Equation (A.6) can be simplified as:

$$\sigma^2 = \frac{8}{NJ|\mathcal{R}|^2}\sum_{\tau=1}^{N-1} R_\tau^2. \tag{A.7}$$

.

Appendix B. Genetic-Based Kernel Search

1. Parent population generation: An initial set of binary sequences of length N is randomly generated. They are called parent sequences, and denoted by $\boldsymbol{\wp} = \{\wp_0\wp_1 \dots \wp_{N-1}\}$. Each parent sequence has exactly G non-zero elements at indices $i_0, i_1, \dots, i_{G-1}$ which correspond to reserved tones in the set $\mathcal{R}$. The population size or the number of parent sequences is a constant $N_\wp$.

2. Ranking parent sequences: Generate a kernel corresponding to each parent sequence using (4.17). For each of the kernel constructed, its merit factor is defined by:

$$\mathrm{MF}_{\boldsymbol{k}} = \max_{J \le n \le (N-1)J} |k[n]| \tag{B.1}$$

which is the secondary peak magnitude of the kernel signal. The ranking is then done to order the parent sequences by their merit factors.

3. Crossover and mutate: This step consists of two consecutive processes. The first process is called crossover since it is inspired from the similar process in the biological evolution, in which two genomes crossover to create two new offspring genomes by switching some portions of their bodies. This operation helps the offspring inherit the characteristics from their parents. The second process, named as a mutation, takes the responsibility to create some new characteristics for the offspring generations. It is made by probabilistically changing some random values in their sequences. After these two processes, a new population, which includes both the parent population formed in the previous step and a number of new offspring sequences, is created. An illustration of these two processes is provided in Figure 1.

   Not all the sequences in the parent population cross over, but a portion of them does. The percentage of crossover, or the crossover rate, is preset by some constant probability of ξ. When two parent sequences cross over, a random point is selected to make the reference boundary to exchange elements, which is called a *crossover point*. All the elements from the reference point towards the end of the two sequences are

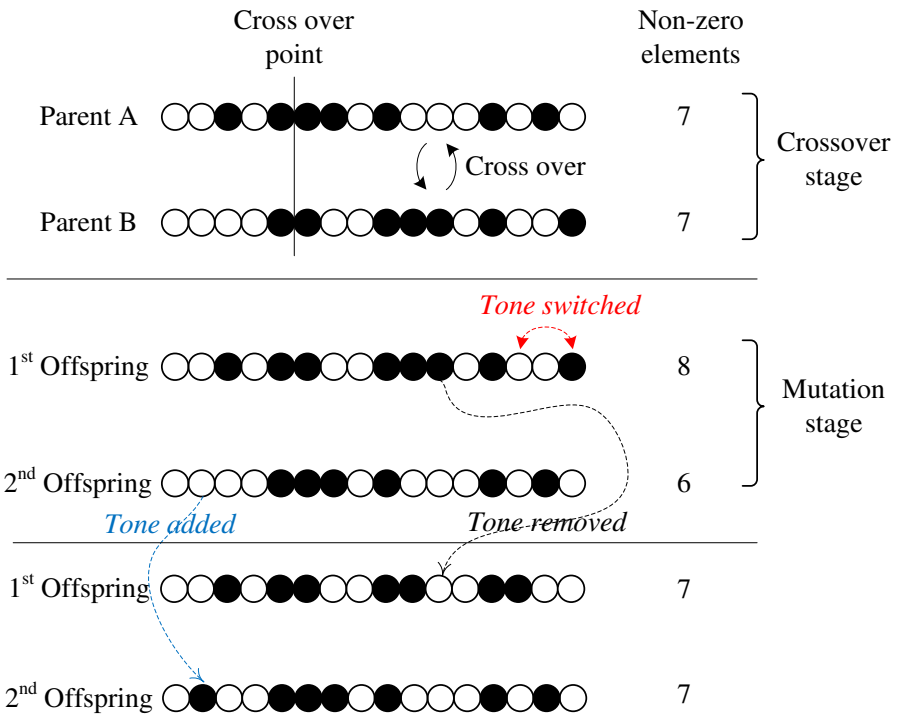

Figure 1 Illustration of crossover and mutation processes for $N = 16, G = 7$.

exchanged. After exchanging parts of the parent bodies, two new offspring sequences are generated, ending the crossover process.

The mutation process actually contains two sub-processes which are mutating and correcting. The mutating sub-process aims to introduce some randomly new tone locations in the offspring sequences, whereas the correcting sub-process ensures all the mutated sequences have the same number of tones, or equivalently the same number of non-zero elements, as the rest of the population, that is G.

There are two ways to mutate an offspring sequence, namely switching tones and toggling tones. The former randomly selects a pair of random tone locations in the sequence, and switches their positions. This does not cause the number of tones in the sequence to change. The latter is done by randomly choosing some locations in the sequence and toggling their values, that is from 0 to 1 and vice versa. This, however, might change the number of tones.

The correcting sub-process comes after to fix any unregulated offsprings. If an offspring

sequence has less number of ones than required, then a random tone is added, otherwise, one of its random tones is removed (see Figure 1).

After this step, the population is more crowded since the total number of its member sequences is $N_\wp + \binom{N_\wp}{2}\xi = N_\wp + \xi\frac{N_\wp(N_\wp-1)}{2}$

4. Ranking offspring sequences: For each generated offspring sequence, a corresponding kernel is constructed and its merit factor is computed. The whole population is then sorted by their merit factors in an increasing order, and only $N_\wp$ sequences having smallest merit factors are chosen to make the next generation parents. The search then continues again with Step 3) until the number of iterations N_{it} is reached.

Appendix C. CFTR to GTR transformation

This appendix proves that the CFTR algorithm can be transformed into the GTR algorithm with an adaptive scaling factor β_k instead of a constant γ as in (4.21). At the kth iteration of the CFTR algorithm, the clipping noise is formed in (4.33). Taking the DFT on both sides leads to:

$$\begin{aligned}\mathcal{F}\{\boldsymbol{f}_k\} &= \mathcal{F}\{\boldsymbol{y}_k\} - \mathcal{F}\{g_{\mathcal{T}}(\boldsymbol{y}_k)\} \\ &= \mathcal{F}\{\boldsymbol{x} + \beta_{k-1}\boldsymbol{c}_{k-1}\} - \mathcal{F}\{g_{\mathcal{T}}(\boldsymbol{y}_k)\} \\ &= \mathcal{F}\{\boldsymbol{x}\} + \beta_{k-1}\mathcal{F}\{\boldsymbol{c}_{k-1}\} - \mathcal{F}\{g_{\mathcal{T}}(\boldsymbol{y}_k)\}.\end{aligned} \tag{C.1}$$

Applying $H(\cdot)$ on both sides of (C.1) gives:

$$H(\mathcal{F}\{\boldsymbol{f}_k\}) = H(\mathcal{F}\{\boldsymbol{x}\}) + H(\mathcal{F}\{\beta_{k-1}\boldsymbol{c}_{k-1}\}) - H(\mathcal{F}\{g_{\mathcal{T}}(\boldsymbol{y}_k)\}). \tag{C.2}$$

Since the frequency filter only keeps reserved frequencies unchanged while suppresses other frequencies, it is easily seen that

$$\begin{aligned}H(\mathcal{F}\{\boldsymbol{x}\}) &= 0; \\ H(\mathcal{F}\{\boldsymbol{c}_{k-1}\}) &= \boldsymbol{C}_{k-1}.\end{aligned} \tag{C.3}$$

Therefore, the canceling signal which is formed in (4.34) as a consequence of (C.3) can be simplified into:

$$\begin{aligned}\boldsymbol{c}_k &= \mathcal{F}^{-1}\{\beta_{k-1}\boldsymbol{C}_{k-1}\} - \mathcal{F}^{-1}\{H(\mathcal{F}\{g_{\mathcal{T}}(\boldsymbol{y}_k)\})\} \\ &= \beta_{k-1}\boldsymbol{c}_{k-1} - \mathcal{F}^{-1}\{H(\mathcal{F}\{g_{\mathcal{T}}(\boldsymbol{y}_k)\})\}.\end{aligned} \tag{C.4}$$

Equation (C.4) means that the new canceling signal is made by adding the canceling signal constructed in the previous iteration with a correction term. The correction term can be derived explicitly using the definition of the DFT operation. Denote $\overline{\boldsymbol{Y}}_k = \mathcal{F}\{g_{\mathcal{T}}(\boldsymbol{y}_k)\}$, which is a length-$NJ$ frequency vector of the clipped signal. Its frequency component at

some tone location $0 \le \ell \le NJ-1$ can be found by:

$$\begin{aligned}
\overline{Y}_k[\ell] &= \frac{1}{\sqrt{NJ}} \sum_{n=0}^{NJ-1} g_{\mathcal{T}}(y_k[n])\, \mathrm{e}^{j2\pi \frac{n\ell}{NJ}} \\
&= \frac{1}{\sqrt{NJ}} \left(\sum_{n \notin \mathcal{S}_k} y_k[n]\, \mathrm{e}^{j2\pi \frac{n\ell}{NJ}} + \sum_{n \in \mathcal{S}_k} \left(\mathcal{T} \mathrm{e}^{j\angle y_k[n]} \right)\, \mathrm{e}^{j2\pi \frac{n\ell}{NJ}} \right) \\
&= \frac{1}{\sqrt{NJ}} \left(\sum_{n=0}^{NJ-1} y_k[n]\, \mathrm{e}^{j2\pi \frac{n\ell}{NJ}} - \sum_{n \in \mathcal{S}_k} \left(y_k[n] - \mathcal{T} \mathrm{e}^{j\angle y_k[n]} \right)\, \mathrm{e}^{j2\pi \frac{n\ell}{NJ}} \right) \\
&= Y_k[\ell] - \frac{1}{\sqrt{NJ}} \sum_{n \in \mathcal{S}_k} \left(y_k[n] - \mathcal{T} \mathrm{e}^{j\angle y_k[n]} \right)\, \mathrm{e}^{j2\pi \frac{n\ell}{NJ}}.
\end{aligned} \tag{C.5}$$

Since

$$Y_k[\ell] = \begin{cases} X[\ell], & \text{if } \ell \in \mathcal{D} \\ \beta_{k-1} C_{k-1}[\ell], & \text{if } \ell \in \mathcal{R} \\ 0, & \text{otherwise} \end{cases}$$

one has, for $0 \le m \le NJ-1$:

$$\begin{aligned}
\mathcal{F}^{-1}\{H(\mathcal{F}\{g_{\mathcal{T}}(\boldsymbol{y}_k)\})\}|_m &= \mathcal{F}^{-1}\{H(\overline{\boldsymbol{Y}}_k)\}|_m \\
&= \frac{1}{\sqrt{NJ}} \sum_{\ell \in \mathcal{R}} \left(Y_k[\ell] - \frac{1}{\sqrt{NJ}} \sum_{n \in \mathcal{S}_k} \left(y_k[n] - \mathcal{T} \mathrm{e}^{j\angle y_k[n]} \right)\, \mathrm{e}^{j2\pi \frac{n\ell}{NJ}} \right) \mathrm{e}^{-j2\pi \frac{\ell m}{NJ}} \\
&= \frac{1}{\sqrt{NJ}} \sum_{\ell \in \mathcal{R}} \beta_{k-1} C_{k-1}[\ell] \mathrm{e}^{-j2\pi \frac{\ell m}{NJ}} \\
&\qquad - \frac{1}{NJ} \sum_{\ell \in \mathcal{R}} \sum_{n \in \mathcal{S}_k} \left(y_k[n] - \mathcal{T} \mathrm{e}^{j\angle y_k[n]} \right) \mathrm{e}^{j2\pi \frac{n\ell}{NJ}} \mathrm{e}^{-j2\pi \frac{\ell m}{NJ}} \\
&= \beta_{k-1} c_{k-1}[m] - \frac{1}{NJ} \sum_{\ell \in \mathcal{R}} \sum_{n \in \mathcal{S}_k} \left(y_k[n] - \mathcal{T} \mathrm{e}^{j\angle y_k[n]} \right) \mathrm{e}^{j2\pi \frac{\ell(n-m)}{NJ}} \\
&= \beta_{k-1} c_{k-1}[m] - \frac{1}{NJ} \sum_{n \in \mathcal{S}_k} \left[\left(y_k[n] - \mathcal{T} \mathrm{e}^{j\angle y_k[n]} \right) \sum_{\ell \in \mathcal{R}} \mathrm{e}^{j2\pi \frac{\ell(n-m)}{NJ}} \right].
\end{aligned} \tag{C.6}$$

On the other hand, from (4.17), one also has:

$$\sum_{\ell \in \mathcal{R}} \mathrm{e}^{j2\pi \frac{\ell(n-m)}{NJ}} = |\mathcal{R}| k_m[n],$$

where $k_m[n]$ is the nth sample of the cyclically shifted kernel by m positions to the right, i.e., $\circlearrowright_m(\boldsymbol{k})$. As a result, the correction term in (C.4) is:

$$\mathcal{F}^{-1}\{H(\mathcal{F}\{g_{\mathcal{T}}(\boldsymbol{y}_k)\})\} = \beta_{k-1}\boldsymbol{c}_{k-1} - \frac{|\mathcal{R}|}{NJ}\sum_{n\in\mathcal{S}_k}\left(y_k[n] - \mathcal{T}\mathrm{e}^{j\angle y_k[n]}\right)\circlearrowright_m(\boldsymbol{k}), \tag{C.7}$$

which transforms Equation (C.4) into:

$$\boldsymbol{c}_k = \frac{|\mathcal{R}|}{NJ}\sum_{n\in\mathcal{S}_k}\left(y_k[n] - \mathcal{T}\mathrm{e}^{j\angle y_k[n]}\right)\circlearrowright_m(\boldsymbol{k}). \tag{C.8}$$

Therefore, the equivalent form of Equation (4.35) is:

$$\boldsymbol{y}_{k+1} = \boldsymbol{x} - \beta_k\frac{|\mathcal{R}|}{NJ}\sum_{n\in\mathcal{S}_k}\left(y_k[n] - \mathcal{T}\mathrm{e}^{j\angle y_k[n]}\right)\circlearrowright_m(\boldsymbol{k}). \tag{C.9}$$

References

[1] Ha H. Nguyen, *Introduction to OFDM. EE810 Lecture Notes.* University of Saskatchewan, 2013.

[2] Y. Rahmatallah and S. Mohan, "Peak-to-average power ratio reduction in OFDM systems: A survey and taxonomy," *IEEE Commun. Surv. Tutor*, vol. 15, pp. 1567–1592, Mar. 2013.

[3] Cable Center, "The cable history timeline." `https://www.cablecenter.org/resources/exhibits/cable-history-timeline.html`, 2014. [Online; accessed 17-July-2018].

[4] Cable Television Laboratories, Inc., "Physical layer specification," in *Data-Over-Cable Service Interface Specifications, DOCSIS 3.1*, CableLabs, May 2018.

[5] ZCorum, "The DOCSIS evolution and how 3.1 will change everything." `http://www.zcorum.com/wp-content/uploads/DOCSIS-Evolution-and-How-3.1-Will-Change-Everything.pdf`, 2015. [Online; accessed 17-July-2018].

[6] D. Kim, H. Lee, and D. Hong, "A survey of in-band full-duplex transmission: From the perspective of PHY and MAC layers," *IEEE Commun. Surv. Tutor*, vol. 17, pp. 2017–2046, Feb. 2015.

[7] MACOM Technology Solutions Inc., "MAPD-009918-C209C0 2-Way 0° Power Divider (5 – 1000) MHz Datasheet." `https://www.macom.com/products/product-detail/MAPD-009918-C209C0`. [Online; accessed 28-July-2018].

[8] MACOM Technology Solutions Inc., "MAFL-007988-CD0550 CATV Diplex Filter Datasheet." `https://www.macom.com/products/product-detail/MAFL-007988-CD0550`. [Online; accessed 28-July-2018].

[9] Ha H. Nguyen and E. Shwedyk, *A First Course in Digital Communications.* Cambridge University Press, 2009.

[10] C. Tellambura, "Computation of the continuous-time PAR of an OFDM signal with BPSK subcarriers," *IEEE Commun. Letters*, vol. 5, pp. 185–187, May 2001.

[11] H. E. Rowe, "Memoryless nonlinearities with Gaussian inputs: Elementary results," *Bell System Tech. J.*, vol. 61, pp. 1519–1525, Sept. 1982.

[12] C. Rapp, "Effects of HPA-nonlinearity on a 4-DPSK/OFDM-signal for a digital sound broadcasting signal," *Proc. of 2nd European Conference on Satellite Communications*, pp. 179–184, Oct. 1991.

[13] A. A. Saleh, "Frequency-independent and frequency-dependent nonlinear models of TWT amplifiers," *IEEE Trans. Commun.*, vol. 29, pp. 1715–1720, Nov. 1981.

[14] J. Armstrong, "Peak-to-average power reduction for OFDM by repeated clipping and frequency domain filtering," *Electronics Letters*, vol. 38, pp. 246–247, Feb. 2002.

[15] A. K. Gurung, F. S. Al-Qahtani, A. Z. Sadik, and Z. M. Hussain, "One-Iteration-Clipping-Filtering (OICF) scheme for PAPR reduction of OFDM signals," in *International Conference on Advanced Technologies for Communications*, pp. 207–210, Oct. 2008.

[16] K. Anoh, C. Tanriover, and B. Adebisi, "On the optimization of iterative clipping and filtering for PAPR reduction in OFDM systems," *IEEE Access*, vol. 5, pp. 12004–12013, June 2017.

[17] H. Kuo and S. Cheung, "Optimization of windowing and peak-windowing techniques for WCDMA systems," in *IEEE International Conference on Acoustics Speech and Signal Processing Proceedings*, vol. 4, pp. 313–316, May 2006.

[18] M. Ojima and T. Hattori, "PAPR reduction method using clipping and peak-windowing in CI/OFDM system," in *Proc. IEEE Veh. Technol. Conf.*, pp. 1356–1360, Sept. 2007.

[19] S. Cha, M. Park, S. Lee, K.-J. Bang, and D. Hong, "A new PAPR reduction technique for OFDM systems using advanced peak windowing method," *IEEE Transactions on Consumer Electronics*, vol. 54, pp. 405–410, July 2008.

[20] G. Chen, R. Ansari, and Y. Yao, "Improved peak windowing for PAPR reduction in OFDM," in *Proc. IEEE Veh. Technol. Conf.*, pp. 1–5, Apr. 2009.

[21] S. Lu, D. Qu, and Y. He, "Sliding window tone reservation technique for the peak-to-average power ratio reduction of FBMC-OQAM signals," *IEEE Commun. Letters*, vol. 1, pp. 268–271, July 2012.

[22] J. Hou, J. Ge, and F. Gong, "Tone reservation technique based on peak-windowing residual noise for PAPR reduction in OFDM systems," *IEEE Trans. Veh. Technol.*, vol. 64, pp. 5373–5378, Jan. 2015.

[23] X. Huang, J. Lu, J. Chuang, and J. Zheng, "Companding transform for the reduction of peak-to-average power ratio of OFDM signals," *IEEE Trans. Wireless Commun.*, vol. 3, pp. 2030–2039, Nov. 2004.

[24] E.-V. Cuteanu, "PAPR reduction of ofdm signals using adaptive companding scheme," in *International Conference on Applied Electronics*, pp. 1–4, Sept. 2013.

[25] K. Anoh, B. Adebisi, K. M. Rabie, and C. Tanriover, "Root-based nonlinear companding technique for reducing PAPR of precoded OFDM signals," *IEEE Access*, vol. 6, pp. 4618–4629, Dec. 2017.

[26] R. W. Bauml, R. F. Fischer, and J. B. Huber, "Reducing the peak-to-average power ratio of multicarrier modulation by selected mapping," *Electronics Letters*, vol. 32, pp. 2056–2057, Oct. 1996.

[27] S. Y. Le Goff, S. S. Al-Samahi, B. K. Khoo, C. C. Tsimenidis, and B. S. Sharif, "Selected mapping without side information for PAPR reduction in OFDM," *IEEE Trans. Wireless Commun.*, vol. 8, pp. 182–184, July 2009.

[28] E. Hong and D. Har, "Peak-to-average power ratio reduction in OFDM systems using all-pass filters," *IEEE Trans. Broadcast.*, vol. 56, pp. 114–119, Dec. 2009.

[29] S. H. Muller and J. B. Huber, "OFDM with reduced peak-to-average power ratio by optimum combination of partial transmit sequences," *Electronics Letters*, vol. 33, pp. 368–369, Feb. 1997.

[30] L. J. Cimini and N. R. Sollenberger, "Peak-to-average power ratio reduction of an OFDM signal using partial transmit sequences," *IEEE Commun. Letters*, vol. 4, pp. 86–88, Mar. 2000.

[31] A. Jayalath and C. Tellambura, "Adaptive PTS approach for reduction of peak-to-average power ratio of OFDM signal," *Electronics Letters*, vol. 36, pp. 1226–1228, July 2000.

[32] Y.-J. Cho, J.-S. No, and D.-J. Shin, "A new low-complexity PTS scheme based on successive local search using sequences," *IEEE Commun. Letters*, vol. 16, pp. 1470–1473, July 2012.

[33] P. Van Eetvelt, G. Wade, and M. Tomlinson, "Peak to average power reduction for OFDM schemes by selective scrambling," *Electronics Letters*, vol. 32, pp. 1963–1964, Oct. 1996.

[34] A. D. S. Jayalath and C. Tellambura, "The use of interleaving to reduce the peak-to-average power ratio of an OFDM signal," in *Proc. IEEE Global Telecommun. Conf.*, vol. 1, pp. 82–86, Dec. 2000.

[35] S.-H. Wang, K.-C. Lee, C.-P. Li, and H.-J. Li, "A low-complexity symbol interleaving-based PAPR reduction scheme for OFDM systems," in *Proc. IEEE Int. Conf. Commun.*, pp. 4693–4697, June 2013.

[36] J. Tellado and J. M. Cioffi, "Efficient algorithms for reducing PAR in multicarrier systems," in *IEEE International Symposium on Information Theory*, p. 191, Aug. 1998.

[37] J. Tellado, *Multicarrier modulation with low PAR: applications to DSL and wireless*. Springer Science & Business Media, 2006.

[38] D. L. Jones, "Peak power reduction in OFDM and DMT via active channel modification," in *Conference Record of the Thirty-Third Asilomar Conference on Signals, Systems, and Computers*, vol. 2, pp. 1076–1079, Oct. 1999.

[39] B. S. Krongold and D. L. Jones, "PAR reduction in OFDM via active constellation extension," *IEEE Trans. Broadcast.*, vol. 49, pp. 258–268, Sept. 2003.

[40] K. Bae, J. G. Andrews, and E. J. Powers, "Adaptive active constellation extension algorithm for peak-to-average ratio reduction in OFDM," *IEEE Commun. Letters*, vol. 14, pp. 39–41, Dec. 2009.

[41] A. E. Jones, T. A. Wilkinson, and S. Barton, "Block coding scheme for reduction of peak to mean envelope power ratio of multicarrier transmission schemes," *Electronics Letters*, vol. 30, pp. 2098–2099, Dec. 1994.

[42] D. Wulich, "Reduction of peak to mean ratio of multicarrier modulation using cyclic coding," *Electronics Letters*, vol. 32, p. 432, Feb. 1996.

[43] M.-J. Hao and C.-H. Lai, "Precoding for PAPR reduction of OFDM signals with minimum error probability," *IEEE Trans. Broadcast.*, vol. 56, pp. 120–128, Nov. 2009.

[44] J. A. Davis and J. Jedwab, "Peak-to-mean power control in OFDM, Golay complementary sequences, and Reed-Muller codes," *IEEE Trans. Inform. Theory*, vol. 45, pp. 2397–2417, Nov. 1999.

[45] C. V. Chong, R. Venkataramani, and V. Tarokh, "A new construction of 16-QAM Golay complementary sequences," *IEEE Trans. Inform. Theory*, vol. 49, pp. 2953–2959, Nov. 2003.

[46] S. C.-H. Huang, H.-C. Wu, S. Y. Chang, and X. Liu, "Novel sequence design for low-PMEPR and high-code-rate OFDM systems," *IEEE Trans. Commun.*, vol. 58, pp. 405–410, Feb. 2010.

[47] M.-C. Lin, K.-C. Chen, and S.-L. Li, "Turbo coded OFDM system with peak power reduction," in *Proc. IEEE Veh. Technol. Conf.*, vol. 4, pp. 2282–2286, Oct. 2003.

[48] Y.-C. Tsai, S.-K. Deng, K.-C. Chen, and M.-C. Lin, "Turbo coded OFDM for reducing PAPR and error rates," *IEEE Trans. Wireless Commun.*, vol. 7, pp. 84–89, Jan. 2008.

[49] K. Bani, R. Bansode, and B. Mishra, "Novel technique for PAPR reduction in OFDM system using $\pi/4$-shifted-DQPSK modulation & turbo code," in *International Conference on Devices, Circuits and Systems (ICDCS)*, pp. 627–633, Mar. 2012.

[50] S. Kimura, T. Nakamura, M. Saito, and M. Okada, "PAR reduction for OFDM signals based on deep clipping," in *International Symposium on Communications, Control and Signal Processing*, pp. 911–916, Mar. 2008.

[51] D. Guel and J. Palicot, "Transformation of any Adding Signal Technique in Tone Reservation Technique for PAPR Mitigation thanks to Frequency Domain Filtering," *International Journal on Advances in Telecommunications*, vol. 4, pp. 205–216, 2011.

[52] X. Li and L. J. Cimini, "Effects of clipping and filtering on the performance of OFDM," *IEEE Commun. Letters*, vol. 2, pp. 131–133, May 1998.

[53] Y. Tang, W. Shieh, and B. S. Krongold, "DFT-spread OFDM for fiber nonlinearity mitigation," *IEEE Photonics Technology Letters*, vol. 22, pp. 1250–1252, June 2010.

[54] S. Boyd and L. Vandenberghe, *Convex Optimization*. Cambridge University Press, 2004.

[55] S. Zabre, J. Palicot, Y. Louet, and C. Lereau, "SOCP approach for OFDM peak-to-average power ratio reduction in the signal adding context," in *International Symposium on Signal Processing and Information Technology*, pp. 834–839, Aug. 2006.

[56] Q. Liang, Q. Wen, Y. Xiao, and S. Li, "A comparison of SCR and active-set methods for PAPR reduction in OFDM systems," in *International Conference on Networks Security, Wireless Communications and Trusted Computing*, vol. 1, pp. 489–495, Apr. 2009.

[57] D. Guel and J. Palicot, "FFT/IFFT pair based digital filtering for the transformation of adding signal PAPR reduction techniques in tone reservation techniques," in *Fifth International Conference on Wireless and Mobile Communications*, pp. 200–204, Aug. 2009.

[58] H. Li, T. Jiang, and Y. Zhou, "An improved tone reservation scheme with fast convergence for PAPR reduction in OFDM systems," *IEEE Trans. Broadcast.*, vol. 57, pp. 902–906, Oct. 2011.

[59] X. Lv and Y. Wan, "Efficient tone reservation peak-to-average power ratio reduction system with optimal clipping for orthogonal frequency division multiplexing systems," *IET Communications*, vol. 9, pp. 2070–2076, Nov. 2015.

[60] J. Bai, Y. Li, W. Cheng, H. Du, and Y. Wang, "A novel peak-to-average power ratio reduction scheme via tone reservation in OFDM systems," *China Communications*, vol. 14, pp. 279–290, Dec. 2017.

[61] D.-W. Lim, H.-S. Noh, J.-S. No, and D.-J. Shin, "Near optimal PRT set selection algorithm for tone reservation in OFDM systems," *IEEE Trans. Broadcast.*, vol. 54, pp. 454–460, June 2008.

[62] Y. Wang, W. Chen, and C. Tellambura, "Genetic algorithm based nearly optimal peak reduction tone set selection for adaptive amplitude clipping PAPR reduction," *IEEE Trans. Broadcast.*, vol. 58, pp. 462–471, Apr. 2012.

[63] J.-C. Chen, M.-H. Chiu, Y.-S. Yang, and C.-P. Li, "A suboptimal tone reservation algorithm based on cross-entropy method for PAPR reduction in OFDM systems," *IEEE Trans. Broadcast.*, vol. 57, pp. 752–756, Apr. 2011.

[64] L. Wang and C. Tellambura, "Analysis of clipping noise and tone-reservation algorithms for peak reduction in OFDM systems," *IEEE Trans. Veh. Technol.*, vol. 57, pp. 1675–1694, May 2008.

[65] J. Ilow and P. Venkatasubramanian, "Applications of level crossing theory to clipping noise characterization in filtered OFDM signals," in *Consumer Communications and Networking Conference*, pp. 470–473, Jan. 2007.

[66] Q. Liuy, R. J. Baxleyz, X. May, and G. T. Zhou, "Peak reduction for multiplexed asynchronous OFDM-FDMA," in *IEEE Military Communications Conference*, pp. 1–6, Oct. 2009.

[67] Q. Liu, X. Ma, G. T. Zhou, and J. Wu, "Peak-to-average power ratio versus instantaneous-to-average power ratio for OFDM," in *42nd Asilomar Conference on Signals, Systems and Computers*, pp. 938–942, Oct. 2008.

[68] Q. Liu, R. J. Baxley, X. Ma, and G. T. Zhou, "On the PTS method and BER-minimizing power allocation of the multi-channel OFDM system," in *IEEE International Conference on Acoustics, Speech and Signal Processing*, pp. 2585–2588, Apr. 2009.